UCLA

UCLA Electronic Theses and Dissertations

Title

Understanding the role of the microenvironment in cardiovascular differentiation

Permalink

https://escholarship.org/uc/item/0cr48276

Author

Gluck, Jessica Marie

Publication Date

2013

Peer reviewed|Thesis/dissertation

UNIVERSITY OF CALIFORNIA

Los Angeles

Understanding the Role of the Microenvironment in Cardiovascular Differentiation

A dissertation submitted in partial satisfaction of the

requirements for the degree Doctor of Philosophy

in Molecular, Cellular & Integrative Physiology

By

Jessica Marie Gluck

2013

ABSTRACT OF THE DISSERTATION

Understanding the Role of the Microenvironment on Cardiovascular Differentiation

By

Jessica Marie Gluck

Doctor of Philosophy in Molecular, Cellular & Integrative Physiology

University of California, Los Angeles, 2013

Professor Joshua Goldhaber, co-chair

Professor W. Robb MacLellan, co-chair

The goal of this work is to understand the role of the microenvironment on cardiovascular differentiation. I sought to investigate the role of extracellular matrix (ECM) proteins on early cardiovascular differentiation and specifically the role of ECM proteins and three-dimensional (3D) environment using an engineered scaffold that mimics the cardiovascular progenitor cell (CPC) niche. Chapter one provides background and outlines the significance of this work. Chapter two describes the development of a 3D scaffold used for later studies. I examined the role of a 3D hydrogel on the induction of CPCs from murine embryonic stem (mES) cells and characterized integrin expression in both undifferentiated and partially differentiated mES cells. These results show that the addition of a 3D element in the microenvironment significantly increases the amount of CPCs induced from mES cells. Chapter three investigates the role of the

microenvironment on cell fate commitment of CPCs. This work demonstrates the effects of both ECM proteins and the addition of a 3D scaffold to CPC culture on both vascular endothelial cell and smooth muscle cell differentiation. I also developed a method to create CPC-derived layered tissue engineered vascular grafts. Chapter four extends this work into a human induced pluripotent stem (hiPS) cell model. I show the effects of the microenvironment do influence cardiac differentiation in a human model, but with differing results from the mouse studies. I also show that the addition of fibronectin in 3D scaffold can greatly enhance vascular differentiation, and that cardiac differentiation is time sensitive.

This works provides insight into the role of the microenvironment on cardiovascular differentiation in both mouse and human stem cell models, introduces a method to create layered tissue engineered vascular grafts, and raises new questions and directions for future work in the area of cardiovascular tissue engineering and cardiovascular differentiation.

The dissertation of Jessica Marie Gluck is approved.

Kristina Boström

Alan Garfinkel

Andrea Kasko

Richard J. Shemin

Joshua Goldhaber, Committee Co-Chair

W. Robb MacLellan, Committee Co-Chair

University of California, Los Angeles

2013

To my family

Mom, Dad, Molly, Bruce, Moo & Winston

with endless gratitude for your constant unconditional love and support

TABLE OF CONTENTS

LIST OF FIGURES

LIST OF TABLES AND EQUATIONS

ACKNOWLEDGEMENTS

There are many people I wish to thank in the preparation of this dissertation and their support throughout my PhD journey. A very special thank you goes to my two mentors Dr. W. Robb MacLellan and Dr. Richard Shemin. Dr. MacLellan, I would not have completed my PhD without your guidance and support the last five years. I am grateful for your extremely high standards in research and patience as I found my way. I've learned so much from you and I hope this work has made you proud! Dr. Richard Shemin also deserves special recognition for his constant support and guidance. He took a chance by accepting a graduate student and gave me a lab "home" for which I am very grateful. I have truly enjoyed being part of his never-ending quest for a Nobel Prize!

Thank you to Dr. Joshua Goldhaber for all of his kind encouragement, attendance at my MCIP student seminars and support as my co-chair. I am very grateful to the rest of my committee, Dr. Kristina Boström, Dr. Alan Garfinkel, and Dr. Andrea Kasko for their time, patience and support. Even with a rocky start, I have learned so much and grown so much as a researcher—thank you for advice and input! I hope you are proud of your influence on my work.

I would not be where I am today without the mentorship and (better still) friendship of Dr. Sepideh Heydarkhan-Hagvall. Her unwavering belief in me has been the best gift from my PhD journey. She has taught me so much; not only in the lab, but her life lessons will stay with me always. I can only hope I have even half the impact on my future lab mates and students as she had on me. I'm so lucky to have made a lifelong friend and I hope I have made you proud! I have to thank all the students I had the privilege of working with in the lab over the last five years; they have taught me just as much as I hope they have learned from me: Connor Delman,

Last, but certainly not least. To my family, thank you so much for your constant support even when it meant living 3,000 miles (and 3 time zones) away from you! Thanks to Team Fun for all our adventures, which were not only incredible times but lasting memories. I am very lucky to have such a close family that supports and encourages each other to pursue our dreams. Bruce, my new brother, thank you for all the laughter and encouragement. I'm so excited you're part of the fam now; we are very lucky to have you! My parents, who have always been world's best role models and cheerleaders, words cannot express just how grateful I am to you. You always encourage and inspire me. I am forever indebted for all you have done to help and support me along the way and am so fortunate to have such wonderful parents. Molly—I am so lucky you're my sister and my very best friend! Thank you for listening to all my science stories (even when you didn't understand them) and helping me survive this last stage of my professional student status! Your constant support and endless encouragement mean the world to me! The unconditional love from my family has made this PhD possible. I love you all very much. My cup runneth over.

Co-author Acknowledgements

Chapter Two contains versions of the following manuscripts:

"Gluck JM, Rahgozar P, Ingle NP, Rofail F, Petrosian A, Cline MG, Jordan MC, Roos KP, MacLellan WR, Shemin RJ, Heydarkhan-Hagvall S. Hybrid co-axial electrospun nanofibrous scaffolds with limited immunological response for tissue engineering. Journal of Biomedical Materials Research Part B, 2011; 99B: 180-190."

"Gluck JM, Chyu J, Delman C, Heydarkhan-Hagvall S, MacLellan WR, Shemin RJ. Hyaluronan-based three-dimensional microenvironment potently induce cardiovascular progenitor cell population. BioMed Research International, 2013, under review."

"Gluck JM, Delman C, Full S, Shemin RJ, Heydarkhan-Hagvall S. Stem cell extracellular matrix interactions in three-dimensional system via integrins. Journal of Regenerative Medicine, 2013, under review"

Chapters Three and Four contain versions of the following manuscripts, which are in preparation for publication:

"Gluck JM, Delman C, Chyu J, Full S, Heydarkhan-Hagvall S, Shemin RJ, MacLellan WR. Microenvironment influences cardiovascular differentiation of murine cardiovascular progenitor cells."

"Gluck JM, Chyu J, Delman C, Heydarkhan-Hagvall S, Shemin RJ, MacLellan WR. Extracellular matrix proteins in the microenvironment enhance cardiac differentiation of human induced pluripotent stem cells."

VITA

2002-2005	BS, Textile Technology College of Textiles North Carolina State University Raleigh, NC
2005-2007	MS, Textile Apparel, Technology & Management minor Biomedical Engineering College of Textiles North Carolina State University Raleigh, NC
2005-2007	Graduate Teaching and Research Assistant Dr. Martin W. King College of Textiles North Carolina State University Raleigh, NC
2007-2008	MS, Biomedical Engineering Henry Samueli School of Engineering and Applied Science University of California, Los Angeles Los Angeles, CA
2008-present	Graduate Student Researcher Department of Cardiothoracic Surgery David Geffen School of Medicine University of California, Los Angeles Los Angeles, CA
2010	Teaching Assistant UCLA Life Sciences Core University of California, Los Angeles Los Angeles, CA

PUBLICATIONS

Gluck JM*, Chyu J, Delman C, Heydarkhan-Hagvall S, MacLellan WR, Shemin RJ.
Hyaluronan-based three-dimensional microenvironment potently induce cardiovascular
progenitor cell population. *BioMed Research International*, **2013** under review

Gluck JM*, Delman C, Full S, Shemin RJ, Heydarkhan-Hagvall S. Stem cell extracellular matrix interactions in three-dimensional system via integrins. *Journal of Regenerative Medicine*, **2013** under review

Gluck JM*, Rahgozar P, Ingle NP, Rofail F, Petrosian A, Cline MG, Jordan MC, Roos KP, MacLellan WR, Shemin RJ, Heydarkhan-Hagvall S. Hybrid co-axial electrospun nanofibrous scaffolds with limited immunological response created for tissue engineering. *Journal of Biomedical Materials Research Part B*, **2011**; 99B: 180-190.

Heydarkhan-Hagvall S, Gluck JM*, Delman C, Jung M, Ehsani N, Full S, Shemin RJ. The effect of vitronectin on the differentiation of embryonic stem cells in a 3D culture system. *Biomaterials*, **2012**: 33; 2032-2040.

Schenke-Layland K, Nsair A, van Handel B, Angelis E, Gluck JM*, Votteler M, Goldhaber JI, Mikkola HKA, Kahn M, MacLellan WR. Recapitulation of the embryonic cardiovascular progenitor cell niche. *Biomaterials*, **2011**; 32: 2748-2756.

Schenke-Layland K, Rofail F, Heydarkhan S, Gluck JM*, Ingle NP, Angelis E, Choi C, MacLellan WR, Beygui RE, Shemin RJ, Heydarkhan-Hagvall S. The use of three-dimensional nanostructures to instruct cells to produce extracellular matrix for regenerative medicine strategies. *Biomaterials*, **2009**; 30: 4665-4675.

CHAPTER ONE

A. Introduction

Heart disease is a leading cause of morbidity and mortality in the United States [1,2]. Conventional therapies range from lifestyle changes to drug therapy to surgical intervention, with heart transplantation being the final option [3,4]. Recently, regenerative therapies and stem cell-based approaches in particular have garnered much interest [5]. Stem cells combined with tissue engineering principles could potentially be used to fabricate cardiovascular tissue, which can be used as both a more realistic *in vitro* culture model and potentially as tissue replacement for heart disease patients *in vivo*. One such example is stem cell niches. Much work has been conducted to determine what comprises the niche environment of cardiac progenitor cells (CPCs) found in small populations *in vivo* and the mechanisms by which this cell population then differentiates to form committed cardiovascular tissue. Previously, we established the role of extracellular matrix (ECM) proteins in the development of CPCs from mouse stem cell lineages [6]. We also determined a key influence on the expansion of the CPC population from an embryonic stem (ES) cell population is the addition of a three-dimensional (3D) microenvironment in the form of hydrogels and electrospun nanofibrous scaffolds.

I propose to use tissue engineering principles and biomaterials to engineer human cardiovascular grafts. I will investigate 1) how a 3D microenvironment induces a mouse CPC population, 2) the mechanism(s) by which the microenvironment and ECM proteins influence differentiation of mouse CPCs, and 3) how the microenvironment alters the cardiovascular differentiation potential of human induced pluripotent stem (iPS) cells. Through this research, I envision providing a better, more complete understanding of how cardiovascular tissue is formed

and how the microenvironment interacts with the progenitor cell niche and drives differentiation using tissue engineering principles and both synthetic and natural biomaterials.

B. Stem Cell Biology and Regenerative Medicine

Cardiovascular disease remains one of the leading causes of death in the developed world; as such, much focus has been dedicated to developing new and better treatments. Because of the nature of cardiovascular disease, many researchers have turned to regenerative medicine as a possible avenue of developing more effective and possibly preventative treatments. By understanding how cardiovascular tissue is formed, it becomes easier to understand how disease states develop and how to prevent and treat those disease states.

Stem cell biology has become a major focus of recent cardiovascular research. The idea of regenerative medicine in practice is evident in the ability of the liver and skeletal muscle to regenerate itself. Cardiovascular injuries, however, do not result in regeneration. Myocardial infarctions can lead to the loss of over a billion cardiomyocytes [7]. The hearts that survive the cardiac injury are then forced to work "overtime" to maintain marginal cardiac function. Over time, that increased work leads to congestive heart failure [8]. It has been proposed that heart failure could be reversed if new myocardium could be introduced to the damaged region of the heart.

Numerous cell types have been evaluated for their potential to repair cardiac tissue [9]. Skeletal muscle satellite cells were among the first candidate cell type investigated [10,11]. Transplantation of theses myoblasts did not result in the necessary integration and development of gap junction proteins to properly electromechanically couple with other myoblasts or host cardiac myocytes [12]. After Ferrari et al [13] reported cells from bone marrow can contribute to

skeletal muscle regeneration in 1998 researchers began to investigate the potential for myocardial regeneration. Several groups reported that bone marrow cells can contribute to cardiac repair on a small scale using genetic tracking models and lethally irradiated wild-type mice [14-17]. However, controversy has arisen as there has been difficulty reproducing the results from these studies. Researchers agree that endogenous bone marrow-derived cells can contribute to cardiac repair rarely through cell fusion but whether bone marrow cells can lead to large-scale cardiac repair is still unanswered. Mesenchymal stem cells (MSCs) are found in the stroma of bone marrow. Work from the Caplan group led to the identification of a multipotent stem cell population from these marrow stromal cells [18]. Pittenger confirmed the multilineage potential of the MSCs from clonal studies [19]. Many groups [20] have pursued studying the potential of MSCs for cardiac repair, including direct injection of MSCs to large animal model infarcted hearts [21] and finding that MSCs have demonstrated ability to hone to the site of cardiac injury [22].

In response, to these variable results with adult stem cell researchers have turned their attention to pluripotent stem cells, ES cells and iPS cells. Human ES cells were derived in 1998 [23] from the inner cell mass of a preimplantation stage mammalian embryo. These undifferentiated ES cells are capable of proliferation, self-renewal, and the generation of large number of differentiated cell progeny [24-26]. As the cell differentiates, it commits to a specific cell-type lineage, with decreasing differentiation potential and is described as a progenitor cell. Progenitor cells along with adult stem cells are capable of limited differentiation in specific tissues [27]. In particular, ES cells provide researchers with a unique opportunity to study and analyze the particular pathway of differentiation to a cardiovascular lineage [28-30]. ES cells

have demonstrated clear evidence of cardiac potential by expressing the necessary molecular elements required for electromechanical coupling with host myocardium [31-33].

Mouse ES cells have been successfully differentiated into cardiac tissue *in vitro* using a variety of methods. Undifferentiated mES cells express several pluripotency markers, including Oct3/4, FGF-5, Nodal, Sox2, etc. A variety of parameters can determine the differentiation potential of ES cells, namely the number of cells, media, FBS, growth factors/small molecules, and the specific cell line being used [32,34]. Doetschman et al were amongst the first to describe that removal of ES cells from the conditions that maintain pluripotency results in spontaneous aggregation and the formation of embroyid bodies (EBs) [35]. Several days after EB formation led to beating cardiomyocytes *in vitro*. The rate of beating contraction increases with continued differentiation and will eventually slow with maturation. During early stages of differentiation, myofibrils are present but lack uniformity and organization. A and I bands are normally evident in these early stages [32]. With prolonged differentiation and maturation ES cell-derived cardiomyocytes become elongated with developed myofibrils and sarcomeres and develop cell-cell junctions consistent with those observed *in vivo* [34].

In vitro, mES cell-derived cardiomyocytes exhibit developmentally appropriate cardiac gene expression [36-38]. In particular mES cell-derived cardiomyocytes are known to express the following: transcription factors Nkx2.5 and GATA-4, as well as myosin light chain (MLC)-2v, α-myosin heavy chain (α-MHC), β-myosin heavy chain (β-MHC), atrial natriuretic factor (ANF) and Na^+-Ca^{2+} exchanger and phospholamban [39]. Sarcomeric proteins are developed in ES cell-derived cardiomyocytes in this typical order: titin (Z-disk), α-actinin, myomesin, titin (M band), MHC, SM-α-actin, cardiac troponin T and other cardiac specific markers such

Connexin43 [39]. mES cell-derived cardiomyoctyes have also shown development of electrophysiological specialization into ventricular, atrial and nodal/pacemaker cell subtypes [38].

The capacity of ES cells to differentiate into almost all types of tissue underlies their attractiveness as a cell source for regenerative medicine. However, the implantation of direct ES cells leads to the formation of teratomas *in vivo*. Therapeutic use will require deriving purified populations of ES cell-derived cardiomyocytes or progenitor cells free of undifferentiated stem cells. Many studies have been conducted to identify and characterize the complex steps of cardiogenesis [40,41]. Endogenous factors have been identified as inducers of cardiac differentiation, including: transforming growth factor β (TGFβ), bone morphogenic proteins (BMPs), fibroblast growth factors, nitric oxide, and various members of the Wnt signaling family [42-47]. Small molecules have also been reported to promote cardiac differentiation, including retinoic acid, ascorbic acid, dynorphin B, activin A, and ROCK inhibitor [47-51].

Human ES cell differentiation to cardiovascular lineages has been harder to achieve but hES cell-derived cardiomyocytes show the expected molecular, structural, and electrophysiological properties of nascent embryonic myocardium [33,52,53]. Several different methods have been investigated, but the methods for cardiovascular differentiation are constantly evolving.

Nuclear reprogramming resets the fate of somatic cells to a primordial ES cell-like state producing induced pluripotent stem cells. Somatic cell nuclear transfer showed that an oocyte can return an adult cell nucleus to a pluripotent state [54, 55]. First introduced by Yamanaka [56] in 2006, four transcription factors were retrovirally overexpressed to create what is known as an iPS cell. These four factors, Oct4, Sox2, c-Myc, and Klf4 created iPS cells with morphology and growth properties similar to that of an ES cell. Human iPS cells have been created using Oct4,

Sox2, Nanog, and LIN28 [57]. These cells have shown normal karyotype, express telomerase activity, cell surface markers, and genes that are used to identify ES cells. Recently, it has been established that mouse iPS cells have the potential to differentiate into cardiovascular and hematopoietic lineages [58]. Human iPS cells have also been shown to differentiate into functional cardiomyocytes [59-61]. These cells were subjected to electrophysiology studies, which demonstrated their capacity for differentiation into nodal, atrial, and ventricular phenotypes, as well as exhibiting the necessary molecular markers used to define cardiomyocytes. It is thought iPS cells could provide an alternative method to using ES cells, which are subject to ethical and procurement controversy. Progress in the field has made stem cell therapies an attractive model for regenerative medicine in cardiovascular research.

C. Cardiovascular Progenitor Cell Niche

In vivo, endogenous stem cells reside in tissue-specific anatomically defined clusters called "niches." Schofield first proposed the idea of a stem cell niche almost 35 years ago [62]. The first experimental evidence was demonstrated in invertebrates. Germ cells of *Dosophila melanogaster* and *Caenorhabditis elegans* reside in the distal end of a tapered structure, and depend upon interactions with somatic cells at the end of that structure to maintain stem cell features [63-65]. Stem cell niches have been identified and studied in the haematopoietic, skin epithelial, intestinal, and neural systems as well as the germ line in mice [66,67]. Bone marrow has been one of the most extensively studied stem cell systems and the microenvironment of their natural niche has led to further studies of the contribution of the niche to stem cell properties [66,68,69]. The concept of the stem cell niche has been extensively researched in the

last decade [70] but many gaps remain in our understanding the regulatory mechanisms within the niche.

Cell fate within the stem cell niche is thought to be controlled both spatially and temporally, as well as through cell-cell and cell-matrix interactions. Paracrine and autocrine factors are also thought to regulate cell fate within the niche—there is mounting evidence that stem cells secrete a variety of growth factors, cytokines, chemokines and bioactive lipids which regulate biology and interactions within the surrounding microenvironment. These factors are thought to inhibit apoptosis, stimulate proliferation, and promote vascularization [71]. Additionally, interactions with resident niche cells or the surrounding niche ECM are thought to play an equally important role. Two signaling families known to regulate stem cell fate are thought to play key roles within the niche regulation: TGFβ and Wnt [72]. These signaling regulators show conservation between species and tissues that self-renew. Wnts activate transcription through a complex pathway involving β-catenin [73]. TGFβ signaling is regulated through BMPs [74-76]. Additionally, factors secreted from stem cells within the niche that are thought to have an impact on cell fate regulation are the following: vascular endothelial growth factor (VEGF), stem cell factor (SCF), hepatocyte growth factor (HGF), insulin-like growth factor-1 and -2 (IGF-1, IGF-2), and stromal-derived factor-1 (SDF-1) [71,77]. BMP4 has been shown to regulate the haematopoietic stem (HS) cell niche by controlling the number of HS cells within the niche through N-cadherin and β-catenin [78].

The niche ECM is believed to play an important role in cell fate regulation. Those cell-matrix interactions within the niche are in turn mediated via cadherins and integrins [71,79]. β1 integrins are differentially expressed on primitive cells and selectively expressed on stem cell populations through presumed interactions with matrix glycoprotein ligands [80-83]. The

presence or absence of tenascin C, a known neural ECM component can alter the number and function of neural stem cells in the subventricular zone [84]. Tenascin C is thought to modulate stem cell sensitivity to BMP4 and fibroblast growth factor-2 (FGF2), resulting in an increased ability to generate glial cells [84]. The deletion of tenascin C is also thought to participate in the regulation of the HS cell niche [85]. The glycine-arginine-aspartic acid (RGD) amino acid sequence found on many ECM components and matrix ligands, including fibronectin and osteopontin, has been shown to regulate HS cells [86,87]. Osetopontin is known to interact with $\alpha 4$ and $\alpha 5\beta 1$ integrins and it has been shown that osetopontin production can regulate osteoblast activation and HS cell production [87,88]. $\beta 1$ integrins have been implicated in HS cell regulation [89] and have also been used to identify epidermal stem cells [82]. It has also been shown that $\beta 1$ deletion gives rise to an increased production of epithelial stem cells due to impaired Hedgehog signaling [90] and that $\beta 1$ integrin triggers the expression of stemness transcriptional regulators through a synthetic matrix engineered to bind and activate specific $\beta 1$ heterodimers [91].

The physical organization of the niche is thought to be equally important. Ephrins are thought to mediate structural boundaries in neural and vascular tissue. Graduated expression of ephrin B2 and its transmembrane tyrosine kinase receptors EphB2 and EphB3 organize mouse intestinal epithelial cells [92]. Furthermore, the physical properties of the niche ECM have also been implicated to play a role in cell fate regulation. Collagen I gels mimicking the elasticity of muscle induced MSCs to upregulate myogenic markers, while more rigid gels caused MSCs to differentiate down an osteogenic lineage [93]. Additionally, a study using hES cells and muscle-derived stem cells were plated on rigid spots of 576 different combinations of 25 various acrylate-based polymers found that there was a wide range of variation in cell attachment,

proliferation, and lineage induction [94]. Neuron differentiation is favored on soft matrices whereas more rigid surfaces promote glial differentiation from neural stem cells [95]. Most cells are found to adhere more strongly, spread, and to assemble cytoskeleton structures to stiff substrates as compared to soft substrates [96]. With gradients of elasticity, cells are found to accumulate on more stiff substrates in a process called "durotaxis," [97] which might explain why MSCs hone to sites of injury and fibrosis [98]. Studies have found that after a myocardial infarct, fibrotic tissue that forms is more rigid (20-60kPa, common for cartilage and pre-calcified bone) compared to surrounding 'normal' tissue [99,100]. MSCs injected into a mouse infarct model can develop into bone within the heart tissue [101]. This may be due to the stiff nature of the fibrotic tissue that forms following a cardiac injury. Fibroblasts have been shown to differentiate to myofibroblasts *in vitro* when exposed to a stiff matrix (more than 20kPa) and TGFβ [100]. Likewise, it also well documented that stem cells maintained on rigid tissue culture dishes (~10^6kPa [102]) will spread and exhibit higher amounts of actin-myosin stress fibers. Synthetic 3D culture systems using a hyaluronic acid (HA) hydrogels were able to support and maintain hES cells in an undifferentiated state, in part due to the fact HA is a common ECM component [103]. The exact mechanism for stem cells to sense the matrix are not yet clear, although it is known that growth factor- and integrin-coupled cell motility, contractility, and anchorage are regulated by Rac and Rho [104,105]. Rac isoforms regulate engraftment and marrow retention in HS cells with Rac activation occurring through β1 integrin adhesion to the matrix [104]. Similar signaling is found in MSCs [105]. Inhibition of the Rho kinase effector, ROCK causes deactivation of myosin and selectively blocks rigid-directed osteogenesis [106,107]. Inhibition of ROCK in hES cells dramatically enhanced survival [108]. Neonatal cardiomyocytes show that ROCK inhibition blocks cells dysfunction that occurs with exposure

9

to rigid substrates [109], suggesting that future ES cell cardiomyocyte differentiation could benefit from both ROCK inhibition and careful attention to the microenvironment.

Cardiovascular progenitor cells (CPCs) are thought to reside in niches found in the developing right atria, ventricle and outflow tract. These CPCs have been shown to differentiate into all three cardiovascular cell lineages: vascular endothelial cells, vascular smooth muscle cells, and cardiomyocytes [110]. It has been proposed that there is a rare endogenous population of CPCs in the adult myocardium exists which are able to repair small damages [111]. CPCs express embryonic (SSEA-1) and stem cell-related (abcg2, c-Kit, isl-1, sca-1) markers [112-114]. It has been shown that stem cells are able to initially differentiate to this CPC state [28,58]. These progenitor cells are at one of the earliest stages in mesodermal differentiation towards a cardiovascular lineage. As such, it is theorized that a CPC population could be used as stem cell therapy for regenerative medicine therapies or treatments.

Various markers have identified mouse CPCs, including Isl-1, Nkx2.5, and Flk-1 (also known as KDR). Isl-1$^+$ progenitor cells were first identified via *in vivo* lineage tracing in 2005 by Laugwitz et al [115] in postnatal rat, mouse and human myocardium. The Isl-1$^+$ cells remained undifferentiated progenitor cells in very small, discrete populations within the developing myocardium and it was shown that these cells maintain the capacity to differentiate to a mature cardiac cell with the ability to cycle Ca^{2+} and generate action potentials. Flk-1$^+$ murine progenitor cells were later characterized and identified from a mES cell population and shown within an *in vitro* setting to have the capability to differentiate into cardiomyocytes, vascular endothelial cells and vascular smooth muscle cells [116]. Further evidence was presented by Moretti et al [117] to characterize a multipotent progenitor cell with the distinction Isl-1$^+$/Nkx2.5$^+$/Flk-1$^+$ with the capability to differentiate into all three major cardiac lineages.

Similar progenitors have been identified in differentiating hES cells. This KDR^{low}/c-Kit^{neg} progenitor cell when exposed to cardiogenic growth factors (BMP4, bFGF, ActivinA, VEGF, and DKK1) differentiated to cardiac myocytes. hES cell-derived cardiomyocytes were shown to express cardiac markers including troponin T, as well as generate action potentials and electrically couple to each other [118]. Isl-1$^+$ human progenitors have also been characterized and shown to contribute to the right ventricle and inflow/outflow tracts [119].

Stem cell niches have been widely studied in the last 10 years. Contributions of the niche are thought to regulate cell fate decisions through the 3D nature of the niche and ECM components found in the niche. CPCs are thought to reside in a small niche within the endogenous heart. The exact nature and mechanism of the niche's contribution to cell fate is still unknown and more work needs to be done to identify the contributing components and factors of the niche to CPC commitment to further cardiovascular differentiation.

D. Stem Cell Niche-ECM Interaction

The cardiac stem cell niche is defined as a 3D microenvironment that regulates self-renewal, proliferation, and differentiation through cell-cell and cell-matrix interactions. This makes the native ECM's role in cardiac development very important to understand. In the absence of signals coming from the ECM, cells undergo apoptosis. Various studies have shown the importance of ECM support for angiogenesis and cardiovascular physiology [120]. However, the exact nature of the ECM's role during cardiac development is still unknown.

The extracellular matrix was first defined morphologically as extracellular material visible as fibrils or sheets in the electron microscope. The definition has evolved to reflect broader view and includes essentially all secreted molecules that are immobilized outside cells

[121]. Major components of the ECM include collagens, glycoproteins, and proteoglycans; within these groups fall laminins, fibronectin, tenascin, vitronectin, amongst many other macromolecules. Binding specificity of the ECM to cells can constitute large sequences and/or be dependent upon "active" conformation states or be as short as 3 distinct amino acids, namely the well-known RGD sequence that was first identified as the "fibronectin receptor." [122]. The ECM provides the necessary structural support as well as essential support for cell migration, tissue organization, and even differentiation.

The structure of adhesion sites between cells *in vitro* and the ECM were first described by Abercrombie [123,124] forty years ago using interference-reflection microscopy and electron microscopy. These studies showed that ECM-cell adhesion occurs at specialized small regions along the ventral plasma membrane, leaving only a gap of ~10-15nm. These sites are called focal contacts or focal adhesions and have been shown to associate with actin microfilaments, playing a role in the regulation of the actin cytoskeleton. Focal adhesions are integrin-based interactions that mediate cell-substrate adhesion and can be used as bidirectional signaling tools between extracellular molecules and the cytoplasm [125-127]. Focal adhesions anchor actin filament bundles and mediate a strong adhesion to the substrate. Once a focal adhesion is stable and mature, it is the anchoring point for α5β1 integrins to translocate centripetally on lamellae towards the cell body. This maturation of the focal adhesion and translocation begins the formation of fibrillar adhesions. These structures are made up of extracellular fibrils of fibronectin, which also facilitate further fibronectin fibrillogenesis to occur in a tension-dependent manner [128, 129]

Cell adhesion to the matrix is one of the most important regulated processes during development. The family of integrins largely mediates these cell-matrix adhesions. Cells of all

type interact with the ECM namely via integrins. Integrin receptors are the primary receptors for ECM adhesion and provide a transmembrane link between the ECM and actin cytoskeleton [130]. Integrins are non-covalently linked, heterodimeric molecules containing both an α and β subunit. These subunits are both type 1 transmembrane proteins. To date, 19 α-integrin and 8 β-integrin subunits have been identified, leading to 25 αβ heterodimers, which have been seen in almost every cell type [131]. Integrins are known to control many cellular processes, including mediating the attachment of cells to the ECM. They can act both directly and indirectly on signal transduction pathways, activating signals from both inside and outside of the cell [132].

Integrin function can also be controlled from within the cell; which is called "inside-out" signaling and is characterized by events that induce a conformational change, which leads to a higher ligand binding affinity. "Inside-out" signaling has been seen with the β-integrin cytoplasmic tail associating with talin and kindling proteins [132,133]. There is evidence to support that "inside-out" signaling pathways stimulate integrin clustering, which contributes to increased integrin affinity [133], however, the extent and mechanism(s) of this are not clearly defined. In contrast, "outside-in" signaling is typically initiated by integrins associating with ECM proteins. Integrins have the capability to initiate "outside-in" signaling by recruiting various molecules, including focal adhesion kinase (FAK) and Src, signaling intermediates such as phosphatidylinositol-3 kinase, Rho and Rac GTPases, and actin-binding cytoskeleton proteins such as talin, α-actinin, paxillin, tensin, and vinculin, which in turn generate signals for migratory and proliferatory functions of the cells [134]. "Outside-in" signaling can also be seen through integrin association with growth factor receptors, including epidermal growth factor (EGF) receptor and fibroblast growth factor (FGF) receptor. Integrins are able to turn signals from the ECM by co-clustering serine threonine, and tyrosine kinases, phosphatases, and adaptor

proteins in focal adhesions outside the cell which are able to lead to internal signaling pathways promoting cell migration and actin remodeling.

Integrin subunits are known to associate specific ligands, In particular, β subunits have non-specific roles in ligand binding activity, while the α subunit provide high specificity of signal transduction [135]. α integrin subunit cytoplasmic tails contain a conserved GFFKR amino acid sequence that is crucial for a salt bridge-mediated interaction with the β chain [133,136]. The cytoplasmic domain of the β1 subunit plays an important role in cytoskeletal association [137].

Adhesion of ES cells to ECM proteins is essential for differentiation [91,132,138,139]. Undifferentiated ES cells express a subset of integrins, some of which may be up- or down-regulated during differentiation, indicating the potential importance of integrins in maintaining an undifferentiated ES cell state [140-142]. Different ES cell lines have reported high expression levels of integrin subunits α5, α6, αv, β1, and β5 [91,131].

β1-associated subunits α1, α2, α3, α6, and α7 are regulated developmentally [143,144]. Collagen IV is known to associate with α1, α2, α3, αV, β1 and β8 while laminin is known to associate with α1, α2, α3, α6, α7, α10, αV, β1, β3, β4 and β8 subunits. The following integrin subunits have been identified to interaction with fibronectin: α2, α3, α4, α5, α8, α9, αV, β1, β3, β5 and β7. Vitronectin is known to associate with α8, αV, β1, β3, and β5 subunits [134,145-148]. Further integrin specificity can be found in Table 1.

Integrin subunit	Known ECM ligands
α1β1	Collagen, laminin
α2β1	Collagen, laminin, α3β1, fibronectin
α3β1	Fibronectin, invasin, thrombospondin, laminin
α4β1	Fibronectin, VCAM1, invasin, MAdCAM-1, osteopontin
α5β1	Fibronectin, L1-CAM, denatured collagen, fibrinogen, invasion, osteopontin
α6β1	Laminin, merosin, kalinin, invasion, sperm fertilin
α7β1	Laminin
α8β1	Tenascin, fibronectin, vitronectin, osteopontin
α9β1	Tenascin, fibronectin, thrombospondin, VCAM, collagen, laminin, osteopontin
αVβ1	Fibronectin, vitronectin, LAP-TGFβ, osteopontin
αIIβ1	Collagens
α10β1	Laminin, collagen
α11β1	Collagen
αMβ2	ICAM-1, fibrinogen, *Candida albicans*, Factor X, iC3b, neutrophil inhibitory factor
αxβ2	Collagen, iC3b, fibrinogen, ICAM
αVβ3	Fibronectin, vitronectin, von Willebrand factor, thrombospondin, tenascin, DEL1, osteopontin, adenovirus penton base protein, bone sialoprotein, denatured collagen, disintegrins, fibrinogen, HIV Tat protein, laminin, MMP-2, prothrombin, fibrillin, LAP-TGFβ, PECAM-1, MFG-E8, BSP
αIIβ3	Collagens
αIIbβ3	*Borrelia burgdorferi*, denatured collagen, decorsin, disintegrins, fibronectin, fibrinogen, plasminogen, prothrombin, thrombospondin, vitronectin, von Willebrand factor
α6β4	Laminin 5
αVβ4	Collagen, laminin, fibronectin
αVβ5	Vitronectin, fibronectin, osteopontin, DEL1, adenovirus penton base protein, bone sialoprotein, HIV Tat protein, MFG-E8, BSP
αVβ6	Tenascin, fibronectin, LAP-TGFβ, osteopontin
αEβ7	E-cadherin
α4β7	Fibronectin, MAdCAM-1, VCAM-1, osteopontin
αVβ8	Fibronectin, LAP-TGFβ

Table 1-1. Integrin-ECM interactions Compiled from data from the following references: [122,134,146]

The concept of the ECM regulating stem cells was established in mammalian stem cells where in the skin β1 integrins are known to be differentially expressed on primitive cells and participate in constrained localization of a stem-cell population through interaction with ECM

glycoprotein ligands [82,83]. In particular, Li et al [142] demonstrated the ability of laminin to overcome a β1 integrin deficiency in mouse embryonic stem cells. They found that basement membrane assembly and differentiation in the developing embryo requires laminin polymerization. EBs lacking β1 integrin are unable to form a basement membrane and the complete knockout of β1 integrin is an embryonic lethal mutation [149]. Exogenous laminin treatment was able to 'recover' the EBs lacking β1 and they were able to form normal basement membrane. Similarly, Hayashi et al, found that mES cells cultured on fibronectin and laminin activated integrin and ERK1/2 signaling, while cells cultured on type I and type IV collagen or poly-D-lysine remained undifferentiated [143]. Braam et al demonstrated that αVβ5 integrin mediated adhesion to vitronectin, α5β1 mediated adhesion to fibronectin, and α6β1 mediated adhesion to laminin and entactin [147]. Additionally, they found that recombinant vitronectin supported human ES cells in an undifferentiated state as the only reliable alternative to Matrigel. Further evidence of the importance of integrin-ECM interactions during development is the fact that an α5 integrin germ line deletion in mice leads to embryonic lethality at E9.5/E10 [150,151]. α4-null mouse embryos die at E9.5-E11.5 due to failure of allantois-chorion fusion or at E11.5-E14 due to massive heart hemorrhage. The α4β1 integrin binds with fibronectin and VCAM-1 and it is the lack of these interactions that cause the embryonic lethality [152,153].

Integrin-ECM interactions have also been implicated in angiogenesis [154]. Vitronectin, fibronectin, fibrinogen, and oestopontin are known to interact with the αV integrin subunit, which is widely expressed on blood vessels. Various studies have established the clear role of αVβ3 and αVβ5 integrins for angiogenesis during tumor growth and development [155-158]. Using organ culture systems with branching organs such as lungs, kidneys or salivary glands have shown that branching morphogenesis involves specific, repetitive steps starting with the

formation of a cleft in the basement membrane. Sakai et al [159] demonstrated that fibronectin and its major receptor, the α5β1 integrin, are required for this step of branching morphogenesis. This study highlights the importance of the ECM-cell interaction during development and helps to further understanding of the ECM's role during development.

ECM studies have been based primarily on conventional 2D *in vitro* models. However, the importance of the 3D aspect of the matrix is clear when examining epithelial cells, where polarity is crucial for structure and function [160]. As cell biology understanding evolves, whether the discrete cell adhesion structures identified in a 2D setting actually exist in cells cultured in a 3D model system has been questioned. Our basic understanding of cell-matrix adhesions is predicated on biology techniques and assays developed within the last 30 years for conventional *in vitro* 2D culture. As cells in native ECM tissue exist in a 3D nature, recent studies have begun to explore the validity of established literature as well as further understand the properties of the 3D ECM and how it affects cellular function.

Early studies reported that fibroblasts embedded within a cell-derived 3D matrix or collagen gel *in vitro* had integrins and vinculin make up some of the cell-matrix adhesion [126,161]. These studies have highlighted the importance of 3D culture techniques to accurately understand cell-matrix adhesions. Specifically, Cukierman et al [125], demonstrated that focal adhesions on 2D substrates form firm adhesions to relative stiff substrates. Fibroblasts generate their own matrix and develop 3D matrix adhesions over the course of several days. However, when cells were added to a cell-free 3D matrix, they began generating matrix adhesions within minutes. They were also able to establish that along with three-dimensionality, integrin α5β1 and fibronectin were required. Tamariz et al [161] showed that fibroblasts within a 3D collagen matrix are not only capable of local remodeling but undergo morphological changes and create

mature focal adhesions. They identified the importance of Rho kinase as it is essential for maturation of fibroblast morphology and formation of focal adhesions. Zhou et al establishes the essential nature of 3D conformation for neovessel formation [128]. Angiogenesis and vasculogenesis are processes that disrupt a 2D configuration of endothelium to create vessels and this group demonstrates that fibronectin fibrillogenesis is what regulates that transition to a 3D conformation. It has been well established that focal adhesions require tension with the ECM.

Hakkinen, et al compared the effects of 2D vs 3D microenvironments with human foreskin fibroblasts [162] using four commonly used substrates: cell-derived matrix, basement membrane extract, collagen, and fibrin. They were able to characterize the cellular results and found that each microenvironment has its own unique influence on various aspects of cellular behavior. This type of study highlights the advantages of optimizing a 3D substrate for specific tissues and functions. Furthermore, the use of 3D matrices in cell culture demonstrates the variation in cell morphology observed in 2D vs. 3D. Mammary epithelial cells grown in 3D aggregate, form cell-cell contacts, polarize and establish spherical acini [163], while those cultured on 2D simply form a cellular monolayer [164,165]. Further investigation is needed to establish the understanding of 3D matrix-cell adhesions. Geraldo et al [166] have shown that initial studies to characterize distinct adhesion structures observed in synthetic 3D matrices. They found that the 3D nature of collagen I matrices influence adhesome proteins, which then regulate cell migration, as well as further characterizing the differences in cellular morphology cultured in 2D vs. 3D. The growing amount of evidence highlighting the differences in cellular morphology and behavior between 2D and 3D confirms the necessity of continuing along this avenue of research.

Although, the complex nature of cell-matrix interactions has been studied, there still remains much that is unknown. Cell-ECM interactions are largely mediated via integrins, which can then generate signaling cascades and alter cellular morphology, function and behavior. It has also been shown that cell-ECM interactions can influence development and differentiation. Recent research has focused on investigating the role of a more physiologically relevant 3D substrate on cell-ECM interactions.

E. Cardiovascular Tissue Engineering

Cardiovascular researchers have begun to look at tissue engineering as a future strategy for regenerative therapies. Currently, it is common practice to use biomaterials for grafts and stent-grafts as well as artificial heart valves [1,2]. Tissue engineered structures could also be used to create a bioengineered myocardial patch to provide reinforcement to weakened tissue and promote endogenous healing properties, as well as total replacement of diseased tissues. The ultimate goal of tissue engineering and regenerative medicine is to mimic the native ECM for both therapeutic treatment of defects and failing tissues as well as the possibility of replacement of those tissues. In particular, nanotechnology has become a useful tool for tissue engineers [167-170]. Development of 3D scaffolds that mimic the natural fibrous ECM can allow for diffusion of nutrients, metabolites and soluble factors necessary to the seeded cells until they are able to produce their own functional ECM [171,172]. There are a number of various issues to consider in scaffold design, including: pore size and morphology, porosity, mechanical properties, surface characteristics, biocompatibility and biodegradability. There are various methods to create a scaffold including: electrospinning (random, aligned, and co-axial nanofibrous meshes), self-assembly (hydrogels), and phase separation (macroporous polymer substrates) [173].

Cardiovascular specific tissue engineering studies have employed all types of scaffolds. The choice of polymer to use for scaffold fabrication can be broken into two main categories: natural or synthetic [174]. Within these categories, there are many options for both degradable and permanent polymers. Natural polymers that have been used in cardiovascular studies include: alginate, collagen, gelatin, elastin, and hyaluronic acid [173,175-181]. Polyurethane (PU), poly(ε-caprolactone) (PCL), poly(lactic acid), and poly(glycolic acid) (PGA) are amongst the most commonly used synthetic polymers for cardiovascular tissue engineering [182-191].

Numerous scaffolds types have been studied for their cardiac tissue engineering potential. Weinberg and Bell first reported collagen gels used as scaffolds for engineering arterial vasculature with smooth muscle cells in 1986 [192]. The collagen gel made up the exterior of the construct, with a suspension of endothelial cells in the lumen. The structure was not mechanical stable and ruptured at low pressures. Later studies by L'Heureux et al [193] fabricated a structure made entirely of human origin collagen, which were seeded with smooth muscle cells and able to reach higher burst pressures. More recent studies have included other natural polymers, including elastin. Collagen I has been electrospun with elastin and PLGA to create an artificial artery with similar compliance to a native bovine iliac artery [194]. Scaffolds made of collagen I have been used with neonatal rat cardiomyocytes to create myocardial tissue with sustained contractions [195]. Patches made from collagen I and seeded with MSCs were implanted in a rat model following a myocardial infarction [196]. The animals showed reduction in the left ventricular diameter at systole, as well as increased anterior wall thickness and a 30% increase in ejection shortening. Initial results showed that the MSCs seeded did engraft in the surrounding the tissue, although MSCs or MSC-derived cells were not detected at four weeks. Fibrin has been used to create a small diameter vascular graft [197]. The *in vivo* studies in which the constructs were

implanted in the left external jugular vein of 10-12 week old lambs maintained 71% blood flow at 15 weeks post implantation and showed significant remodeling with native collagen and elastin production as well as maintained mechanical integrity for the duration of the study. PLA was combined with fibrin to create small diameter vascular grafts (5mm) for a large animal model study [198]. The grafts were implanted in adult sheep. After six months, the grafts showed no thrombus formation on the luminal surface of the graft. Furthermore, there were no calcifications or aneurysm formation as well as strong evidence of native cell engraftment and remodeling. PGA-based copolymer scaffolds have been used with bone marrow-derived vascular cells to develop tissue-engineered veins [199]. PLGA-collagen scaffolds have been seeded with and ECs to create a patch for the pulmonary trunk in a canine model [200]. After six months, the patches exhibited evidence of elastin and collagen remodeling similar to what would be seen in native tissues and the histological sections showed a morphology resembling native arteries. Chitosan scaffolds have been created that support contractile heart muscle [201]. Decellularized ECM has also been used in various forms for cardiovascular tissue engineering. An ECM emulsion derived from porcine small intestine submucosa was used as method to initiate native remodeling and induce paracrine effects at the injection site following an infarct in a rat model [202]. The study showed a significant increase in c-kit$^+$ cells at the injection site. Echocardiography studies showed improved fractional shortening, ejection fraction and stroke volume after 42 days.

Cardiovascular tissue engineering has also recently explored electrospinning as a method of scaffold creation that has proven to have a high success rate. Electrospinning technology can be utilized to create customized electrospun nonwoven mats consisting of essentially any polymer and create microenvironments upon which different cell types have been known to

proliferate and thrive. The technology was first patented in 1934 [203] and has gained popularity in lab settings for the ease with which it can be employed to create nanofibrous scaffolds [204,205]. Scaffolds can be made to specification for explicit needs, including varying mechanical and physical properties to correctly mimic the target tissues. The high surface area to volume ratio produced in these scaffolds promotes cell adhesion, migration, and allows for the appropriate diffusion of biochemical signals necessary for growth and exchange of nutrients and metabolic waste [171,206,207]. Electrospinning has been used to successfully produce scaffolds with many different polymers, both natural and synthetic [172,204-208].

Many investigators have electrospun collagen with a synthetic polymer to eliminate needing to crosslink the material with a fixing agent such as glutaraldehyde to preserve the material for implantation. Stitzel et al [209] created layered electrospun scaffolds of PLA and collagen, which promoted the alignment of smooth muscle cells along the direction of the length of the fiber. Another example of a layered electrospun scaffold is from Kidoaki et al [210] who used segmented PUs with collagen I and gelatin and was used as a prototype for a small diameter vascular graft. Poly(L-lactide-co-e-caprolactone) (PLLA-CL) copolymer was electrospun with to produce a scaffold with mechanical properties similar to that of a human coronary artery [211]. Human smooth muscle and endothelial cells were cultured on the PLLA-CL scaffolds and demonstrated good cellular adhesion and strong migration to the interior of the scaffold, suggesting this material could be a promising copolymer to be used for myocardial tissue engineering. Collagen and PGA have been electrospun to create varying types of composite scaffolds, which were then seeded with c-kit^{+} progenitor cells [212]. The scaffolds with nanofibers and collagen demonstrated good cellular attachment and proliferation and represent a good 3D model for cardiac engineering. Another group combined PCL with various

combinations of collagen, elastin, and gelatin, which were then electrospun [5]. The scaffolds were then seeded with adipose-derived stem cells. After two weeks, the cells were shown to have adhered to the fibrous scaffolds and proliferate along the length of the fibers, which could potentially be used for the creation of vascular grafts or myocardial tissue. Electrospun polydioxanone (PDO) scaffolds were seeded with MSCs derived from umbilical cord blood to create a replacement right ventricular outflow tract (RVOT), which was then implanted in a lamb model [213]. After eight months, the scaffolds showed no stenosis or aneurysm formation, as well as less fibrosis and calcification than the control animals. MSC-derived cells with native cells were shown within the scaffold region to have undergone ECM formation and remodeling. These electrospun PDO scaffolds represent an attractive option for complete replacement of the RVOT in congenital diseases. Hong et al [214] decellularized heart valve matrix from a porcine aortic valve leaflet and then coated with electrospun poly-4-hydroxybutyrate. The resulting scaffold was then seeded with MSCs. After 14 days in culture, the cell seeded scaffolds exhibited the mechanical properties similar to that of a native porcine heart valve and represents an option for a hybrid scaffold made of natural and synthetic material.

Biopolymer hydrogels have been created with proven abilities to promote cell survival, minimize scar tissue formation, and enhance transplanted cell engraftment [215]. Because of the macroporous nature of hydrogels, they closely mimic the native ECM. Additionally, the structure of hydrogels can be altered to more closely mimic the target tissue and has been shown to enhance cell signaling *in vitro* [216]. Another advantageous property of hydrogels for tissue engineering is their ability to incorporate larger biopolymers such as hyaluronan, which are extremely difficult to handle in other types of scaffold formation [217]. The ability for cells to be completely encapsulated with the hydrogel network allows for these culture models create 'true

3D' microenvironments as opposed to fibrous or porous scaffolds which require cellular infiltration to become a 'true 3D' model system.

Recent work has focused on the use of hydrogels to create a favorable environment to drive cardiac differentiation as well as support implantation of cell therapies to a cardiac injury. Chiu et al developed collagen I hydrogels to evaluate the spatial and temporal effects of TGFβ, BMP4 and VEGF on chicken derived embryonic heart valve progenitor cells [218]. They found that a small concentration of TGFβ (10ng/mL) was useful to promote tissue remodeling and initiate myofibroblast differentiation, but VEFG and BMP4 did not. Methylacrylate-gelatin hydrogels were created and used to encapsulate porcine valvular interstitial cells (VICs) [219]. After two weeks, the hydrogels supported and promoted active myofibroblast differentiation. The cells were observed to exhibit morphology similar to that of native VICs, as well as promote collagen I deposition and produce smooth muscle α-actin. Prokoph et al [220] created heparin-polyethylene glycol (PEG) hydrogels that were functionalized with stromal cell-derived factor-1α (SDF-1α). Human endothelial progenitor cells were used and showed increased migration towards the releasing growth factor. The hydrogels were implanted in mice subcutaneously, which showed native cell infiltration and increased vascularization after seven days. Deng et al [221] encapsulated human circulating progenitor cells in hydrogels made from collagen and chitosan. After seven days, cells had differentiated and showed increased populations of CD31^{+} and CD133^{+} cells, as well as increasing VE-cadherin. An *in vivo* subcutaneous implantation showed vascular growth in mice after seven days. The hydrogels made of collagen-chitosan demonstrated the ability to recruit vWF[+] and CXCR4^{+} endothelial cells compared to hydrogels made of collagen only. VEGF nanoparticles were created and added to fibrin hydrogels [222]. Using an assay for angiogenic potential with the chorioallantoic membrane of a chicken embryo,

the host vasculature invaded the gel and created a capillary network within the implanted hydrogel. Increasingly clustered growth factor nanoparticles promoted more endothelial tube branch compared to a homogenous distribution. Recently, cardiosphere-derived cells (which are currently being used in clinical trials as a cell therapy [223]) were encapsulated in a hyaluronan-based hydrogel and injected into the infarct border zone of a SCID mouse [224]. Three weeks post injection, cells showed good engraftment into the myocardium and there was a noticeable improvement in left ventricular ejection fraction. Wang et al [225] created oligo[poly(ethylene glycol) fumarate] (OPF) hydrogels and encapsulated mES cells. After fourteen days *in vitro* cells demonstrated the ability to differentiate into cardiomyocytes. Hydrogels with partially differentiated mES cells were injected into the left ventricular wall of a rat myocardial infarction model. Histological analysis showed good engraftment and retention of injected cells in the area of the injection site. After four weeks, the graft size had increased compared to controls. Additionally, the infarct size and collagen deposition had decreased and there was a significant increase in left ventricular fractional shortening.

More specifically to the CPC niche environment, CPC commitment and further differentiation can be directed by the microenvironment and that an *in vitro* 3D culture model can be used to promote cardiac differentiation in a mouse ES model. Collagen IV was identified as an ECM component with the ability to induce trophoectoderm differentiation in mES cells [226]. Collagen IV, which can be detected in the mouse embryo as early as the 32-64-cell stage [227] induced expression of haematopoietic, endothelial, and smooth muscle genes specific to the mesoderm, as well as a panel of trophoectoderm-markers. Collagen I, laminin, and fibronectin did not show the same ability to drive differentiation to trophoblasts. Collagen IV and laminin are present within the endogenous mouse and human CPC niche, while collagen I and

fibronectin are found outside the niche. Adding ECM proteins to mES cells can induce a CPC population [6]. The addition of collagen IV with a synthetic 3D electrospun matrix made of PCL-gelatin nanofibers induced the highest CPC population of the study [5]. Further studies demonstrated that laminin- or vitronectin-coated 3D scaffolds induced an even higher population of Flk-1^{+} CPCs as compared to 2D culture conditions [228].

Cardiovascular tissue engineering has progressed rapidly and tissue engineered scaffolds have demonstrated effectiveness at improving cardiac function for various cardiovascular tissues, including heart valves. Scaffolds have also been investigated for their effectiveness and efficiency in directing stem cell fate towards cardiovascular lineages. In particular, tissue engineered substrates have demonstrated an increased effectiveness to induce a CPC population.

F. Conclusion

Stem cell biology and regenerative medicine has made considerably strides in the last two decades and continues to be a promising area of research. Cardiovascular research in particular has benefited from the evolving field of stem cell biology. Various stem cell sources have been implicated as several potential candidates for stem cell therapies. CPCs have been identified and characterized in both animal and human models. These progenitor cells reside in discrete niches but the exact structure of the niche is still poorly understood. However, it is known that the 3D nature of the niche as well as the ECM components contribute greatly to cell fate decision and regulation of maintaining a stem cell- or progenitor cell-like state. Tissue engineering principles have been used to recapitulate native ECM in efforts to drive differentiation. In particular, our recent studies [6, 228] show that the unique niche microenvironment greatly induces a CPC population.

My studies have focused on understanding the nature of the microenvironment's contribution to cardiovascular differentiation. I first developed co-axial electrospun scaffolds to use as a 3D culture system from both natural and synthetic polymers. I then examined the contribution of the microenvironment to terminal differentiation in a mouse model comparing 2D and 3D culture systems with various ECM proteins. I finally translated this work into a human system to determine the role of the microenvironment in differentiating human iPS cells to cardiomyocytes. Taken together, my work has shown the importance of the unique microenvironment in cardiovascular differentiation of stem cells using biomaterials and tissue engineering principles.

G. References

1. Malik S, Wong ND, Franklin SS, Kamath TV, L'Italien GJ, Pio JR, Williams GR. Impact of the metabolic syndrome on mortality from coronary heart disease, cardiovascular disease, and all causes in United States adults. Circulation. 2004;110:1245-1250.

2. Hunt SA, Baker DW, Chin MH, et al. ACC/AHA Guidelines for the evaluation and management of chronic heart failure in the adult: Executive Summary; A report of the American College of Cardiology/American Heart Association Task Force on practice guidelines (committee to revise the 1995 guidelines for the evaluation and management of heart failure): Developed in collaboration with the International Society for Heart and Lung Transplantation, Endorsed by the Heart Failure Society of America. Circulation. 2001;104:2996-3007.

3. Ornish D, Brown SE, Scherwitz LW, et al. Can lifestyle changes reverse coronary heart disease? Lancet 1990;336:129-133.

4. Fonarow GC, Gawlinski A, Moughrabi S, Tillisch JH. Improved treatment of coronary heart disease by implementation of a cardiac hospitalization atherosclerosis management program (CHAMP). Am J Cardiol 2001;87:819-822.

5. Heydarkhan-Hagvall S, Schenke-Layland K, Dhanasopon AP, Rofail R, Smith H, Wu BM, Shemin R, Beygui RE, MacLellan WR. Three-dimensional electrospun ECM-based hybrid scaffolds for cardiovascular tissue engineering. Biomaterials. 2008;29(19):2907-2914

6. Schenke-Layland K, Nsair A, Van Handel B, Angelis E, Gluck JM, Votteler M, Goldhaber JI, Mikkola HK, Kahn M, MacLellan WR. Recapitulation of the embryonic cardiovascular progenitor cell niche. Biomaterials, 2011; 32: 2748-2756

7. Laflamme MA, Murry CE. Regenerating the heart. Nat Biotechnol, 2005; 23: 845-856.

8. Sutton MG, Sharpe NE. Left ventricular remodeling after myocardial infarction: pathophysiology and therapy. Circulation, 2000; 101: 2981-2988.

9. Atala A, Lanza RP (2000) Methods of Tissue Engineering. New York, Academic Press.

10. Marelli D, Desrosiers C, el-Alfy M, Kao RL, Chiu RC. Cell transplantation for myocardial repair: an experimental approach. Cell Transplant, 1992; 1: 383-390.

11. Chiu RC, Zibatis A, Kao RL. Cellular cardiomyoplasty: myocardial regeneration with satellite cell implantation. Ann Thorac Surg, 1995: 60: 12-18.

12. Reinecke H, MacDonald GH, Hauschka SD, Murry CE. Electromechanical coupling between skeletal and cardiac muscle: Implications for cardiac repair. J Cell Biol, 2000; 149: 731-740.

13. Ferrari G, Cusella G, Angelis D, Coletta M, Paolucci E, Stornaiuolo A, Cossu G, Mavilio F. Muscle regeneration by bone marrow-derived myogenic progenitors. Science, 1998; 279: 1528-1530.

14. Bittner RE, Schofer C, Weipoltshammer K, Ivanova S, Streubel B, Hauser E, Freilinger M, Hoger H, Elbe-Burger A, Wachtler F. Recruitment of bone-marrow-derived cells by skeletal and cardiac muscle in adult dystrophic mdx mice. Anat Embryol, 1999; 199: 391-396.

15. Jackson KA, Majka SM, Wang H, Pocius J, Hartley CJ, Majesky MW, Entman ML, Michael LH, Hirschi KK, Goodell MA. Regeneration of ischemic cardiac muscle and vascular endothelium by adult stem cells. J Clin Invest, 2001; 107: 1395-1402.

16. Alvarez-Dolado M, Pardal R, Garcia-Verdugo JM, Fike JR, Lee HO, Pfeffer K, Lois C, Morrison SJ, Alvarez-Buylla A. Fusion of bone-marrow-derived cells with Purkinje neurons, cardiomyocytes and hepatocytes. Nature, 2003; 425: 968-973.

17. Orlic D, Kajstura J, Chimenti S, Jakoniuk I, Anderson SM, Li B, Pickel J, McKay R, Nadal-Ginard B, Bodine DM, Leri A, Anversa P. Bone marrow cells regenerate infarcted myocardium. Nature, 2001; 410: 701-705.

18. Caplan AI, Bruder SP. Mesenchymal stem cells: building blocks for molecular medicine in the 21st century. Trends Mol Med, 2001; 7: 259-264.

19. Pittenger MF, Mackay AM, Beck SC, Jaiswal RK, Douglas R, Mosca JD, Moorman MA, Simonetti DW, Craig S, Marshak DR. Multilineage potential of adult human mesenchymal stem cells. Science, 1999; 284: 143-147.

20. Le Blanc K, Ringden O. Immunobiology of human mesenchymal stem cells and future use in hematopoietic stem cell transplantation. Biol Blood Marrow Transplant, 2005; 11: 321-334.

21. Shake JG, Gruber PJ, Baumgartner WA, Senechal G, Meyers J, Redmond M, Pittenger MF, Martin BJ. Mesenchymal stem cell implantation in swine myocardial infarct model: engraftment and functional effects. Ann Thorac Surg, 2002; 73: 1919-1925.

22. Bittira B, Shum-Tim D, Al-Khaldi A, Chiu RC. Mobilization and homing of bone marrow stromal cells in myocardial infarction. Eur J Cardiothorac Surg, 2003; 24: 393-398.

23. Thomson JA, Itskovitz-Eldor J, Shapiro SS, Waknitz MA, Swiergiel JJ, Marshall VS, Jones JM. Embryonic stem cell lines derived from human blastocysts. Science, 1998; 282: 1145-1147.

24. Boheler KR, Czyz J, Tweedie D, Yang H, Anisimov SV, Wobus AM. Differentiation of pluripotent embryonic stem cells into cardiomyocytes. Circulation Research, 2002; 91: 189-201.

25. Wobus AM. Potential of embryonic stem cells. Mol Aspects of Med, 2001; 22: 149-164.

26. Amit M, Carpenter MK, Inokuma MS, Chiu CP, Harris CP, Waknitz MA, Itskovitz-Eldor J, Thomson JA. Clonally derived human embryonic stem cell lines maintain pluripotency and proliferative potential for prolonged periods of culture. Dev Biol, 2000; 227: 271-278.

27. Blau HM, Brazelton TF, Weimann JM. The evolving concept of a stem cell: entity or function? Cell, 2001; 105: 829-841.

28. Heydarkhan-Hagvall S, Schenke-Layland K, Yang JQ, Heydarkhan S, Xu Y, Zuk Pa, MacLellan WR, Beygui RE. Human adipose stem cells: a potential source for cardiovascular tissue engineering. Cells Tissues Organs, 2008;187:263-274.

29. Gerecht-Nir S, Itskovitz-Eldor J. The promise of human embryonic stem cells. Best Pract Res Clin Obstet Gynaecol 2004;18:843-852.

30. Yamashita J, Itoh H, Hirashima M. Ogawa M, Nishikawa S, Yurugi T, Naito M, Nakao K, Nishikawa S. Flk-1-positive cells derived from embryonic stem cells serve as vascular progenitors. Nature 2000;408:92-96.

31. Rust EM, Westfall MV, Samuelson LC, Metzger JM. Gene transfer into mouse embryonic stem cell-derived cardiac myocytes mediated by recombinant adenovirus. In Vitro Cell Dev Biol Anim, 1997; 33: 270-276.

32. Westfall MV, Pasyk KA, Yule DI, Samuelson LC, Metzger JM. Ultrastructure and cell-cell coupling of cardiac myocytes differentiating in embryonic stem cell cultures. Cell Motil Cytoskeleton, 1997; 36: 43-54.

33. Xu C, Police S, Rao N, Carpenter MK. Characterization and enrichment of cardiomyocytes derived from human embryonic stem cells. Circ Res, 2002; 91: 501-508.

34. Fassler R, Rohwedel J, Maltsev V, Bloch W, Lentini S, Guan K, Gullberg D, Hescheler J, Addicks K, Wobus AM. Differentiation and integrity of cardiac muscle cells are impaired with the absence of β1 integrin. J Cell Sci, 1996; 109: 2989-2999.

35. Doetschman TC, Eistetter H, Katz M, Schmidt W, Kemler R. The *in vitro* development of blastocyst-derived embryonic stem cell lines: formation of visceral yolk sac, blood islands and myocardium. J Embryol Exp Morphol, 1985; 87: 27-45.

36. Fijnvandraat AC, et al. Cardiomyocytes derived from embryonic stem cells resemble cardiomyocytes of the embryonic heart tube. Cardiovasc Res, 2003; 58: 399-409.

37. Robbins J, Gulick J, Sanchez A, Howles P, Doetschman T. Mouse embryonic stem cells express the cardiac myosin heave chain genes during development *in vitro*. J Biol Chem, 1990; 265: 11905-11909.

38. Maltsev VA, Wobus AM, Rohwedel J, Bader M, Hescheler J. Cardiomyocytes differentiated *in vitro* from embryonic stem cells developmentally express cardiac-specific genes and ionic currents. Circ Res, 1994; 75: 233-244.

39. Boheler KR, Wobus AM. Myocardial aging and stem cell biology. In: Mattson MP, van Zant G, eds. Stem Cells: A Cellular Fountain of Youth? New York, NY: Elsevier Science; 2002: 141-177.

40. Schultheiss TM, Xydas S, Lassar AB. Induction of avian cardiac myogenesis by anterior endoderm. Development, 1995; 121: 4203-4214.

41. Rudy-Reil D, Lough J. Avian precardiac endoderm/mesoderm induces cardiac myocyte differentiation in murine embryonic stem cells. Circ Res, 2004; 94: e107-116.

42. Behfar A, Zingman LV, Hodgson DM, Rauzier AM, Kane GC, Terzic A, Puceat M. Stem cell differentiation requires paracrine pathway in the heart. Faseb J, 2002; 16: 1558-1566.

43. Kawai T, Takahashi T, Esaki M, Ushikoshi H, Nagano S, Fujiwara H, Kosai K. Efficient cardiomyogenic differentiation of embryonic stem cell by fibroblast growth factor 2 and bone morphogenic protein2. Circ J, 2004; 68: 691-702.

44. Yuasa S, Itabashi Y, Koshimizu U, Tanaka T, Sugimura K, Kinoshita M, Hattori F, Fukami S, Shimazaki T, Okano H, Ogawa Fukuda K. Transient inhibition of BMP signaling by Noggin induces cardiomyocyte differentiation of mouse embryonic stem cells. Nat Biotechnol, 2005; 23: 607-611.

45. Dell'Era P, Ronca R, Coco L, Nicoli S, Metra M, Presta M. Fibroblast growth factor receptor-1 is essential for *in vitro* cardiomyocyte development. Circ Res, 2003; 93: 414-420.

46. Kanno S, Kim PKM, Sallam Lei J, Billiar TR, Shears LL. Nitric oxide facilities cardiomyogenesis in mouse embryonic stem cells. Proc Natl Acad Sci USA, 2004; 12277-12281.

47. Terami H, Hidaka K, Katsumata T, Iio A, Morisaki T. Wnt11 facilitates embryonic stem cell differentiation to Nkx2.5-positive cardiomyocytes. Biochem Biophys Res Commun, 2004, 325: 968-975.

48. Wobus AM, Kaomei G, Shan J, Wellner MC, Rohwedel J, Guanju J, Fleischmann B, Katus HA, Hescheler J, Franz WM. Retinoic acid accelerates embryonic stem cell-derived cardiac differentiation and enhances development of ventricular cardiomyocytes. J Mol Cell Cardiol, 1997; 29: 1525-1539.

49. Takahashi T, Lord B, Schulze PC, Fryer RM, Sarang SS, Gullans SR, Lee RT. Ascorbic acid enhances differentiation of embryonic stem cells into cardiac myocytes. Circulation, 2003; 107: 1912-1916.

50. Laflamme MA, Chen KY, Naumova AV, Muskheli V, Fugate JA, Dupras SK, Reinecke H, Xu C, Hassanipour M, Police S, O'Sullivan C, Collins L, Chen Y, Minami E, Gill EA, Uleno S, Yuan C, Gold J, Murry CE. Cardiomyocytes derived from human embryonic stem cells in pro-survival factors enhance function of infarcted rat hearts. Nat Biotechnol, 2007; 25: 1015-1024.

51. Otani H, Yoshioka K, Nishikawa H, Inagaki C, Nakamura T. Involvement of protein kinase C and RhoA in protease-activated receptor1-mediated F-actin reorganization and cell growth in rat cardiomyocytes. J Pharmacol Sci, 2011; 115: 135-143.

52. Kehet I, Kenyagin-Karsenti D, Snir M, Segev H, Amit M, Gepstein A, Livine E, Binah O, Itskovitz-Eldor J, Gepstein L. Human embryonic stem cells can differentiate into myocytes with structural and functional properties of cardiomyocytes. J Clin Invest, 2001; 108: 407-414.

53. He JQ, Ma Y, Lee Y, Thomson JA, Kamp TJ. Human embryonic stem cells develop into multiple types of cardiac myocytes: action potential characterization. Circ Res, 2003; 93: 32-39.

54. Wilmut I, Schnieke AE, McWhir J, Kind AJ, Campbell KHS. Viable offspring derived from fetal and adult mammalian cells. Cloning and Stem Cells, 2007; 9: 3-7.

55. Hochedlinger K, Jaenisch R. Nuclear reprogramming and pluripotency. Nature, 2006; 441: 1061-1067.

56. Takahashi K, Yamanaka S. Induction of pluripotent stem cells from mouse embryonic and adult fibroblast cultures by defined factors. Cell, 2006; 126: 663-676.

57. Yu J, Vodyanik MA, Smuga-Otto K, Antosiewicz-Bourget J, Frane JL, Tian S, Nie J, Jonsdottir GA, Ruotti V, Stewart R, Slukvin II, Thomson JA. Induced pluripotent stem cell lines derived from human somatic cells. Science, 2007; 318: 1917-1920.

58. Schenke-Layland K, Rhodes KE, Angelis E, Butylkova Y, Heydarkhan-Hagvall S, Gekas C, Zhang R, Goldhaber JI, Mikkola HK, Plath K, MacLellan WR. Reprogrammed mouse fibroblast differentiate into cells of the cardiovascular and hematopoietic lineages. Stem Cells, 2008; 26: 1537-1546.

59. Zhang J, Wilson GF, Soerens AG, Koonce CH, Yu J, Palecek SP, Thomson JA, Kamp TJ. Functional cardiomyocytes derived from human induced pluripotent stem cells. Circ Res, 2009; 104: e30-41.

60. Moretti A, Bellin M, Jung CB, Thies TM, Takashima Y, Bernhausen A, Schiemann M, Fischer S, Moosmang S, Smith AG, Lam JT, Laugwitz KL. Mouse and human induced pluripotent stem cells as a source for multipotent Isl1+ cardiovascular progenitors. Faseb J, 2010; 24: 700-711.

61. Xu H, Yi BA, Wu H, Bock C, Gu H, Lui KO, Park JHC, Shao Y, Riley AK, Domian IJ, Hu E, Willette R, Lepore J, Meissner A, Wang Z, Chien KR. Highly efficient derivation of

ventricular cardiomyocytes from induced pluripotent stem cells with a distinct epigenetic signature. Cell Res, 2012; 22: 142-154.

62. Schofield R. The relationship between the spleen colony-forming cell and the haemopoietic stem cell. Blood Cell, 1978, 4: 7-25.

63. Xie T, Spralding AC. A niche maintaining germ line stem cells in the Drosophila ovary. Science, 2000; 290: 328-330.

64. Kiger AA, White-Cooper H, Fuller MT. Somatic support restrict germline stem cell self-renewal and promote differentiation. Nature, 2000; 407: 750-754.

65. Crittenden SL, Bernstein DS, Bachorik JL, Thompson BE, Gallegos M, Petcherski AG, Moulder G, Barstead R, Wickens M, Kimble J. A conserved RNA-binding protein controls germline stem cells in Caenorhabditis elegans. Nature, 2002; 417: 660-663.

66. Li L, Xie T. Stem cell niche: structure and function. Annu Rev Cell Div Biol, 2005; 21: 605-631.

67. Ohlstein B, Kai T, Decotto E, Spralding A. The stem cell niche: theme and variations. Curr Opin Cell Biol, 2004; 16: 693-699.

68. Orkin SH. Diversification of haematopoietic stem cells to specific lineages. Nat Rev Genet, 2001; 1: 57-64.

69. Weissman IL, Anderson DJ, Gage F. Stem and progenitor cells: origins, phenotypes, lineage commitments, and transdifferentiations. Annu Rev Cell Dev Biol, 2001; 17: 387-403.

70. Walker MR, Patel KK, Stappenbeck TS. The stem cell niche. J Pathol, 2009; 217: 169-180.

71. Ratajczak MZ, Kucia M, Jadczyk T, Greco NJ, Wojakowski W, Tendera M, Ratajczak. Pivotal role of paracrine effects in stem cell therapies in regenerative medicine: can we translate stem cell-secreted paracrine factors and microvesicles into better therapeutic strategies? Leukemia, 2012; 26: 1166-1173.

72. Watt FM, Hogan BLM. Out of eden: stem cells and their niches. Science, 2000; 287: 1427-1430.

73. Peifer M. Signal transduction: neither straight nor narrow. Nature, 1999; 400: 213-215.

74. Lo L, Sommer L, Anderson DJ. 74-MASH1 maintains competence for BMP2 induced neuronal differentiation in post migratory neural crest cells Curr Biol, 1997; 7: 440-450.

75. Jan YN, Jan LY. Asymmetric cell division. Nature, 1998; 392: 775-778.

76. Xie T, Spralding AC. *decapentaplegic* is essential for the maintenance and division of germline stem cells in the drosophila ovary. Cell, 1998; 94: 251-260.

77. Janowska-Wieczorek A, Majka M, Ratajczak J, Ratajczak MZ. Autocrine/paracrine mechanisms in human hematopoiesis. Stem Cells, 2001; 19: 99-107.

78. Zhang J, Niu C, Ye L, Huang H, He X, Tong WG, Ross J, Haug J, Johnson T, Feng JQ, Harris S, Widemann LM, Mishina Y, Li L. Identification of the haematopoietic stem cell niche and control of the niche size. Nature, 2003; 425: 836-841.

79. Song X, Zhu CH, Doan C, Xie T. Germline stem cells anchored by adherens junctions in the Drosophila ovary niche. Science, 2002; 296: 1855-1857.

80. Brizzi MF, Tarone G, Defilippi P. Extracellular matrix, integrins, and growth factors as tailors of the stem cell niche. Curr Opin Cell Biol, 2012; 24: 645-651.

81. Scadden DT. The stem-cell niche as an entity of action. Nature, 2006; 441: 1075-1079.

82. Jones PH, Watt FM. Separation of human epidermal stem cells from transit amplifying cells on the basis of differences in integrin function and expression. Cell, 1993; 73: 713-324.

83. Jensen UB, Lowell S, Watt FM. The spatial relationship between stem cells and their progeny in the basal layer of human epidermis: a new view based on whole-mount labeling and lineage analysis. Development, 1999; 126: 2409-2418.

84. Garcion E, Halilagic A, Faissner A, Ffrench-Constant C. Generation of an environmental niche for neural stem cell development by the extracellular matrix molecule tenascin C. Development, 2004; 131: 3423-3432.

85. Ohta M, Sakai T, Saga Y, Aizawa S, Saito M. Suppression of hematopoietic activity in tenascin-C deficient mice. Blood, 1998; 91: 4074-4083.

86. Stier S, Ko Y, Forkert R, Lutz C, Neuhaus T, Grunewald E, Cheng T, Dombkowski D, Calvi LM, Rittling SR, Scadden DT. Osteopontin is a hematopoietic stem cell niche component that negatively regulates stem cell pool size. J Exp Med, 2005; 201: 1781-1791.

87. Nilsson SK, Johnston HM, Whitty GA, Williams B, Webb RJ, Denhardt DT, Bertoncello I, Bendall LJ, Simmons PJ, Haylock DN. Osteopontin, a key component of the hematopoietic stem cell niche and regulator of primitive hematopoietic progenitor cells. Blood, 2005; 106: 1232-1239.

88. Vermeulen M, Pesteur FL, Gagnerault MC, Mary JY, Sainteny F, Lepault F. Role of adhesion molecules in the homing and mobilization of murine hematopoietic stem and progenitor cells. Blood, 1998; 92: 894-900.

89. Laird DJ, von Andrian UH, Wagers AJ. Stem cell trafficking in tissue development, growth, and disease. Cell, 2008; 132: 612-630.

90. Jones RG, Li X, Gray PD, Kuang J, Clayton F, Samowitz WS, Madison BB, Gumucio DL, Kuwada SK. Conditional deletion of beta1 integrins in the intestinal epithelium causes a loss of Hedgehog expression, intestinal hyperplasia, and early postnatal lethality. J Cell Biol, 2006; 175: 505-514.

91. Lee ST, Yun JI, Jo YS, Mochizuki M, van der Vlies AJ, Kontos S, Ihm JE, Lim JM, Hubbell JA. Engineering integrin signaling for promoting embryonic stem cell self-renewal in a precisely defined niche. Biomaterials, 2010; 31: 1219-1226.

92. Batlle E, Henderson JT, Beghtel H, van den Born MMW, Sancho E, Huls G, Meeldijk J, Robertson J, van de Wetering M, Pawson T, Clevers H. β-catenin and TCF mediate cell positioning in the intestinal epithelium by controlling the expression of EphB/ephrinB. Cell, 2002; 111: 251-263.

93. Engler AJ, Carag-Krieger C, Johnson CP, Raab M, Tang HY, Speicher DW, Sanger JW, Sanger JM, Discher DE. Embryonic cardiomyocytes beat best on a matrix with heart-like elasticity: scar-like rigidity inhibits beating. J Cell Sci, 2008; 121: 3794-3802.

94. Anderson DG, Levenberg S, Langer R. Nanoliter-scale synthesis of arrayed biomaterials and application to human embryonic stem cells. Nat Biotechnol, 2004; 22: 863-866.

95. Saha K, Keung AJ, Irwin EF, Li Y, Little L, Schaffer DV, Healy KE. Substrate modulus directs neural stem cell behavior. Biophys J, 2008; 95: 4426-4438.

96. Discher DE, Janmey P, Wang YL. Tissue cells feel and respond to the stiffness of their substrate. Science, 2005; 310: 1139-1143.

97. Lo CM, Wang HB, Dembo M, Wang YL. Cell movement is guided by the rigidity of the substrate. Biophys J, 2000; 79: 144-152

98. Pittenger MF, Martin BJ. Mesenchymal stem cells and their potential as cardiac therapeutics. Circ Res, 2004; 95: 9-20.

99. Berry MF, Engler AJ, Woo J, Pirolli TJ, Bish LT, Jayasankar V, Morine KJ, Gardner TJ, Discher DE, Sweeney HL. Mesenchymal stem cell injection after myocardial infarction improves myocardial compliance. Am J Physiol Heart Circ Physiol, 2006; 290: H2196-H2203.

100. Wipff PJ, Rifkin DB, Meister JJ, Hinz B. Myofibroblast contraction activates latent TGF-beta1 from the extracellular matrix. J Cell Biol, 2007; 179: 1311-1123.

101. Breitbach M, Bostani T, Roell W, Xia Y, Dewald O, Nygren JM, Fries JWU, Tiemann K, Bohlen H, Hescheler J, Welz A, Bloch W, Jacobsen SEW, Fleischmann BK. Potential risks of bone marrow cell transplantation into infarcted hearts. Blood, 2007; 110: 1362-1369.

102. Gilbert PM, Havenstrite KL, Magnusson KEG, Sacco A, Leonardi NA, Kraft P, Nguyen NK, Thrun S, Lutolf, Blau HM. Substrate elasticity regulates skeletal muscle stem cell self-renewal in culture. Science, 2010; 329: 1078-1081.

103. Gerecht S, Burdick JA, Ferreira LS, Townsend SA, Langer R, Vunjak-Novakovic G. Hyaluronic acid hydrogel for controlled self-renewal and differentiation of human embryonic stem cells. Proc Natl Acad Sci USA, 2007; 104: 11298-11303.

104. Williams DA, Zheng Y, Cancelas JA. Rho GTPases and regulation of hematopoietic stem cell localization. Methods Enzymol, 2008; 439: 365-393.

105. Kratchmarova I, Blagoev B, Haack-Sorensen M, Kassem M, Mann M. Mechanism of divergent growth factor effects in mesenchymal stem cell differentiation. Science, 2005; 308: 1472-1477.

106. Engler AJ, Sen S, Sweeney HL, Discher DE. Matrix elasticity directs stem cell lineage specification. Cell, 2006; 126: 677-689.

107. McBeath R, Pirone DM, Nelson CM, Bhadriraju K, Chen CS. Cell shape, cytoskeletal tension, and RhoA regulate stem cell lineage commitment. Dev Cell, 2004; 483-495.

108. Watanabe K, Ueno M, Kamiya D, Nishiyama A, Matsumura M, Wataya T, Takahashi JB, Nishikawa S, Muguruma K, Sasai Y. A ROCK inhibitor permits survival of dissociated human embryonic stem cells. Nat Biotechnol, 2007; 25: 681-686.

109. Jacot JG, McCulloch AD, Omens JH. Substrate stiffness affects the functional maturation of neonatal rat ventricular myocytes. Biophys J, 2008; 95: 3479-3487.

110. Oh H, Bradfute SB, Gallardo TD, Nakamura T, Gaussin V, Mishina Y, Pocious J, Michael LH, Behringer RR, Garry DJ, Entman ML, Schneider MD. Cardiac progenitor cells from adult myocardium: homing, differentiation, and fusion after infarction. Proc Natl Acad Sci 2003;100(21):12313-12318.

111. Mouquet F, Pfister O, Jain m, Oikonomopouls A, Ngoy S, Summer R, Fine A, Liao R. Restoration of cardiac progenitor cells after myocardial infarction by self-proliferation and selective homing of bone marrow-derived stem cells. Cir Res 2005;97:1090-1092.

112. Beltrami AP, Barlucchi L, Torella D, Baker M, Limana F, Chimenti S, Kasahara H, Rota M, Musso E, Urbanek K, Leri A, Kajstura J, Nadal-Ginard B, Anversa P. Adult cardiac stem cells are multipotent and support myocardial regeneration. Cell, 2003; 114: 763-776.

113. Ott HC, Matthiesen TS, Brechtken J, Grindle S, Goh SK, Nelson W, Taylor DA. The adult human heart as a source for stem cells: repair strategies with embryonic-like progenitor cells. Nat Clin Pract Cardiovasc Med, 2007; 4: S27-S39.

114. Davis DR, Kizana E, Terrovitis J, Barth AS, Zhang Y, Smith RR, Miake J, Marban E. Isolation and expansion of functionally-competent cardiac progenitor cells directly from heart biopsies. J Mol Cell Cardiol, 2010; 49: 312-321.

115. Laugwitz KL, Moretti A, Lam J, Gruber P, Chen Y, Woodard S, Lin LZ, Cai CL, Lu MM, Reth M, Platoshyn O, Yuan JXJ, Evans S, Chien KR. Postnatal isl1+ cardioblasts enter fully differentiated cardiomyocytes lineages. Nature, 2005; 433: 647-653

116. Kattman SJ, Huber TL, Keller GM. Multipotent Flk1+ cardiovascular progenitor cells give rise to the cardiomyocyte, endothelial and vascular smooth muscle lineages. Dev Cell, 2006; 11: 723-732.

117. Moretti A, Caron L, Nakano A, Lam JT, Bernshausen A, Chen Y, Qyang Y, Bu L, Sasaki M, Martin-Puig S, Sun Y, Evans SM, Laugwitz KL, Chien KR. Multipotent embryonic Isl1+ progenitor cells lead to cardiac, smooth muscle and endothelial cell diversification. Cell, 2006; 127: 1151-1165.

118. Yang L, Soonpaa MH, Adler ED, Roepke TK, Kattman SJ, Kennedy M, Henckaerts E, Bonham K, Abbott GW, Linden RM, Field LJ, Keller GM. Human cardiovascular progenitor cells develop from a KDR+ embryonic-stem-cell-derived population. Nature, 2008; 453: 524-528.

119. Bu L, Jiang X, Martin-Puig S, Caron L, Zhu S, Shao Y, Roberts DJ, Huang PL, Domian IJ, Chien KR. Human ISL1 heart progenitors generate diverse multipotent cardiovascular cell lineages. Nature, 2009; 460: 113-117.

120. Ingber, DE. Mechanical signaling and the cellular response to extracellular matrix in angiogenesis and cardiovascular physiology. Circ Res. 2002; 91: 877-887.

121. Guidebook to the Extracellular Matrix and Adhesion Proteins. Edited by Kreis T, Vale R. Oxford University Press, Oxford/NY/Toyko, 1993.

122. Plow EF, Haas TA, Zhang L, Loftus J, Smith JW. Ligand binding to integrins. J Biol Chem, 2000; 275(29): 21785-21788.

123. Abercrombie M, Heaysman JEM, Pegrum SM. The locomotion of fibroblasts in culture. Experimental Cell Research, 1971; 67: 359-367.

124. Abercrombie M, Dunn GA. Adhesions of fibroblasts to substratum during contact inhibition observed by interference reflection microscopy. Experimental Cell Research, 1975; 92: 57-62.

125. Cukierman E, Pankov R, Stevens D, Yamada KM. Taking cell-matrix adhesions to the third dimension. Science, 2001; 294: 1708-1712.

126. Hynes RO. Integrins: versatility, modulation, and signaling in cell adhesion. Cell, 1992; 69:11-25.

127. Huang S, Ingber DE. The structural and mechanical complexity of cell-growth control. Nature Cell Biol, 1999; 1: E131-E138.

128. Zhou X, Rowe RG, Hiraoka N, George JP, Wirtz D, Mosher DF, Virtanen I, Chernousov MA, Weiss SJ. Fibronectin fibrillogenesis regulates three-dimensional neovessel formation. Genes Dev, 2008; 22: 1231-1243.

129. Cukierman, Pankov, Yamada KM. Cell interactions with three-dimensional matrices. Curr Opin Cell Biol, 2002; 14: 633-639.

130. Moiseeva EP. Adhesion receptors of vascular smooth muscle cells and their functions. Cardiovasc Res, 2001; 52: 372-386.

131. Caswell PT, Vadrevu S, Norman JC. Integrins: masters and slaves of endocytic transport. Nature Rev Mol Cell Biol, 2009; 10: 843-853.

132. Hynes RO. Integrins: bidirectional, allosteric signaling machines. Cells, 2002; 110: 673-687.

133. Abram CL, Lowell CA. The ins and outs of leukocyte integrin signaling. Annu Rev Immunol, 2009; 27: 339-362.

134. Avraamides CJ, Garmy-Susini B, Varner JA. Integrins in angiogenesis and lymphangiogenesis. Nature Rev, 2008; 8: 604-617.

135. Rosso F, Giordano A, Barbarisi M, Barbarisi A. From cell-ECM interactions to tissue engineering. Journal of Cellular Physiology, 2004; 199: 174-180.

136. Luo BH, Carman CV, Springer TA. Structural basis of integrin regulation and signaling. Annu. Rev. Immunol, 2007; 25: 619-647.

137. Schaffert CS, Sorrell MF, Tuma DJ. Expression and cytoskeletal association of integrin subunits is selectively increased in rat perivenous hepatocytes after chronic ethanol administration. Alcohol Clin Exp Res, 2001; 25: 1749-1757.

138. Danen EH, Yamada KM. Fibronectin, integrins, and growth control. J Cell Physiol, 2001; 189: 1-13.

139. Ramirez F, Rifkin DB. Cell signaling events: a view from the matrix. Matrix Biol, 2003; 22: 101-107.

140. Hata RI. Where am I? How a cell recognizes its positional information during morphogenesis. Cell Biol Int, 1996; 20: 59-65.

141. Boudreau N, Bissell MJ. Extracellular matrix signaling: integration of form and function in normal and malignant cells. Curr Opin Cell Biol, 1998; 10: 640-646.

142. Li S, Harrison D, Carbonetto S, Fassler R, Smyth N, Edgar D, Yurchenco PD. Matrix assembly, regulation, and survival functions of laminin and its receptors in embryonic stem cell differentiation. J Cell Biol, 2002; 157(7): 1279-1290.

143. Hayashi Y, Furue M, Okamoto T, Ohnuma K, Myoishi Y, Fukuhara Y, Abe T, Sato JD, Hata RI, Asashima. Integrins regulate mouse embryonic stem cell self-renewal. Stem Cells, 2007;25: 3005-3015.

144. Sutherland AE, Calarco PG, Damsky CH. Developmental regulation of integrin expression at the time of implantation in the mouse embryo. Development, 1993; 119: 1175-1186.

145. Humphries MJ. The molecular basis and specificity of integrin-ligand interactions. J Cell Sci, 1990; 97: 585-592.

146. Humphries JD, Byron A, Humphries MJ. Integrin ligands at a glance. J Cell Sci, 2006; 119: 3901-3903.

147. Braam SF, Zeinstra L, Litjens S, Ward-van Oostwaard D, van den Brink S, van Laake L, Lebrin F, Kats P, Hochstenbach R, Passier R, Sonnenberg A, Mummery CL. Recombinant vitronectin is a functionally defined substrate that supports human embryonic stem cell self-renewal via αVβ5 integrin. Stem Cells, 2008; 26: 2257-2265.

148. Heino J. The collagen receptor integrins have distinct ligand recognition and signaling functions. Matrix Biol, 2000; 19: 319-323.

149. Fassler R, Meyer M. Consequences of lack of beta1 integrin gene expression in mice. Genes Dev, 1995; 9: 1896-1908.

150. Yang JT, Rayburn H, Hynes RO. Embryonic mesodermal defects in α5 integrin-deficient mice. Development, 1993; 119: 1093-1105.

151. Yang JT, Bader BL, Kreidberg JA, Ullman-Cullere M, Trevithick JE, Hynes RO. Overlapping and independent functions of fibronectin receptor integrins in early mesodermal development. Dev Biol, 1999; 215: 264-277.

152. Gurtner GC, Davis V, Li H, McCoy MJ, Sharpe A, Cybulsky MK. Targeted disruption of the murine VCAM1 gene: essential role of VCAM-1 in chorioallantoic fusion and placentation. Genes Dev, 1995; 9: 1-14.

153. Kwee L, Baldwin HS, Shen HM, Stewart CL, Buck CA, Labow MA. Defective development of the embryonic and extraembryonic circulatory systems in vascular cell adhesion molecule (VCAM-1) deficient mice. Development, 1995; 121: 489-503.

154. Avraamides CJ, Garmy-Susini B, Varner JA. Integrins in angiogenesis and lymphangiogenesis. Nature Reviews, 2008; 8: 604-617.

155. Brooks PC, Clark RA, Cheresh DA. Requirement of vascular integrin αVβ3 for angiogenesis. Science, 1994; 264: 569-571.

156. Brooks PC, Montgomery AMP, Rosenfield M, Reisfeld RA, Hu T, Klier G, Cheresh DA. Integrin αVβ3 antagonists promote tumor regression by inducing apoptosis of angiogenic blood vessels. Cell, 1994; 79: 1157-1164.

157. Friedlander M, Brooks PC, Shaffer RW, Kincaid CM, Varner JA, Cheresh DA. Definition of two angiogenic pathways by distinct αV integrins. Science, 1995; 270: 1500-1502.

158. Friedlander M, Theesfeld CL, Sugita M, Fruttiger MS, Thomas MA, Chang S, Cheresh DA. Involvement of integrins αVβ3 and αVβ5 in ocular neovascular diseases. Proc. Natl. Acad. Sci, 1996; 93: 9764-9769.

159. Sakai T, Larsen M, Yamada KM. Fibronectin requirement in branching morphogenesis. Nature, 2003; 423: 876-881.

160. Roskelley CD, Bissell MJ. Dynamic reciprocity revisited: a continuous, bidirectional flow of information between cells and the extracellular matrix regulates mammary epithelial cell function. Biochem Cell Biol, 1995; 73: 391-397.

161. Tamariz E, Ginnell F, Modulation of fibroblast morphology and adhesion during collagen matrix remodeling. Mol Biol Cell, 2002; 13: 3915-3929.

162. Hakkinen KM, Harunaga JS, Doyle AD, Yamada KM. Direct comparisons of the morphology, migration, cell adhesions, and actin cytoskeleton of fibroblasts in four different three-dimensional extracellular matrices. Tissue Engineering Part A, 2001; 17: 713-724.

163. Debnath J, Brugge JS. Modeling glandular epithelial cancers in three-dimensional cultures. Nat Rev Cancer, 2005; 5: 675-688.

164. Nelson CM, Bissell MJ. Of extracellular matrix, scaffolds, and signaling: Tissue architecture regulates development, homeostasis, and cancer. Annu Rev Cell Dev Biol, 2006; 22: 287-309.

165. Berrier AL, Yamada KM. Cell-Matrix Adhesion, J Cell Physiol, 2007; 213: 565-573.

166. Geraldo S, Simon A, Elkhatib N, Louvard D, Fetler L, Vignjevic DM. Do cancer cells have distinct adhesions in 3D collagen matrices and *in vivo*? Eur J Cell Biol, 2012; 91: 930-937.

167. Langer R and Vacanti JP, Tissue Engineering. Science, 1993;260(5110):920-926.

168. Nerem RM. Tissue engineering: confronting the transplantation crisis. Proc Inst Mech Eng [H], 2000;214(1): 95-99.

169. Vacanti JP. Tissue engineering: the design and fabrication of living replacement devices for surgical reconstruction and transplantation. Lancet, 1999;354(supp 1): S132-S134.

170. Li M, Gandhi MR, Ko FK, Weiss AS, Lelkes PI. Electrospun protein fibers as matrices for tissue engineering. Biomaterials, 2005; 26(30):5999-6008.

171. Zong X, Chung CY, Yin L, Fang D, Hsiao BS, Chu B, Entcheva E. Electrospun fine-textured scaffolds for heart tissue constructs. Biomaterials, 2005; 26(26): 5330-5338.

172. Khil MS, Kim KY, Kim SZ, Lee KH, Novel fabricated matrix via electrospinning for tissue engineering. J Biomed Mater Res B Appl Biomater, 2005; 15(72): 117-124.

173. Leor J, Aboula-Etzion S, Dar A, Shapiro L, Barbash IM, Battler A, Granot Y, Cohen S. Bioengineered cardiac grafts: a new approach to repair the infarcted myocardium? Circulation, 2000; 102: III56.

174. Giraud MN, Armbruster C, Carrel T, Tevaearai HT. Current state of the art in myocardial tissue engineering. Tissue Eng, 2007; 13: 1825-1836.

175. Dar A, Shachar M, Leor J, Cohen S. Optimization of cardiac sell seeding and distribution in 3D porous alginate scaffolds. Biotechnol Bioeng, 2002; 80: 305-312.

176. Yost MJ, Baicu CF, Stonerock CE, Goodwin RL, Price RL, Davis JM, Evans H, Watson PD, Gore CM, Sweet J, Creech L, Zile MR, Terracio L. A novel tubular scaffold for cardiovascular tissue engineering. Tissue Eng, 2004; 10: 273-284.

177. Feng Z, Matsumoto T, Nomura Y, Nakamura T. An electro-tensile bioreactor for 3D culturing of cardiomyocytes; A bioreactor that stimulates the myocardium's electrical and mechanical response *in vivo*. IEEE Eng Med Biol Mag, 2005; 24: 73-79.

178. van Luyn MJ, Tio RA, Gallego y van Seijen XJ, Plantinga JA, de Leij LF, DeJongste MJ, van Wachem PB. Cardiac tissue engineering: characteristics of in unison contracting two- and three-dimensional neonatal rat ventricle cell (co)-cultures. Biomaterials, 2002; 23: 4793-4801.

179. Giraud M, Siepe M, Ayuni E, Tevaerai H, Carrel T. A hydrogel based engineered skeletal muscle graft (ESMG) for cardiac repair. Faseb J, 2005; 19: A1659.

180. Akhyari P, Fedak PW, Weisel RD, Lee TY, Verma S, Mickle DA, Li RK. Mechanical stretch regimen enhances the formation of bioengineered autologous cardiac muscle grafts. Circulation, 2002; 106: I137-I142.

181. Birla RK, Borschel GH, Dennis RG, Brown DL. Myocardial engineering *in vivo*: formation and characterization of contractile, vascularized three-dimensional cardiac tissue. Tissue Eng, 2005; 11: 803-813.

182. Ozawa T, Mickle DA, Weisel RD, Koyama N, Ozawa S, Li RK. Optimal biomaterial for creation of autologous cardiac grafts. Circulation, 2002; 106: I176-182.

183. Alperin C, Zandstra PW, Woodhouse KA. Polyurethane films seeded with embryonic stem cell-derived cardiomyocytes for use in cardiac tissue engineering applications. Biomaterials, 2005; 26: 7377-7386.

184. McDevitt TC, Woodhouse KA, Hauschka SD, Murry CE, Stayton PS. Spatially organized layers of cardiomyocytes on biodegradable polyurethane films for myocardial repair. J Biomed Mater Res A, 2003; 66: 586-595.

185. Siepe M, Giraud MN, Pavlovic M, Receputo C, Beyersdorf P, Menasche P, Carrel T, Tevaearai HT. Myoblast-seeded biodegradable scaffolds to prevent post-myocardial infarction evolution toward heart failure. J Thorac Cardiovasc Surg, 2006; 132: 124-131.

186. Shin M, Ishii O, Sueda T, Vacanti JP. Contractile cardiac grafts using a novel nanofibrous mesh. Biomaterials, 2004; 25: 3717-3723.

187. Papadaki M, Bursac N, Langer R, Merok J, Vunjak-Novakovic G, Freed LE. Tissue engineering of functional cardiac muscle: molecular, structural, and electrophysiological studies. Am J Physiol Heart Circ Physiol, 2001; 280: H168-H178.

188. Park H, Radisic M, Lim JO, Chang BH, Vunjak-Novakovic G. A novel composite scaffold for cardiac tissue engineering. In Vitro Cell Dev Biol Anim, 2005: 41: 188-196.

189. Carrier RL, Rupnick M, Langer R, Schoen FJ, Freed LE, Vunjak-Novakovic G. Perfusion improves tissue architecture of engineered cardiac muscle. Tissue Eng, 2002; 8: 175-188.

190. Carrier RL, Papadaki M, Rupnick M, Schoen FJ, Bursac N, Langer R, Freed LE, Vunjak-Novakovic G. Cardiac tissue engineering: cell seeding, cultivation parameters, and tissue construct characterization. Biotechnol Bioeng, 1999; 64: 580-589.

191. Levenberg S, Roukema J, Macdonald M, Garfein ES, Kohane DS, Darland DC, Marini R, van Blitterswijk, Mulligan RC, D'Amore PA, Langer R. Engineering vascularized skeletal muscle tissue. Nat Biotechnol, 2005; 23: 879-884.

192. Weinberg CB, Bell E. A blood vessel model constructed from collagen and cultured vascular cells. Science, 1986; 231: 397-400.

193. L'Heureux N, Germain L, Labbe R, Auger FA. *In vitro* construction of a human blood vessel from cultured vascular cells: a morphologic study. J Vasc Surg, 1993; 17: 499-509.

194. Stitzel J, Liu J, Lee SJ, Komura M, Berry J, Soker S, Lim G, van Dyke M, Czerw R, Yoo JJ, Atala A. Controlled fabrication of a biological vascular substitute. Biomaterials, 2006; 27: 1088-1094.

195. Kofidis T, Akhyari P, Wachsmann B, Boublik J, Mueller-Stahl K, Leyh R, Fischer S, Haverich A. A novel bioartificial myocardial tissue and its prospective use in cardiac surgery. Eur J Cardiothorac Surg, 2002; 22: 238-243.

196. Simpson D, Liu H, Fan TM, Nerem R, Dudley SC. A tissue engineering approach to progenitor cell delivery results in significant cell engraftment and improved myocardial remodeling. Stem Cells, 2007; 25: 2350-2357.

197. Swartz DD, Russell JA, Andreadis ST. Engineering of fibrin-based functional and implantable small-diameter blood vessel. Am J Physiol Heart Circ Physiol, 2005; 288: H1451-H1460.

198. Koch S, Flanagan TC, Sachweh JS, Tanios F, Schnoering H, Deichmann T, Ella V, Kellomaki M, Gronloh N, Gries T, Tolba R, Schmitz-Rode T, Jockenhoevel S. Fibrin-polylactide-based tissue-engineered vascular graft in the arterial circulation. Biomaterials, 2010; 31: 4731-4739.

199. Roh JD, Brennan MP, Lopez-Soler RI, Fong PM, Goyal A, Dardik A, Breuer CK. Construction of an autologous tissue-engineered venous conduit from bone marrow-derived vascular cells: optimization of cell harvest and seeding techniques. J Pediatriac Surg, 2007; 42: 198-202.

200. Iwai S, Sawa Y, Ichikawa H, Taketani S, Uchimura E. Chen G, Hara M, Miyake J, Matsuda H. Biodegradable polymer with collagen microsponge serves as a new bioengineered cardiovascular prosthesis. J Thor Cardiovasc Surg, 2004; 128: 472-479.

201. Blan NR, Birla RK. Design and fabrication of heart muscle using scaffold-based tissue engineering. J Biomed Mater Res A, 2008; 86A: 195-208.

202. Zhao ZQ, Puskas JD, Xu D, Wang NP, Mosunjac M, Guyton RA, Vinten-Johansen J, Matheny R. Improvement in cardiac function with small intestine extracellular matrix is associated with recruitment of c-kit cells, myofibroblasts, and macrophages after myocardial infarction. J Am Coll Cardiol, 2010; 55: 1250-1261.

203. Formhals A. US Patent 1,975,5042; 1934.

204. Theron SA, Zussman E, Yarin AL. Experimental investigation of the governing parameters in electrospinning of polymer solutions. Polymer, 2004; 45:217-230.

205. Reneker DH, Kataphinan W, Theron A, Zussman E, Yarin AL. Nanofiber garlands of polycaprolactone by electrospinning. Polymer, 2002; 43: 6785-6794.

206. Bhattarai SR, Yi HK, Hwang PH, Cha DI, Kim HY. Novel biodegradable electrospun membrane: scaffold for tissue engineering. Biomaterials, 2004; 25: 2595-2602.

207. Li WJ, Caterson EJ, Tuan RS, Ko FK. Electrospun nanofibrous structure: a novel scaffold for tissue engineering. J Biomed Mater Res, 2002;60:613.

208. Chew SY, Yim EKF, Leon KW. Sustained release of proteins from electrospun biodegradable fibers. Biomacromolecules, 2005;6:2017-2024.

209. Stitzel JD, Pawlowski KJ, Wnek GE, Simpson DG, Bowlin GL. Arterial smooth muscle cell proliferation on a novel biomimicking biodegradable vascular graft scaffold. J Biomater Appl, 2001; 16: 22-33.

210. Kidoaki S, Kwon IK, Matsuda T. Mesoscopic spatial designs of nano- and microfiber meshes for tissue-engineering matrix and scaffold based on newly devised multilayering and mixing electrospinning techniques. Biomaterials, 2005; 26: 37-46.

211. Xu C, Inai R, Kotaki M, Ramakrishna S. Electrospun nanofiber fabrication as synthetic extracellular matrix and its potential for vascular tissue engineering. Tissue Eng, 2004; 10: 1160-1168.

212. Hosseinkhani H, Hosseinkhani M, Hattori S, Matsuoka R, Kawaguchi. Micro and nano-scale *in vitro* 3D culture system for cardiac stem cells. J Biomed Mater Res A, 2010; 94A: 1-8.

213. Kalfa D, Bel A, Chen-Tournoux A, Martina AD, Rochereau P, Coz C, Bellamy V, Bensalah M, Vanneaux V, Lecourt S, Mousseaux E, Bruneval P, Larghero J, Menasche P. A polydioxanone electrospun valve patch to replace the right ventricular outflow tract in a growing lamb model. Biomaterials, 2010; 31: 4056-4063.

214. Hong H, Dong GN, Shi WJ, Chen S, Guo C, Hu P. Fabrication of biomatrix/polymer hybrid scaffold for heart valve tissue engineering *in vitro*. ASAIO J, 2008; 54: 627-632.

215. Zhong J, Chan A, Morad L, Kornblum HI, Fan G, Carmichael ST. Hydrogel matrix to support stem cell survival after brain transplantation in stroke. Neurorehabilitation and Neural Repair, 2010; 24(7): 636-644.

216. Hosack LW, Firpo MA, Scott JA, Prestwich GD, Peattie RA. Microvascular maturity elicited in tissue treated with cytokine-loaded hyaluronan-based hydrogels. Biomaterials, 2008; 29: 2336-2347.

217. Shu XZ, Ghosh K, Liu Y, Palumbo FS, Luo Y, Clark RA, Prestwich GD. Attachment and spreading of fibroblasts on an RGD peptide-modified injectable hyaluronan hydrogel. J Biomed Mater Res, 2004; 68A: 365-375.

218. Chiu YN, Norris RA, Mahler G, Recknagel A, Butcher JT. Transforming growth factor β, bone morphogentic protein, and vascular endothelial growth factor mediate phenotype maturation and tissue remodeling by embryonic valve progenitor cells: relevance for heart valve tissue engineering. Tissue Eng, 2010; 16: 3375-3383.

219. Benton JA, DeForest CA, Vivekanandan V, Anseth KS. Photo crosslinking of gelatin macromers to synthesize porous hydrogels that promote valvular interstitial cell function. Tissue Eng, 2009; 15: 3221-3230.

220. Prokoph S, Chavakis E, Levental KR, Zieris A, Freudenberg U, Dimmeler S, Werner C. Sustained delivery of SDF-1α from heparin-based hydrogels to attract circulating pro-angiogenic cells. Biomaterials, 2012; 33: 4792-4800.

221. Deng C, Zhang P, Vulesevic B, Kuraitis D, Li F, Yang AF, Griffith M, Ruel M, Suuronen EJ. A collagen-chitosan hydrogel for endothelial differentiation and angiogenesis. Tissue Eng, 2010; 16: 3099-3109.

222. Anderson SM, Siegman SN, Segura T. The effect of vascular endothelial growth factor (VEGF) presentation within fibrin matrices on endothelial cell branching. Biomaterials, 2011; 32: 7432-7443.

223. ClinicalTrials.gov [Internet]. Bethesda (MD): National Library of Medicine (US). 2012 July- . Identifier NCT01496209. Regenerative cardiosphere injection to strengthen dysfunctional hearts (RECONSTRUCT); 2011 Dec 19 [cited 2012 Sept 20]; Available from: http://clinicaltrials.gov/ct2/show/NCT01496209?term=marban&rank=1

224. Cheng K, Blusztajn A, Shen D, Li TS, Sun B, Galang G, Zarembinski TI, Prestwich GD, Marban E, Smith RR, Marban L. Functional performance of human cardiosphere-derived cells delivered in an in situ polymerizable hyaluronan-gelatin hydrogel. Biomaterials, 2012; 33: 5317-5324.

225. Wang H, Liu Z, Li D, Guo X, Kasper FK, Duan C, Zhou J, Mikos AG, Wang C. Injectable biodegradable hydrogels for embryonic stem cell transplantation: improved cardiac remodeling and function of myocardial infarction. J Cell Mol Med, 2012; 16: 1310-1320.

226. Schenke-Layland K, Angelis E, Rhodes KE, Heydarkhan-Hagvall S, Mikkola HK, MacLellan WR. Collagen IV induces trophoectoderm differentiation of mouse embryonic stem cells. Stem Cells, 2007; 25: 1529-1538.

227. Dziadek M, Timpl R. Expression of nidogen and laminin in basement membranes during mouse embryogenesis and in teratocarcinoma cells. Dev Biol, 1985; 111: 372-382.

228. Heydarkhan-Hagvall S, Gluck JM, Delman C, Jung M, Ehsani N, Full S, Shemin RJ. The effect of vitronectin on the differentiation of embryonic stem cells in a 3D culture system. Biomaterials, 2012; 33 (7), 2032-2040.

CHAPTER TWO

<u>**A. Chapter Introduction**</u>

I first examined the effects of the microenvironment on induction of mouse embryonic stem (mES) cells into cardiovascular progenitor cells (CPCs). To evaluate the microenvironment effects, I developed a three-dimensional (3D) scaffold system, as well as adapted a hyaluronan-based hydrogel system to assess the effects of 3D nature on CPC induction. I used a co-axial electrospinning system to create mechanically stable scaffolds. I determined that the scaffolds do not elicit an immunological reaction *in vivo* and can be used as an *in vitro* 3D culture system for extended culture time (up to 30 days). We previously determined that the addition of the extracellular matrix (ECM) protein collagen IV enhances the induction of CPCs from mES cells and that the addition of a 3D scaffold further enhances CPC induction. As cells take a prolonged time to migrate into the interior of the scaffold, I used a hydrogel system to completely encapsulate mES cells and create an immediate 3D microenvironment. Integrins are known to mediate cell-cell and cell-matrix interactions. In an effort to understand the regulation of the cell-matrix and cell-scaffold interactions, I examined the integrin expression levels of both undifferentiated and partially differentiated mES cells. Overall, I have examined the role of the ECM proteins and 3D microenvironment on the induction of mES cells to become CPCs.

B. Hybrid co-axial electrospun nanofibrous scaffolds with limited immunological response created for tissue engineering

B1. Introduction

Tissue engineering is a rapidly growing field of study that aims to repair, and/or replace damaged tissues and organs using a combination of structured scaffolds, specific cell types, and biologically active molecules. In general, the goal of tissue engineering is to mimic the endogenous 3D environment of the target tissue as closely as possible. The natural ECM is comprised of a complex network of structural and regulatory proteins that are arranged into a fibrous matrix. Development of 3D scaffolds that can recapitulate the natural ECM will allow cell attachment and migration as well as diffusion of nutrients, metabolites and soluble factors until the seeded cells can produce a new functional matrix and regenerate the desired tissue structures [1-3]. The ideal scaffold must satisfy a number of often conflicting demands: high porosity allowing for cell migration, sufficient surface area and a variety of surface chemistries that encourage cell adhesion, growth, migration, and has a degradation rate that closely matches regeneration rate of the desired natural tissue. Moreover, the scaffold must be biologically inert so as not to stimulate a foreign body response.

A broad range of tissue-engineering matrices have been fabricated from both synthetic and natural polymers using solvent casting and particulate leaching, gas foaming, freeze drying, rapid prototyping, thermally induced phase separating, fiber bonding, melt molding, and electrospinning, as reviewed elsewhere [4-7]. Electrospinning in particular has been used as an effective method to fabricate biomimetic scaffolds comprised of fibrous meshes. The process produces nonwoven scaffolds with a large network of interconnected pores that is conducive to

tissue ingrowth. In conjunction with the porous network, small diameter fibers and high surface area to volume ratio in the electrospun scaffolds promote cell adhesion and migration as well as function as a delivery vehicle for biochemical signals needed for the seeded cells and efficient exchange of nutrients and metabolic waste [8-10]. Electrospinning has successfully been used in the fabrication of scaffolds made from many different polymers including poly(ε-caprolactone) (PCL), poly(lactic acid) (PLA), poly(glycolic acid) (PGA), poly(lactide-co-glycolide) (PLGA) and poly(urethane) (PU) in addition to the natural proteins, such as collagen, elastin and gelatin [9-12].

Synthetic polymers provide many advantages over natural proteins due to price, availability and reliability [13-14]. They possess a wider range of mechanical properties than natural polymers and their lot-to-lot uniformity translates into the production of consistently uniform scaffolds. They can also be combined with natural proteins to produce hybrid scaffolds, which demonstrate beneficial properties of both starting materials. For example, the weak mechanical properties of natural proteins are overcome by combining them with a synthetic polymer, reinforcing the strength and durability of the scaffold while retaining the specific cell affinity of the natural polymer [13]. Many natural polymers exist such as gelatin, a natural biopolymer derived from collagen by controlled hydrolysis, which is a heterogeneous mixture of single or multi-stranded polymers. Gelatin has several potential advantages over other natural proteins, such as its biological origin, biodegradability, biocompatibility, and commercial availability at low cost [15-16].

As with all tissue engineered structures, the body's native tissue reaction to the implanted cell-scaffold construct can cause an immunogenic response. As such, it is necessary to limit that response as much as possible. Macrophage and foreign body giant cells play a crucial role in the

foreign body reaction, and their responses toward implanted materials have significant impact on the proper functioning of medical devices. The formation of a fibrous capsule during the foreign body reaction is one of the most common barriers observed prohibiting normal function of medical devices, such as biosensors, drug delivery systems, eye implants, etc. Material surface chemistry, physical properties, and morphological features all play a part in modulating cellular reactions towards implant materials [17-19].

In this study, we fabricated co-axial electrospun hybrid scaffolds, which combined synthetic materials with natural proteins to overcome limitations seen with scaffolds constructed with either one alone, such as poor cell adhesion and weak mechanical properties. We produced electrospun nanofibers composed of two distinct polymer solutions arranged in a core-sheath configuration. We used scaffolds made of bicomponent fibers with a gelatin-PCL mixture in the sheath and a PU core, which were determined to provide optimal fiber diameter, pore size and strength, leading to enhanced seeding of the electrospun scaffolds with cells *in vitro*. No immunogenic reaction to the fabricated scaffold was observed in this study *in vivo*. The mechanical properties of the scaffold should prove useful for their application in the field of cardiovascular tissue engineering and regenerative medicine.

B2. Materials and Methods

B2.1. Scaffold Fabrication

Unless otherwise noted all reagents were purchased from Sigma Aldrich (St. Louis, MO). In general, relatively volatile solvents are quite suitable for electrospinning polymeric fibers to ensure rapid drying of electrospun mats. We, like others, noted that 1,1,1,3,3,3-hexafluoro-2-propanol (HFP) is sufficiently volatile (Boiling Point 61°C) and has been used as a solvent in
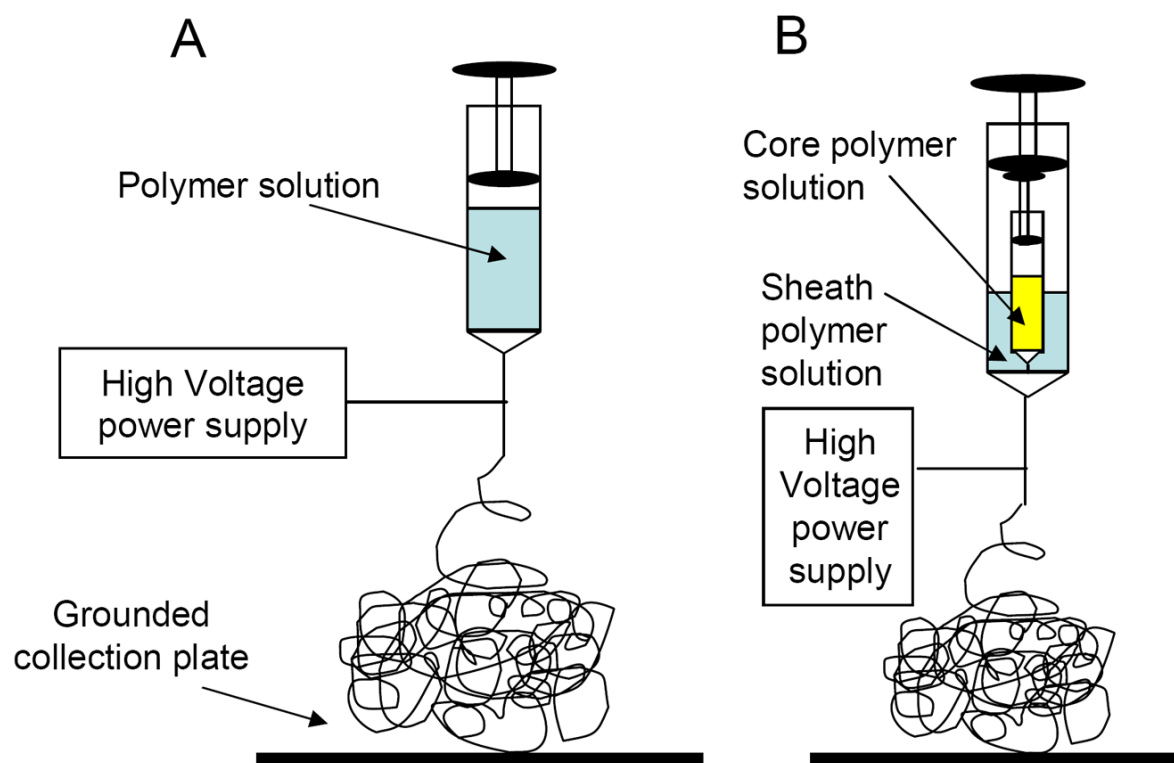
Figure 2-1: Creation of nanofibrous scaffolds A) Schematic of standard system for electrospinning B) Schematic of two-syringe system for electrospinning co-axial scaffolds

which proteins and simpler amino acid sequences have been suspended for various conformational analysis studies [14]. In this study, in order to create a customized electrospun scaffold, a solution of gelatin type B (bovine skin) (10% w/v) and poly(ε-caprolactone) (PCL) (10% w/v) and a solution of PCL alone (10% w/v) were dissolved in HFP. The solution was then loaded into a 10 ml-syringe, to which an 18-gauge blunt ended needle (spinning nuzzle) was attached. A core solution of 5% w/v poly(urethane) (PU) dissolved in HFP was loaded into a 3 ml-syringe, to which a 25-gauge needle was attached. This syringe and needle was then loaded into the 10 ml-syringe containing the sheath solution. The entire syringe system was then loaded into a modified syringe pump, as seen in Figure 2-1. The positive output lead of a high voltage supply (28 kV; Glassman High Voltage Inc., NJ, USA) was attached to the needle on the 10 ml-syringe, spinning nuzzle. In the created electric field, a thin jet was ejected from the solution in

the syringe at a speed of 70μL/min from the raised syringe pump. The grounded target was placed 16 cm under the needle tip and upon introduction of the electric field Taylor cone formation at the base of the spinning nuzzle was observed. By the time the jet reached the target, a dry fiber was collected in the form of a flat 3D mat (300-400 μm thick). After the electrospinning process, the scaffold was then sterilized by soaking scaffolds for 30 minutes in 70% ethanol, and then washed with sterile Dulbecco's phosphate buffered saline (PBS 1x) before seeding with cells for *in vitro* or *in vivo* studies.

B2.2. Ultrastructural Scaffold Analysis

Scanning electron microscopy. For ultrastructural analysis, unseeded scaffold samples were processed for characterization by scanning electron microscopy (SEM) as described previously [14]. Fiber samples were cut from different, randomly selected locations on the electrospun mat to obtain representative fibers. The samples were mounted onto stubs and sputter coated with gold/palladium (Au/Pd to a thickness of ~10μm) using Denton Desk II before scanning with a JEOL 6610 Low-Vacuum SEM (JEOL, Ltd, Tokyo, Japan). Fiber diameters in the electrospun scaffolds were measured on scanning electron micrographs. Average fiber diameter was determined from measurements taken perpendicular to the long axis of the fibers within representative microscopic fields (20 measurements per field). The pores formed at the interstices of the fibers were measured using ImageJ software (free download available at http://rsbweb.nih.gov/ij/). For each sample, at least 5 scanning electron micrographs at 2000x magnification were used for image analysis and pore size measurement.

Transmission electron microscopy. For transmission electron microscopy (TEM), polymer solutions were prepared for regular scaffold fabrication. Gold nanoparticles (GoldSol,

Aurion, The Netherlands) of a 10nm particle size were added to the sheath solution before electrospinning. After scaffold fabrication, scaffolds were embedded in Eponate 12 Resin (Ted Pella, Inc, Redding, CA) and sectioned with a Leica EM UC6 Ultramicrotome before scanning with a JEOL 100CX Transmission Electron Microscope. Images were analyzed using ImageJ software.

Contact angle measurement. For contact angle measurement, the static sessile drop method (ASTM D7334-08 Standard Practice for Surface Wettability of Coatings, Substrates and Pigments by Advancing Contact Angle Measurement) was used with a goniometer to capture images of the scaffolds immediately after a 10µL drop of water was applied to the surface of each scaffold.

B2.3. Mechanical Testing

Electrospun samples were cut into 40mm x 10mm pieces, an average width:length ratio of 3:1, for mechanical testing. Scaffolds that were tested for degradation analysis were left in a desiccator for at least 72 hours to ensure complete dryness before testing. Initial monotonic tensile testing was conducted on an Instron 5564 (Norwood, MA, USA) using a 1N load cell at a speed of 10mm/min and a gauge length of ~30mm with a pneumatic flat jaw clamp.

B2.4.Cell Seeding

Murine fibroblast NIH 3T3 (ATCC, CRL-1658) cells were cultured to a confluent state and at passage 4 were seeded onto the electrospun scaffolds at a density of 10^6 cells/cm^2 to reach a confluent cell layer. The 3T3-seeded scaffold was then cultured for 4 weeks under dynamic

conditions in Dulbecco's Modified Eagle Medium (DMEM) supplemented with 10% FBS at 37ºC and 5% CO_2.

B2.5. Surgical Procedure and Implantation of Scaffolds

UCLA Animal Research Committee approval (protocol # 2010-007-01) was obtained for all procedures. NIH guidelines for the care and use of laboratory animals were observed. Four different groups -- co-axial, co-axial without gelatin (denoted as '*co-axial #2*'), porcine small intestine submucosa (SIS) scaffolds (Cook Medical, Bloomington, IN, USA) and sham were tested at three different time points (2, 4 and 7 weeks). Co-axial #2 scaffolds were fabricated as previously described with the modification of no gelatin in the sheath polymer solution. Anesthesia was induced with 5% isoflurane and maintained with 2% isoflurane. Four 1 x 1- cm sections of sterile scaffold from each group were cut and implanted in the lateral superior region of the subcutaneous dorsum, approximately one-third the distance between the head and tail, c57/BL6J male mice with an average weight of 30g. Inflammation at the implant site, behavioral changes and other adverse reactions to the implant were monitored for the duration of the experiment and no significant abnormalities were observed. Sham control mice had a subcutaneous incision with no scaffold implant.

B2.6. Tissue Collection, Histology and Immunohistochemistry

On weeks 2, 4, and 7 postimplantation, the animals were euthanized and tissue was harvested. Following fixation, the tissue was then embedded in paraffin. Paraffin-embedded tissues were cut into 5-μm sections and stained for different histological analysis using hematoxylin and eosin (H&E) (American Mastertech, Lodi, CA, USA), Masson's trichrome

(American Mastertech, Lodi, CA, USA). [14]. CD 45 (BD Biosciences, dilution 1:100), a mouse monoclonal antibody, and IL-6 (Abcam, dilution 1:400), a rabbit monoclonal antibody were used for immunohistochemistry following standard protocols [14]. Fluorescence images were acquired using a confocal TCS SP2 AOBS laser scanning microscope system (Leica Microsystems Inc., Exton, PA, http://www.leica.com) with x40 (1.3 numerical aperture [NA]). Images were processed with Adobe Photoshop CS3 (Adobe Systems Inc., San Jose, CA, http://www.adobe.com).

To detect the cell attachment on the electrospun scaffolds as well as cell migration through the scaffolds *in vitro*, the scaffolds were analyzed at three time points, 7, 14, and 28 days in culture. Cell-seeded scaffolds were fixed in 4% formaldehyde and paraffin-embedded. To determine cell migration through the interior of the scaffolds, sections were cut in 5μm thicknesses at a vertical cross-section, deparaffinized permeabilized with 0.5% Triton X-100 and nuclei stained with DAPI. To determine the extent of cell migration into the interior of the scaffold, the following equation was used:

$$Equation\ 2\text{-}1{:}\ M{=}(X/T)*100$$

where M is the percent migration, X is the distance migrated from the surface of the scaffold into the interior (as determined via DAPI staining), and T is the thickness of the scaffold.

B2.7. Statistical Analysis

Results are presented as mean±standard error of mean. Statistical significance was tested using ANOVA. Probability values of $P<0.05$ were considered statistically significant.

B3. Results

B3.1 Scaffold Fabrication and Morphology

Gelatin, PU, and PCL were dissolved in HFP and electrospun, either separately or mixed together. Previously, we have determined that a PCL-only scaffold does not sufficiently support
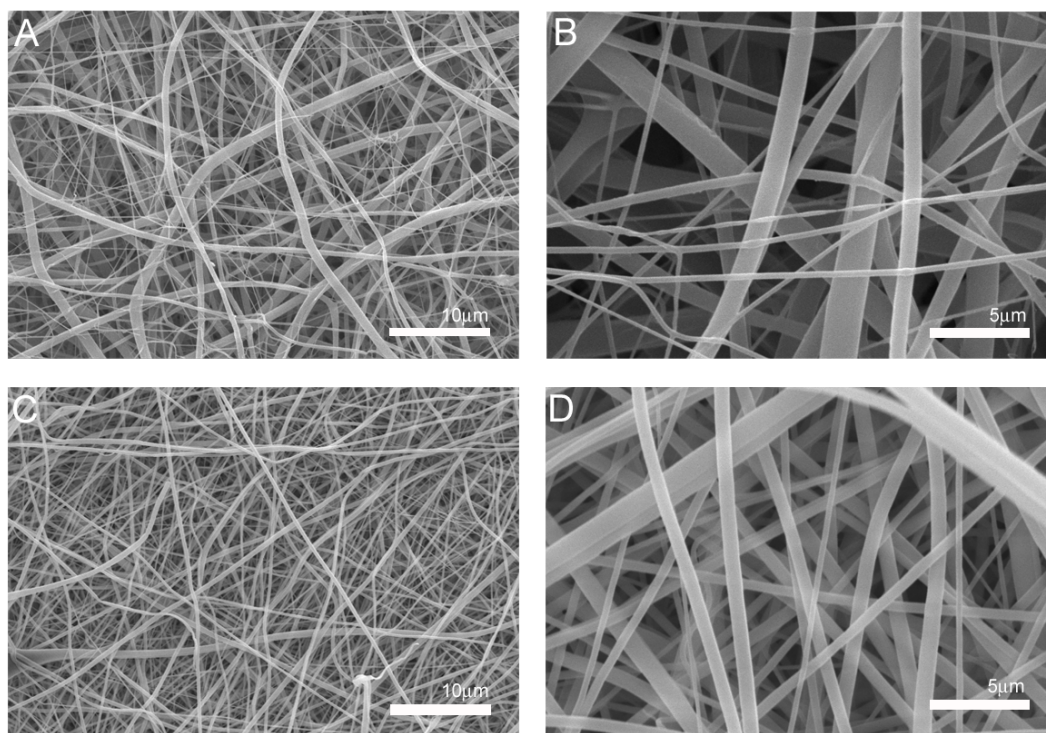
Figure 2-2: Representative SEM micrographs of electrospun scaffold morphology A) Standard 10% PCL-10% gelatin scaffolds at 1,000x with an average fiber diameter of $1.245 \pm 0.413\mu m$ B) Standard scaffolds at 5,000x C) Co-axial scaffold at 1,000x with an average fiber diameter of $0.537 \pm 0.231\mu m$ D) Co-axial scaffold at 5,000x. Scale bar equals $10\mu m$ A and C, Scale bar equals $5\mu m$ B and D.

cell growth and the addition of gelatin is necessary to promote cell adhesion qualities [14]. We have established in previous studies that a minimum polymer concentration is required for pure synthetic nanofibrous scaffold fabrication, thus a minimum polymer concentration of 5% PU was used [14] and 10% PCL-10% gelatin solution was chosen for the hybrid scaffold synthesis based on our previous work. We used these "standard" scaffolds to compare scaffolds prepared via the co-axial system. 5% PU concentration was used for the core of the co-axial system, and a 10% PCL-10% gelatin concentration was used for the sheath (Figure 2-1). SEM and TEM image

analysis of the standard and co-axial electrospun scaffolds showed a 3D nanofibrous mat of random fiber orientation (Figures 2-2 and 2-3).

Analysis of the images obtained from SEM (Figure 2-2) showed uniform fiber morphology for both the standard and co-axial electrospun scaffolds, regardless of needle configuration. However, upon visual observation of the SEM images the standard scaffolds had less fiber volume when compared to the co-axial scaffolds possibly secondary to increased variation in fiber diameter in the standard scaffolds, which is likely related to the development of multiple Taylor cones during the electrospinning process. TEM image analysis (Figure 2-3)
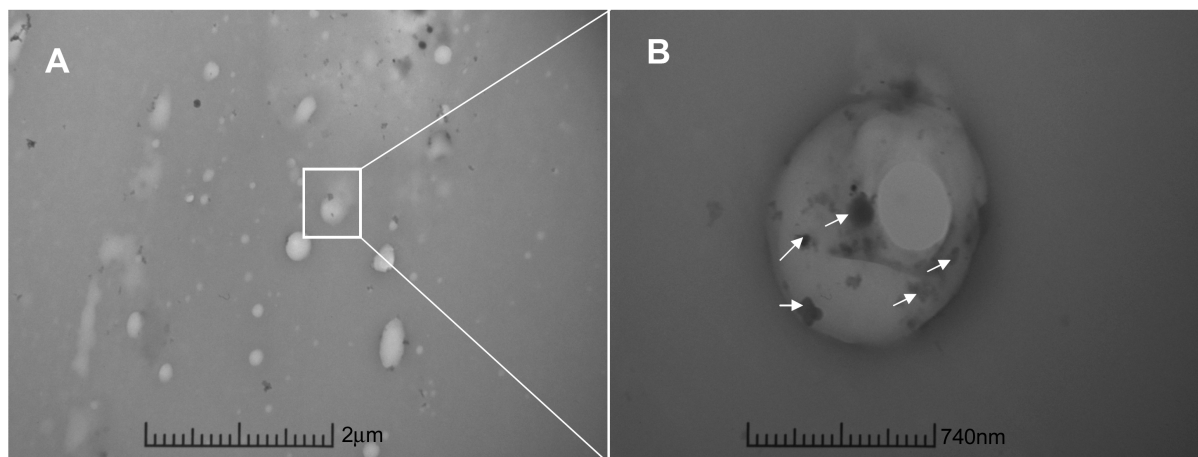
Figure 2-3: Representative TEM micrographs of electrospun scaffold morphology A) TEM micrograph of cross-section of bicomponent nanofibers in the co-axial scaffold. Outer sheath contains gold nanoparticles (small black dots, arrows) to distinguish from inner core. Scale bar = 2μm. B) Further magnification of cross-section of bicomponent nanofiber of co-axial scaffold. Arrows indict gold nanoparticle presence in sheath of fiber. Scale bar = 740nm

confirms the existence of the core-sheath structure in the co-axial scaffolds. Gold nanoparticles were included in the sheath polymer solution to identify the outer sheath. These nanoparticles were visible in the electron micrographs as "black spots." The sheath layer is well delineated and no gold nanoparticles are seen within the core section.

The average fiber diameter and pore size of the various scaffolds are shown in Table 2-1 and Figure 2-4. As shown, the average fiber diameter was significantly smaller for the co-axial scaffolds as compared to the standard scaffold ($P<0.001$). More specifically, the co-axial scaffolds had an average fiber diameter of $0.537\pm0.053\mu$m, while the standard scaffolds had an average fiber diameter of $1.245\pm0.113\mu$m.

Consistent with these findings there were larger pore sizes and more variation of those pore sizes with the standard scaffolds (Figure 2-4). The contact angle of the standard scaffolds was $49.06 \pm 1.77°$, while the co-axial scaffolds had a contact angle of $51.67 \pm 1.10°$. Measurements were taken immediately after the drop was applied to the surface of the scaffold.
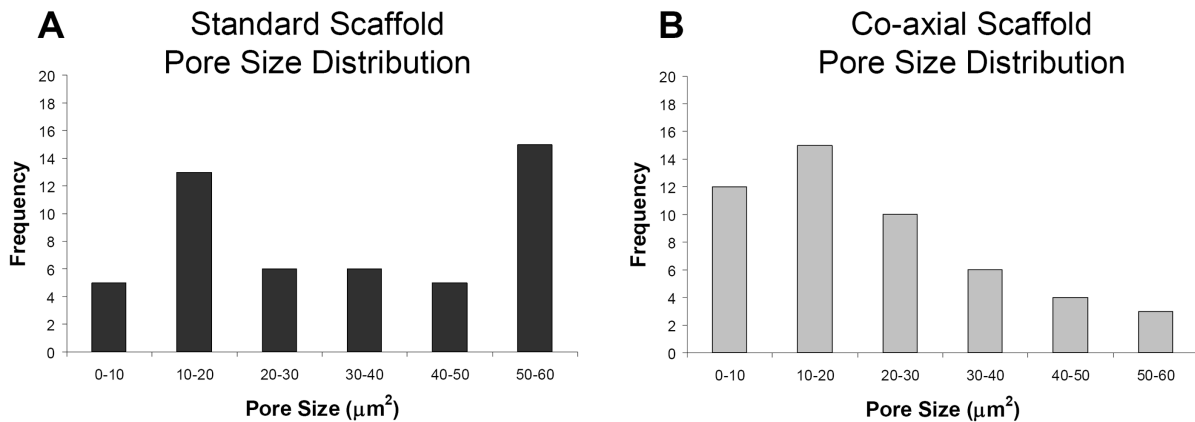
Figure 2-4: Pore size distribution of standard and co-axial scaffolds A) Pore size distribution of standard scaffolds with an average fiber diameter of $1.245 \pm 0.413\mu$m B) Pore size distribution of co-axial scaffold with an average fiber diameter of $0.537 \pm 0.231\mu$m

Within 60 seconds, both scaffolds absorbed the water droplet, respectively. The scaffolds demonstrated similar hydrophilic properties predicting good cell adhesion properties.

B3.3 Mechanical Analysis

The stress and strain properties of the standard versus co-axial scaffolds are shown in Table 2-1. The standard scaffold exhibited the lowest tensile stress value at 0.83 MPa, while the co-axial scaffold exhibited a peak stress of 1.67 MPa. The average strain at peak stress is also shown in Table 2-1. The standard scaffold was only able to withstand a strain of 2.7%, while the co-axial scaffold demonstrated a strain of 36% at peak stress.

Scaffold	Avg. Fiber Diameter (μm)	Young's Modulus (MPa)	Tensile Strength (MPa)	Strain
Standard	1.245 ± 0.113	76.80 ± 14.66	0.83 ± 0.25	0.027 ± 0.013
Co-axial	0.537 ± 0.053	93.36 ± 9.11	1.67 ± 0.47	$0.36 \pm 0.054*$

Table 2-1: Fiber size and mechanical analysis of electrospun scaffolds *$P<0.05$

While the mechanical properties of the two scaffolds demonstrated no significant difference, the co-axial scaffolds were significantly more stable under culture conditions and were able to retain all structural integrity as compared to the standard scaffolds, which lost structural and mechanical integrity after 7 days *in vitro*. As such, the standard scaffolds were not tested as part of a degradation study. After one week in culture, the standard scaffolds could not be physically handled for any volume, mass or tensile measurements (Figure 2-5 and Table 2-2). The co-axial scaffolds exhibited an average volume retention compared to the original volume and mass measured before the samples were subjected to culture media and stored at 37°C of 76.71% after 1 week and 54.37% after 2 weeks in culture-like condition. Likewise the average mass retention was 73.20% after 1 week and 68.30% after 2 weeks in culture-like condition. After 2 weeks the volume and mass loss tapered off and remained steady for a total of 4 weeks. The tensile properties did drop dramatically after 1 week in culture-like condition (Table 2-2):

the modulus of the co-axial scaffolds dropped to 47.92 $\pm$ 2.82 MPa, the tensile strength dropped to 1.41 $\pm$ 0.14 MPa, and the strain dropped to 0.10 $\pm$ 0.018. After 1 week in culture-like condition, the tensile properties remained steady and did not continue to decrease significantly.

	Week 0	Week 1	Week 2	Week 3	Week 4
Young's Modulus (MPa)	93.36 $\pm$ 9.11	47.92 $\pm$ 2.82	47.99 $\pm$ 10.28	46.91 $\pm$ 6.99	40.43 $\pm$ 3.98
Tensile Strength (MPa)	1.67 $\pm$ 0.47	1.41 $\pm$ 0.14	1.42 $\pm$ 0.19	1.63 $\pm$ 0.11	1.29 $\pm$ 0.08
Strain	0.36 $\pm$ 0.05	0.10 $\pm$ 0.02	0.12 $\pm$ 0.05	0.15 $\pm$ 0.02	0.13 $\pm$ 0.01

Table 2-2: Mechanical analysis of co-axial scaffolds over four weeks
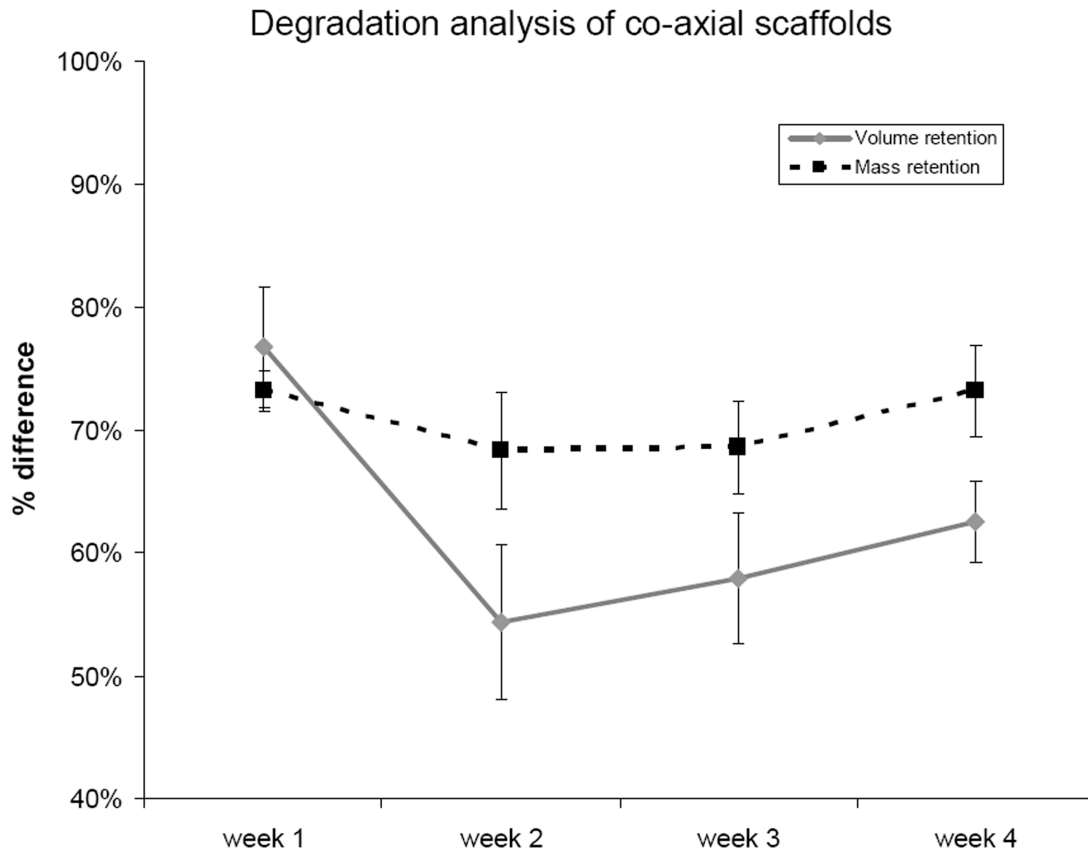
Figure 2-5: Degradation analysis of electrospun scaffolds over four weeks Volume and mass retention of co-axial scaffolds.

<u>B3.4 Cell-Scaffold Interactions</u>

Cell-scaffold interactions were studied *in vitro* by seeding murine NIH 3T3 fibroblasts on both the standard and co-axial scaffolds for analysis at various time points. No additional surface modification of the electrospun scaffolds was necessary to ensure robust attachment of 3T3 cells to the scaffold. After 7 days in dynamic culture, cells began to migrate into the interior of the scaffolds (Figure 2-6). The cells seeded on the standard scaffolds migrated $21.0 \pm 1.4\%$ of the entire scaffold thickness, while cells seeded on the co-axial scaffolds migrated $17.6 \pm 1.1\%$ into the scaffold. After 14 days in culture, the standard scaffolds showed significant evidence of
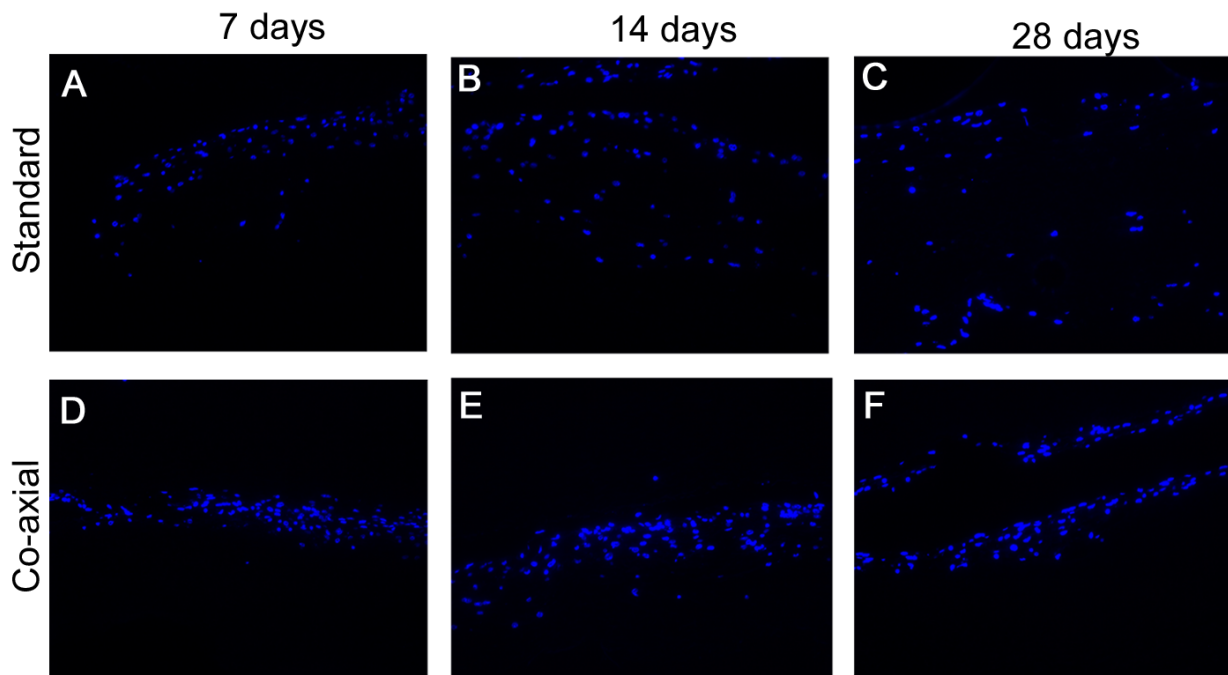
Figure 2-6: 3T3 cells seeded on scaffolds for 7,14, and 28 days Nuclei stained (DAPI) NIH 3T3 fibroblasts cultured on **A-C)** Standard scaffolds, **D-E)** Co-axial scaffolds, scale bar = 100μm.

degradation and had begun to lose their structural and mechanical integrity, thus no cell migration measurements were possible. However the co-axial scaffolds retained their structural integrity and cells migrated $33.5 \pm 1.7\%$ and $31.0 \pm 2.2\%$ after 14 and 28 days respectively.

B3.5 Immunogenicity of Scaffolds
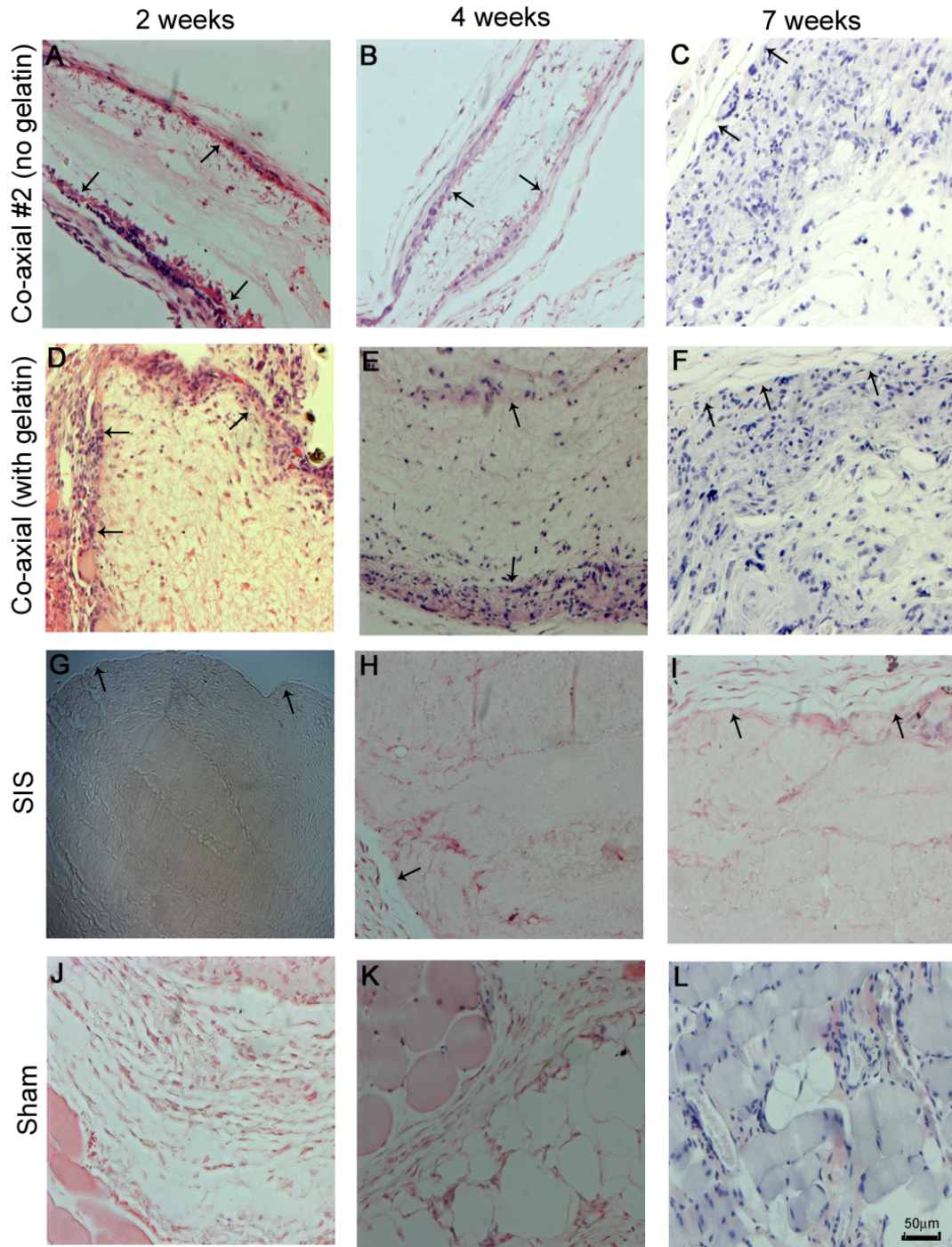
Figure 2-7: H&E staining of implanted scaffolds at 2, 4, and 7 weeks Tissue sections stained with hematoxylin and eosin reveals cellular ingrowth of native cells into electrospun scaffolds (original magnification 20x, scale bar = 50 μm). **A-C)** Co-axial #2 at 2, 4 and 7 weeks respectively. **D-F)** Co-axial at 2, 4, and 7 weeks. **G-I)** SIS scaffolds at 2, 4, and 7 weeks, **J-L)** Sham at 2, 4, and 7 weeks. Arrows indicate scaffold boundaries

To determine the extent of the immune response to the electrospun scaffolds *in vivo,* scaffolds were inserted subcutaneously into mice and H&E staining was done on scaffolds explanted from the animals at 2, 4, and 7 week time points. SIS scaffolds are commonly used for many cardiovascular surgical procedures and were included as a benchmark for immune response levels and cellular infiltration. As depicted in Figure 2-7, nuclei staining is detected at 2 weeks in both electrospun scaffolds (Figures 2-7A and 2-7D), while there is almost no cellular infiltration at any time point for the implanted SIS scaffolds. Because we were unable to detect any cell migration into the scaffold in the SIS scaffolds (Figures 2-7G-I), we did not anticipate finding any cellular ingrowth into the interior of the electrospun scaffolds. However, at later time points, cellular ingrowth of host cells is clearly visible in both the electrospun co-axial scaffolds with and without gelatin. The scaffold boundaries are readily detectable even at the 7 week time point (depicted by arrows, indicating scaffold boundaries), suggesting the slow degradation of the synthetic polymers used in the fabrication of the scaffolds. Immunological response to foreign bodies is often associated with fibrous capsule formation. This is easily detected by trichrome staining, which shows collagen deposition along the longitudinal axis of the implanted scaffold. As shown in Figure 8, relatively small fibrous capsules are seen around all scaffolds (Figures 2-8G-I, depicted as "FC"). Cellular ingrowth is visible at all time points in these scaffolds, suggesting the lack of structure of the fibrous capsules as barriers to the scaffolds. To further characterize the immunological response, we performed an immunohistochemical analysis of the scaffold for IL-6 expression or the presence of CD45 positive cells (Figure 2-9). No CD45 and IL-6 staining was observed suggesting the scaffolds elicit no immunological response.
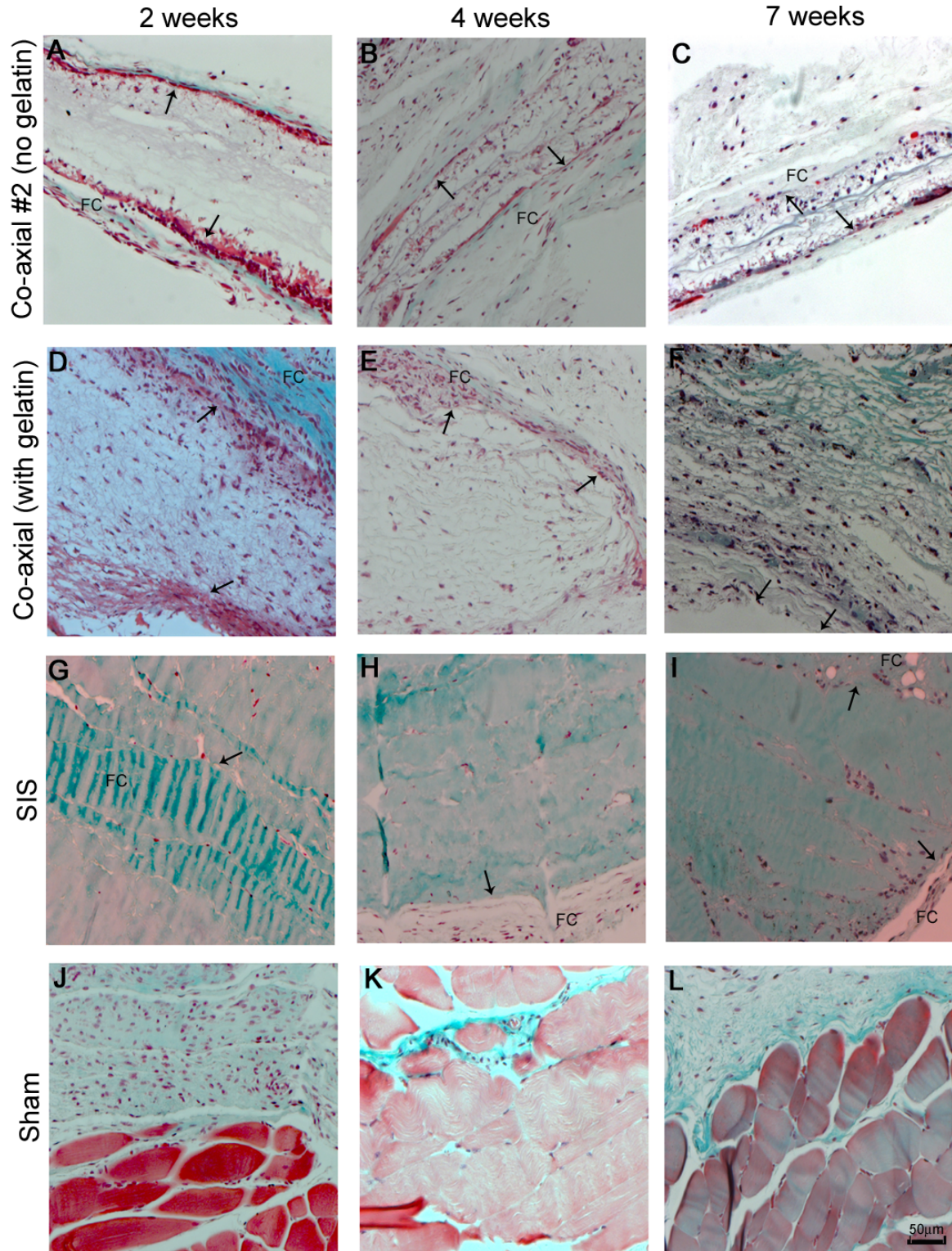
Figure 2-8: Masson's trichrome staining of implanted scaffolds at 2, 4, and 7 weeks Tissue sections stained with Masson's trichrome shows minimal fibrous capsule (FC) formation of electrospun and SIS scaffolds (original magnification 20x, scale bar = 50 µm). **A-C)** Co-axial #2 at 2, 4 and 7 weeks respectively. **D-F)** Co-axial at 2, 4, and 7 weeks. **G-I)** SIS scaffolds at 2, 4, and 7 weeks, **J-L)** Sham at 2, 4, and 7 weeks. Arrows indicate scaffold boundaries.
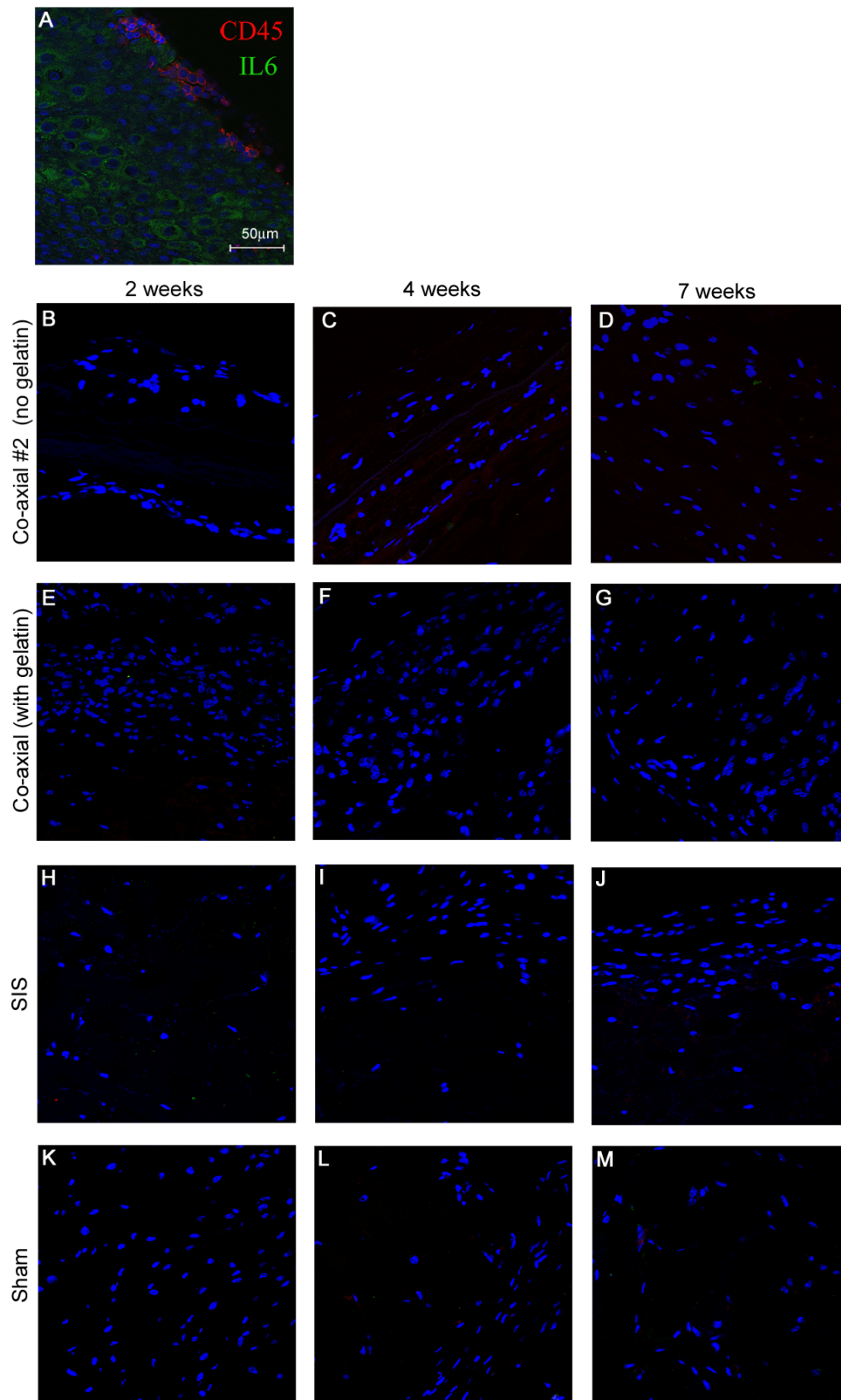
Figure 2-9: Immunofluorescence staining of implanted scaffolds at 2, 4, and 7 weeks Immunohistochemistry staining of implanted scaffolds to detect immunological response by staining for markers CD45 (red) and IL6 (green) and DAPI (blue). **A)** positive control tonsil tissue. **B-D)** Co-axial #2 at 2, 4 and 7 weeks respectively. **E-G)** Co-axial at 2, 4, and 7 weeks. **H-J)** SIS scaffolds at 2, 4, and 7 weeks. **K-M)** Sham at 2, 4, and 7 weeks. Scale bar = 50 μm

B4. Discussion

In the present study we created and characterized hybrid co-axial electrospun scaffolds that incorporated PU and PCL synthetic polymers as well as natural polymers to enhance cell adhesion and migration for future tissue engineering applications. We compared these co-axial scaffolds to conventionally electrospun standard fibrous scaffolds. Co-axial scaffolds, at least theoretically, would incorporate the beneficial properties of all of its components. PU electrospun scaffolds have demonstrated extreme elasticity and better handling characteristics but poor cell adhesion and no degradability (data not shown). In contrast the hybrid polymer solution (10% PCL-10% gelatin) for the outer surface, is inherently stiffer, but has excellent cell adhesion qualities, as determined previously [14]. The mechanical properties of the co-axial scaffold were superior to that of the standard scaffold (Table 2-1). While there are increased values for both the Young's Modulus and tensile strength for the co-axial scaffolds as compared to the standard scaffolds, the differences are not significant. A significant difference exists between the strain properties of the two scaffolds. The co-axial scaffolds exhibit a much higher elastic potential than the standard scaffolds. Overall, the inclusion of PU in our system adds the necessary elasticity to the mechanical properties of our scaffolds. Additionally, the inclusion of PU to the core of the scaffolds helps to maintain the structural and mechanical integrity for long-term studies both *in vitro* and *in vivo*. Likewise, the co-axial scaffolds exhibited superior handling and structural integrity after one week in culture-like conditions (Figure 2-5). The standard scaffolds fell apart during the transfer out of the culture dish to be measured for volume and mass retention. As such, these scaffolds were not included in further degradation or *in vivo* studies. Additionally, after one week of culture-like conditions, SEM image analysis of the standard scaffolds showed no distinguishable fiber boundaries (data not shown). The

morphology of the fibers of the co-axial scaffolds observed through SEM image analysis showed no significant difference in fiber diameter or pore size at each time point (data not shown). The co-axial scaffolds did show signs of degradation after one week in culture. The tensile properties of the scaffolds dropped significantly, but remained steady for the remaining three weeks of the degradation study. The slow degradation was again visible during the *in vivo* studies, as the scaffold borders were still visible in the histological analysis (Figures 2-7 and 2-8).

While both scaffolds have exhibited similar tensile strength, the standard scaffolds demonstrated higher initial cell migration into the interior of the scaffold. However, this migration could not be sustained as the mechanical and structural integrity of the scaffold degraded quickly in aqueous conditions. The longer the scaffolds are submersed in liquid, the less stable they become and gross handling of the scaffolds is impossible without imparting damage to the structure of the scaffold. However, the co-axial scaffolds support less initial migration into the scaffold, but keep their mechanical integrity *in vitro* for at least 28 days. We believe the difference in migration capabilities resides in the differences in fiber diameter and pore sizes. Future work will include fabricating co-axial scaffolds with larger fiber diameters and consequently larger pore sizes (by varying the distance between needle tip and collection plate as well as flow rate), which we will expect to support even better cellular ingrowth.

Scaffolds were implanted subcutaneously to ascertain the extent of immunological response in the murine host. Due to the poor handling and obvious mechanical deterioration of the standard scaffolds over longer time points, we were not able to include these in the *in vivo* study as we were unable to implant the scaffolds in the animals. In addition, we used co-axial scaffolds with no gelatin in the sheath polymer solution to determine if any immunological response would be mounted due to the species difference of the bovine source of gelatin

implanted in the murine host. These scaffolds were denoted "*co-axial #2*" The scaffold morphology was almost identical to that of the co-axial scaffolds with gelatin. Likewise, the mechanical analysis of the co-axial #2 scaffolds without gelatin was very similar to that of the co-axial scaffolds with gelatin (data not shown). SIS scaffolds, which are FDA-approved and used in various surgical procedures routinely, were included as a guideline to demonstrate acceptable immunological response.

Soft tissue response to porous and fibrous biomaterials is influenced, in part, by the microarchitecture of the implant [20-21]. For porous materials like our electrospun scaffolds, effects of change to the pore size have been studied, suggesting that pore size dimensions of at least 10 μm are needed to allow connective tissue ingrowth and to avoid global encapsulation. The fabricated electrospun scaffolds clearly have pore sizes < 10μm (Figure 2-4) and we correctly anticipated the scaffolds to support at least minimal cell migration *in vitro*. Cellular infiltration has rarely been reported on electrospun nanofibers which usually demonstrate a two-dimensional behavior as the distance between layers of fibers is too small to allow cells to migrate through the scaffold without being impinged upon by a layer of fibers underneath the surface layer, thus preventing cellular infiltration. However, as seen in Figures 2-7 and 2-8, cellular infiltration did occur in the interior scaffolds in both the *in vitro* and *in vivo* studies. Interestingly, we observed a greater cell migration from *in vivo* studies than those observed in the *in vitro* studies. Given that the scaffolds were implanted with no cells seeded, the infiltrating cells are clearly those of the murine hosts.

The formation of the fibrous capsule is dependent upon both the physical and mechanical properties of the implanted biomaterial and the thickness of the fibrous capsule can have a significant influence on the functionality of the implant. Scaffolds with smaller pore sizes and a

high surface area-to-volume ratio are more likely to induce dense fibrous capsule formation, thus the thickness of the fibrous capsules can be greatly reduced when implants are more porous with larger pore sizes, in turn promoting greater cellular ingrowth [22-23]. As we observed in Figure 2-8, the fibrous capsule formation around the periphery of both our fabricated electrospun scaffolds and commonly used, commercially available SIS scaffolds was minimal (as depicted by "FC" in Figure 2-8). The presence of native cells in the interior of the scaffold with a small fibrous capsule formation suggests the bovine source of gelatin in the sheath component of the electrospun scaffolds does not elicit a strong immunological response.

As seen in Figure 2-9, we observed a limited immune response with nearly no macrophage or common immunological marker present. Interleukin (IL) 6 was not clearly detected at any of the time points of the implanted electrospun scaffolds. Similarly, CD 45 a common immunological marker was not detected in any of the implanted scaffolds. We can conclude that not only does the bovine source of gelatin not cause an immune response, but neither do the scaffolds themselves. We can also conclude the architecture of the electrospun scaffolds readily supports cell migration and can be used for further tissue engineering applications.

B5. Conclusion

ECM consists of a complex network of structural and regulatory proteins *in vivo*. The multifunctional nature of natural ECM will need to be considered in the design and fabrication of tissue-engineered scaffolds. The introduction of a protein/polymer hybrid such as PCL-gelatin or a co-axial system to include a core of PU and a sheath of PCL-gelatin provides both favorable mechanical properties and binding sites for cell attachment and proliferation. We anticipate these

co-axially electrospun scaffolds to prove extremely useful for tissue engineering applications, particularly those applications that will be used under dynamic conditions. The added elasticity and handling properties from the inclusion of PU to the core of the scaffolds will be extremely beneficial for future cardiovascular tissue engineering applications. We believe electrospinning with natural and synthetic polymers can be used to produce tissue-engineered scaffolds for various applications. These scaffolds better recapitulate key features of the native ECM including its mechanical and biochemical properties. We can conclude the physical properties of our electrospun scaffolds are not only adequate in both fiber diameter and pore size, but will encourage and promote cellular migration and proliferation within the interior of the scaffold. By detecting robust native cell migration into the interior of the scaffold and observing minimal fibrous capsule formation and immunological response *in vivo*, we are confident our electrospun co-axial scaffolds will support further tissue engineering studies.

C. Hyaluronan-based three-dimensional microenvironment potently induce cardiovascular progenitor cell populations

C1. Introduction

The mammalian heart is believed to originate from a common progenitor cell. CPCs further differentiate into the three main cardiovascular lineages: endothelial cells, smooth muscle cells and cardiomyocytes. Using our mES cell model, we have isolated CPCs using Flk-1 (also known as KDR), a cell surface marker for VEGF-R2. Endogenous CPCs are found in anatomical clusters in the developing right atria, ventricle and outflow tract. These clusters are suggestive of a stem cell niche. Niches are 3D microenvironments the regulate self-renewal, proliferation, and differentiation through cell-cell and cell-matrix interactions [24,25]. This makes the role of the native ECM surrounding the CPC niche important to understand.

Hyaluronic acid (HA) is one of the major components found in ECMs throughout the body. It is a linear, high molecular weight polymer with visco-elastic properties [26]. HA is involved in many biological processes, including wound repair, inflammation, and metastasis. The carboxyl group of HA is a major target site for further derivatizing. HA-based hydrogels can be particularly useful to encapsulate various cell types to determine the effects of a 3D microenvironment.

Previously, we have established that the ECM protein collagen IV induces a greater amount of CPCs than other proteins [25]. Additionally, incorporating a modified 2D substrate, a nanofibrous scaffold, into the culture system further induces a CPC population [27]. In order to further examine the full effects of a 3D microenvironment, we will develop a 3D *in vitro* culture system using a HA-based hydrogel.

C2. Materials and Methods

C2.1 Mouse ES cell culture

Murine ES v6.5 cells were purchased from Open Biosystems and maintained in an undifferentiated, feeder-free state in leukemia inhibitory factor (LIF) supplemented medium (Knockout Dulbecco's modified Eagle's medium, Invitrogen, Carlsbad, CA USA) with 15% ES-FBS (Invitrogen), 0.1mM β-mercaptoethanol, 2mM L-glutamine (Invitrogen), 0.1mM nonessential amino acids (Invitrogen), 1000U/mL recombinant LIF (Chemicon, Temecula CA USA), and 2mM HEPES (Invitrogen). Cells were cultured on gelatin-coated (0.1% gelatin in PBS, coated for 2h at 37C) T-75 flasks at 37°C, 5% CO2 in a humidified incubator. Cells were passaged every 2-3 days to maintain an undifferentiated state.

For initial differentiation assays, mES cells were introduced to collagen IV flasks (BD Biosciences, San Jose, CA USA) and maintained in α-minimum essential medium (α-MEM) (Invitrogen) supplemented with 10% ES-FBS (Invitrogen), 0.1mM β-mercaptoethanol, 2mM L-glutamine (Invitrogen), 0.1mM nonessential amino acids (Invitrogen), and 2mM HEPES (Invitrogen). After five days, cells were harvested for FACS analysis, fixed for immunostaining or RNA was collected for PCR analysis.

C2.2 Hydrogel formation

HA-based hydrogels were purchased from Glycosan Biosystems (subsidiary of BioTime, Alameda, CA USA) and crosslinked with a PEGSSDA crosslinker. The hydrogel consists of a hyaluronan-backbone and thiolated gelatin. The PEGSSDA crosslinker allows for easy dissolution of the hydrogel at various time points. To encapsulate mES cells in the hydrogel microenvironment, the manufacturer's protocol was followed. Briefly, the two components of

the hydrogel backbone were dissolved in the provided diH2O and allowed to homogenize for 30min on a rocker plate. mES cells were collected from the culture flask and centrifuged. The cell pellet was then resuspended in the hydrogel backbone components. The cross-linking agent, PEGSSDA is then introduced at 4:1 ratio to the backbone components. Gelation occurs within 30minutes from the cross-linker introduction. Equal volume of media (α-MEM) is added to the hydrogel after 2h. In order to dissolve the hydrogel for further cellular analysis after 5 days, a reducing agent is added to the hydrogel. 40mM L-glutathione solution is added directly to the hydrogel to break up the disulfide bonds formed from the cross-linking agent. After 1-2hrs, the hydrogel-L-glutathione mixture is collected and centrifuged to obtain a cell pellet. The cells are then processed for FACS analysis, RNA collection, or cytospin imaging.

C2.3 Live/Dead Cell Assay

Live/Dead cytotoxicity assay was performed using the kit purchased from Invitrogen specific for mammalian cells and the manufacturer's recommended protocol was followed. Briefly, a solution of sterile PBS with 1:1000 Calcein AM and 1:500 Ethidium homodimer-1 was made. Cells were washed thoroughly with sterile PBS and the live/dead solution was added to the dish. Imaging immediately followed.

C2.4 Fluorescence-activated cell sorter analysis (FACS)

Cells were harvested from both standard 2D and 3D (hydrogel) culture, pelleted via centrifugation, washed in PBS supplemented with 1% ES-FBS and 2% BSA and stained with purified rat anti-mouse Flk-1 antibody (BD Biosciences). The cells were gated by forward scatter (FSC) versus side scatter (SSC) to eliminate debris. A minimum of 10,000 events were counted

for each analysis. All analyses were performed using a Becton Dickinson FACScan analytic flow cytometer (BD Biosciences) with FCS Express software (DeNovo Software, Thornhill, Ontario, Canada) at the UCLA Flow Cytometery Laboratory.

C2.5 Quantitative real-time polymerase chain reaction (PCR)

Total RNA was extracted from cells using TRI Reagent (Sigma-Aldrich) according to the manufacturer's instructions. First-strand cDNA was generated from RNA by using the Quantitect Reverse Transcription kit (Omniscript, Qiagen, Valencia, CA USA). Real-time quantitative PCR was conducted using the ABI PRISM 7900 Sequence Detection System (TaqMan, Applied Biosystems, Carlsbad, CA USA) with the UCLA GenoSeq Core. PCR amplicons were detected by fluorescent detection of SYBR green (QuantiTect SYBR green PCR kit, Qiagen). Data was analyzed using the ΔΔCt method, using ribosomal protein S26 as a stable reference gene for normalization control. Primers used were purchased from Qiagen (QuantiTect Primer Assay).

C2.6 Immunofluorescent staining

mES cells at both undifferentiated and partially differentiated states were fixed using 4% paraformaldehyde in PBS for 20min and rinsed with PBS. All samples were then washed with 0.05% Tween-20 in PBS three times, 5min each, followed by a 15min wash of 0.1% Triton-X in PBS. Three more washes of 0.05% Tween-20 in PBS for 5min each followed. A blocking solution of 1% BSA and 2% goat serum in PBS was used on the cells for 30min followed by incubation with the primary antibody overnight at 4°C. The samples were then washed in PBS. A secondary antibody with Alexa Fluor 488 or 546 conjugation was then applied and incubated at room temperature for 30min. After several washes of fresh PBS, cells were then counterstained

73

with 4'-6-diamidino-2-phenylindole (DAPI) followed by anti ProLong Gold antifade mounting medium (Molecular Probes, Carlsbad, CA USA). Digital images were acquired using a Leica DM IRB inverted microscope system equipped with 20x (0.40 numerical aperture (NA)) and 40x (0.75 NA) objective lenses (Leica Microsystems Inc, Bannockburn, IL USA).

C2.7 Statistical Analyses

All results are presented as mean values $\pm$ standard error of mean (SEM). Statistical significance was assessed by t-test and ANOVA as necessary. $P< 0.05$ was defined as statistically significant.

C3. Results

C3.1 Cells maintained in HA-hydrogel survive

Hyaluronan hydrogels have been studied previously [28,29] and in particular, Hystem-C hydrogels have been characterized [30,31]. We have further investigated the biocompatibility of the encapsulated microenvironment of the hydrogel with mES cells. Using a live/dead cytotoxicity assay, we can see in Figure 2-10 that the environment of the hydrogel supports mES cell growth. We did observation a slower proliferation rate (data not shown) of the cell encapsulated within the hydrogel as compared to cells maintained on gelatin- (for control) and collagen IV-coated dishes in 2D culture conditions. Additionally, we observed different morphology of cells in 2D culture versus 3D culture. Cells supported in 2D culture (Figure 2-10) exhibit a more cluster or colony phenotype, characteristic of stem cell culture, while cells encapsulated in the 3D hydrogel (Figure 2-10C) are maintained in a more single cell suspension-

like phenotype. We also found a larger number of cells in the 2D culture dishes compared to the cells suspended in the hydrogel, which is evident from the images in Figure 2-10.

C3.2. CPC induction in both 2D and 3D microenvironments

We have previously shown that collagen IV in 2D culture conditions induces a greater CPC population and that the addition of an electrospun scaffold further enhances induction of a Flk-1^{+} CPC population [25,27]. While electrospun scaffolds can be classified as a 3D microenvironment, it can take mES cells up to seven days to migrate to the interior of the scaffold (data not shown). In order to investigate the true 3D effects, we encapsulated mES cells
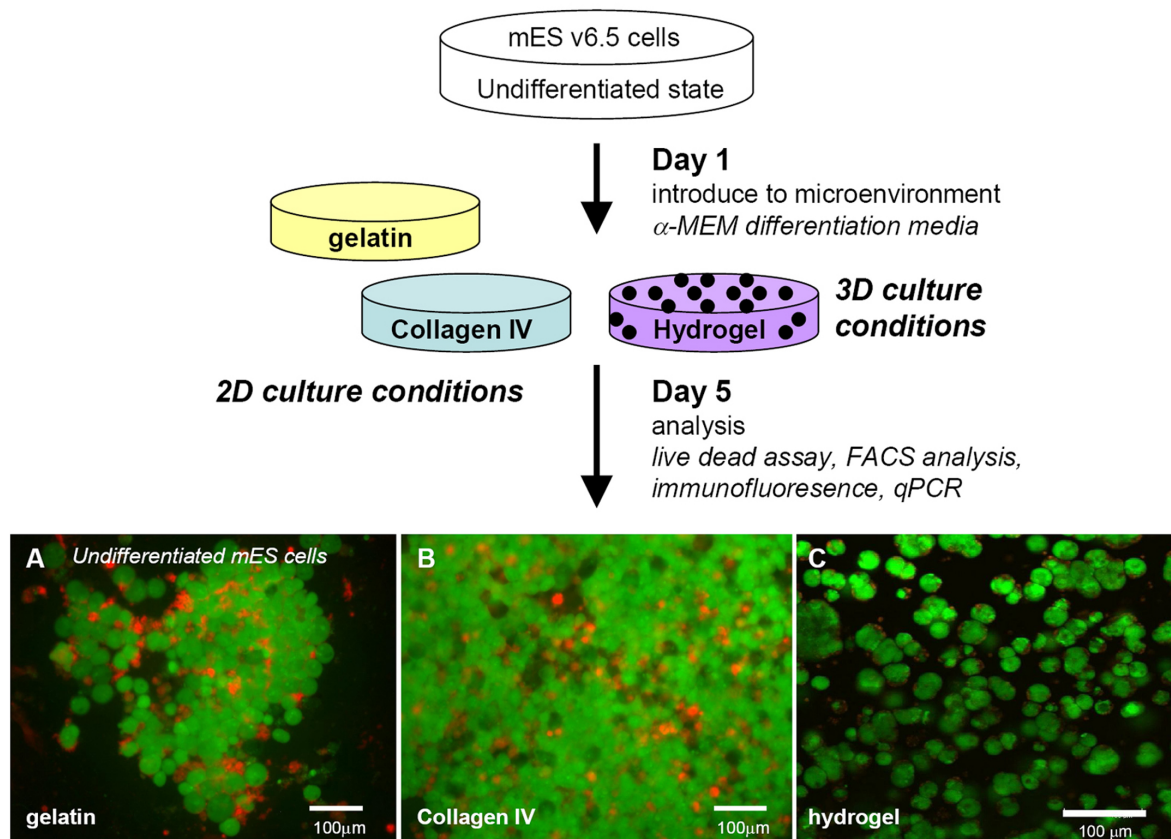
Figure 2-10: Schematic of experimental design mES cells are cultured on either 2D or 3D conditions in differentiation media for five days. mES cells are then evaluated via a cytotoxicity assay, fixed for immunofluorescence, or harvested for FACS analysis and PCR. mES cells on 2D culture conditions with gelatin (undifferentiated) (A) or collagen IV (B) show a high amount of live (green) cells compared to dead cells (red) at 5 days. mES cells encapsulated in the Hystem-C hydrogel (C) also show a high number of live cells.

75

in the Hystem-C hydrogel system. After 5 days, we isolated cells for FACS analysis and checked for CPCs using the Flk-1 surface marker We found that the addition of the 3D microenvironment greatly enhances CPC induction (Figure 2-11). After 5 days in differentiation media, undifferentiated mES cells (0.24 ± 0.04% Flk-1^{+}) expressed less than 1% Flk-1^{+} cells. Collagen IV, the protein previously shown to have the highest capacity to induce a Flk-1^{+} CPC population in 2D conditions [25], had 5.45 ± 0.66 % Flk-1^{+} cells, while 11.32 ± 1.34 % cells encapsulated in the Hystem-C hydrogel expressed the CPC marker. The hydrogel environment induced a significantly higher population of CPCs compared to both undifferentiated mES cells and those cultured on collagen IV-coated 2D dishes.
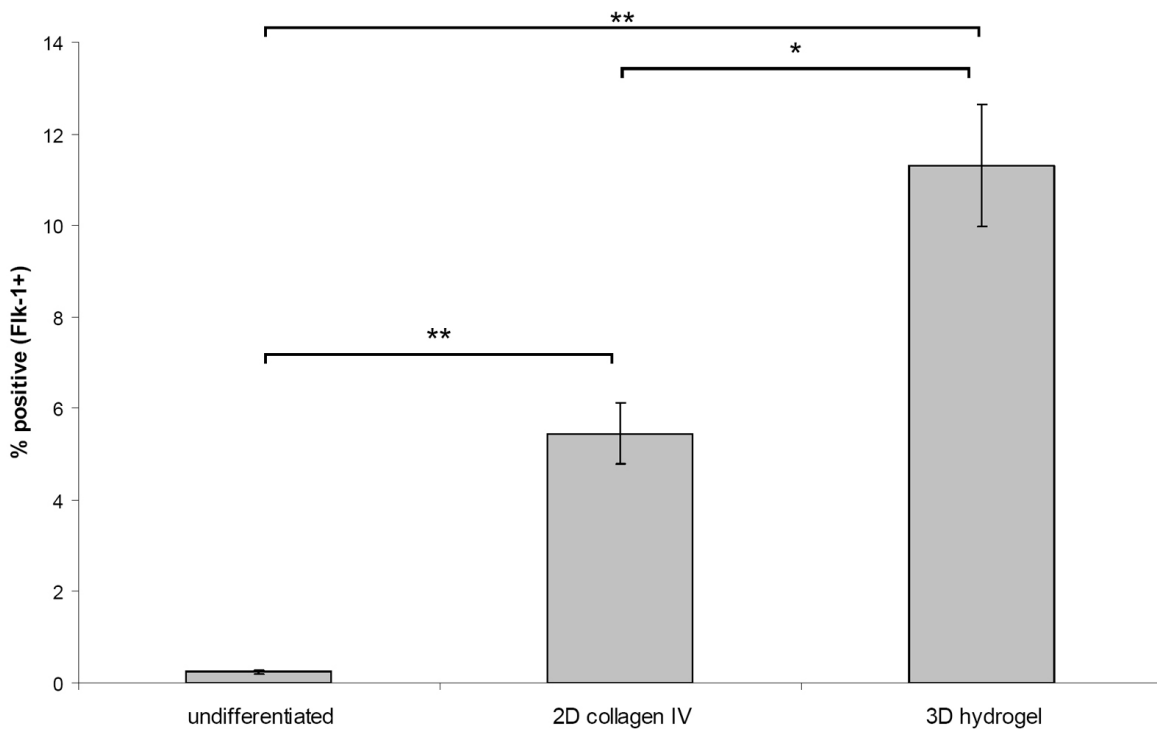
Figure 2-11: FACS analysis of Flk-1^{+} CPC population FACS analysis of Flk-1^{+} cells from undifferentiated mES cells. mES cells cultured on collagen IV-coated 2D dishes and encapsulated in the 3D hydrogel were harvested for FACS analysis after five days in differentiation media. *P-value < 0.005, **P-value <0.0001.

We also performed immunofluorescence staining for selected CPC markers, including Nkx2.5, Isl-1, c-kit, and Flk-1. We used cytospin to stain cells encapsulated within the 3D hydrogel. As seen in Figure 2-12, there is no signal for any CPC markers on the undifferentiated

mES cells (Figure 2-12A,D,G). Cells maintained in differentiation media on 2D collagen IV-coated dishes exhibited expression for Nkx2.5 and Isl1 (Figure 2-12B), as did the cells encapsulated in the 3D hydrogel (2-12C). Encapsulated cells in the 3D hydrogel also displayed positive staining for c-Kit and Isl-1 (2-12F) as did those cells cultured on collagen IV in 2D
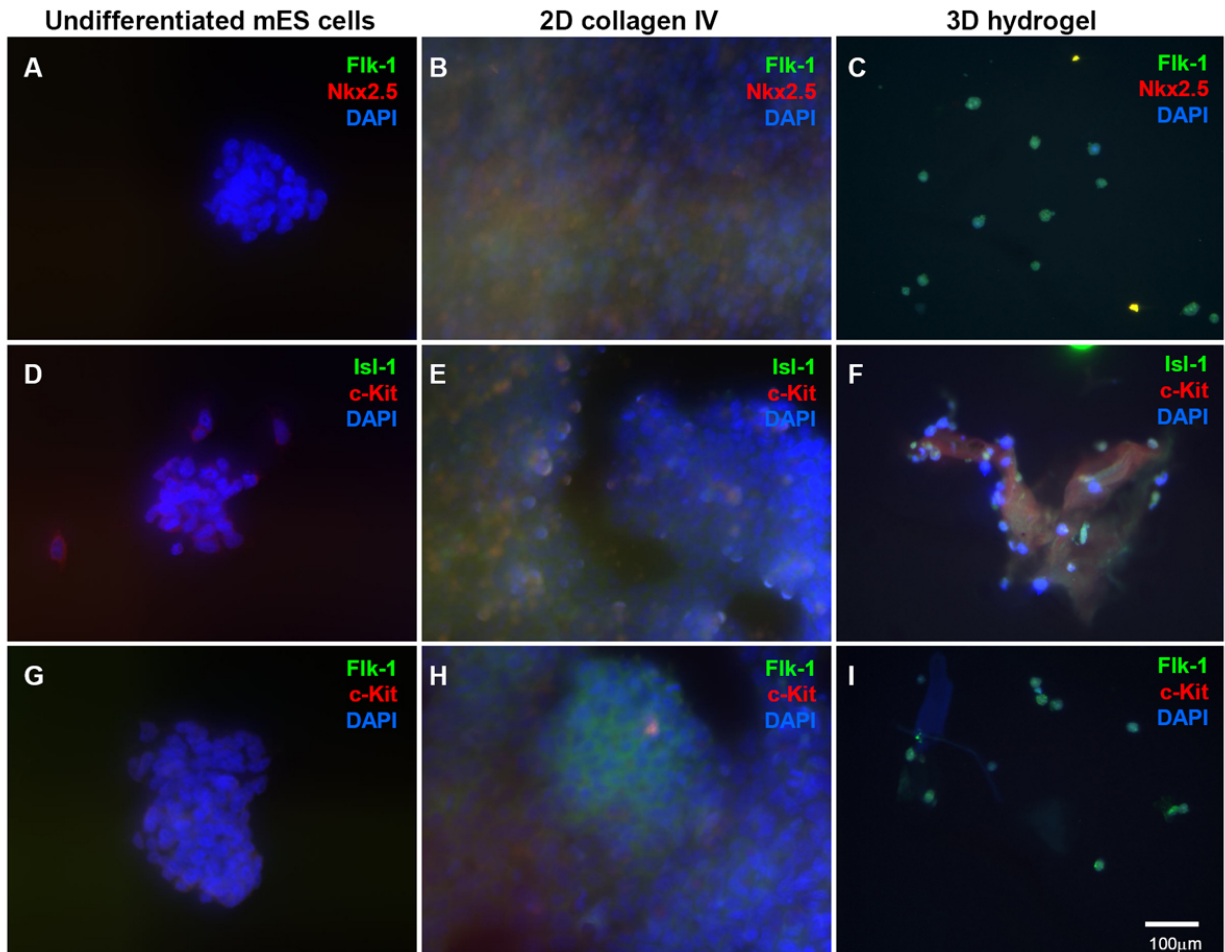
Figure 2-12: Immunofluorescence of CPCs mES cells cultured in 2D culture conditions were immunostained for CPC markers after five days in differentiation media. Undifferentiated mES cells are shown in the first column of panels (A, D, G). Cells cultured on 2D collagen IV-coated dishes are shown in the middle column of panels (B, E, H). Cells encapsulated in the 3D hydrogel are shown in far right column of panels (C, F, I). CPC markers Flk-1 (green) and Nkx 2.5 (red) are shown in the top row (A, B, C). Isl-1 (green) and c-Kit (red) are shown in the middle row (D, E, F) and Flk-1 (green) and c-kit (red) are shown in the bottom row.

conditions (2-12E). Additionally, cells cultured on both 2D collagen IV dishes and the 3D hydrogel both exhibited signals for Flk-1 and c-Kit (2-12H,I). It is notable that the cells maintained on the 2D collagen IV-coated dishes were more plentiful and were almost completely

confluent by day five. Cells maintained in the hydrogel maintained a single-cell morphology, similar to that seen in Figure 2-10C.

To confirm the results we observed from the immunostaining and FACS analysis, we performed qPCR (Figure 2-13). Using undifferentiated mES v6.5 cells as our comparison group, we observed relatively no difference between undifferentiated mES cells and cells cultured on 2D collagen IV for one of the CPC markers Isl1 (Figure 2-13D). mES cells cultured in 2D conditions on collagen IV showed a higher expression for the VEGF receptor surface markers, which are known CPC markers: Flk-1 (5.06 ± 5.01 fold expression, 2-13A), Flt1 (7.85 ± 7.77 fold expression, 2-13B), and Flt4 (0.23 ± 0.13 fold expression, 2-13C). Additionally, we examined the cardiac development genes Nkx2.5 (2.39 ± 1.22 fold expression, 2-13D) and Isl1 ($0.31+0.04$ fold expression, 2-13E). However, when we encapsulated cells in the 3D hydrogel environment, we observed significantly higher expression of the two CPC markers examined. Isl1 expression was increased dramatically when encapsulated in the hydrogel (390.73 ± 70.10) compared to 2D collagen IV (0.31 ± 0.04). The other CPC marker, Nkx2.5 was also significantly increased in the

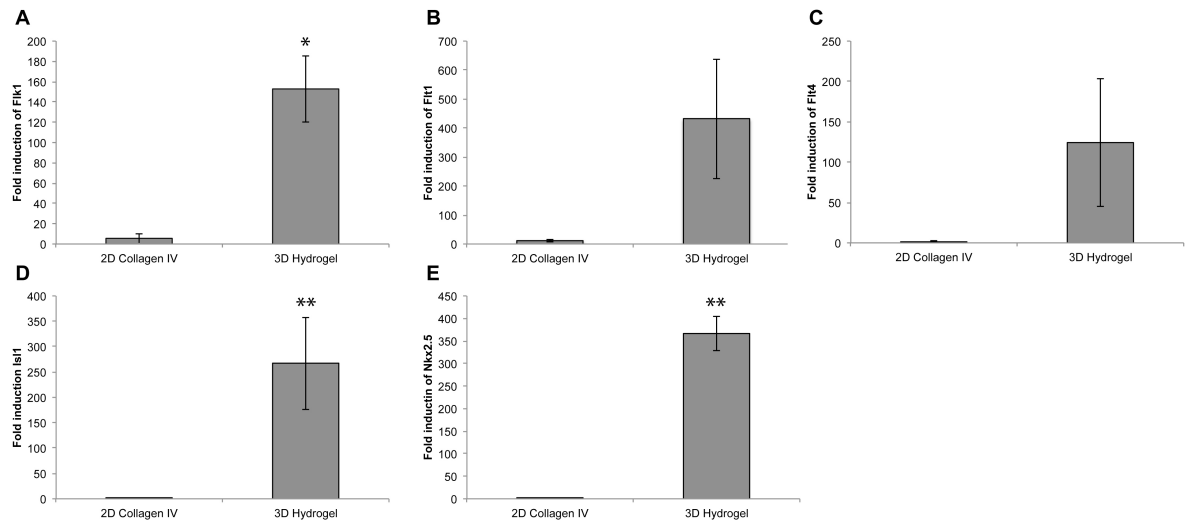***Figure 2-13: qPCR analysis*** qPCR was performed on RNA collected from 2D and 3D culture conditions after five days in differentiation media. The $\Delta\Delta$Ct comparison method was used to calculate the fold-level expression with the undifferentiated mES cells as the reference group. CPC markers Flk-1 (A), Flt1 (B), Flt4 (C), Isl-1 (D), and Nkx2.5 (E) were evaluated. N=3 *p-value < 0.05, **p-value < 0.01

3D hydrogel (147.56$\pm$37.86) compared to 2D collagen IV (2.39$\pm$1.22). Additionally, we observed about 30x significantly higher expression in 3D hydrogel than the 2D collagen IV-cultured cells for Flk-1 (152.50+32.73 fold expression, 2-13A). We also observed a marked increase in expression for Flt1 (338.35$\pm$205.45 fold expression, 2-13B) and Flt4 (35.37$\pm$30.41 fold expression, 2-13E).

C4. Discussion

The role of the ECM within a stem cell niche has been widely studied; however, the role of the ECM within the cardiovascular niche is unknown. Recently, it has been shown that the addition of ECM proteins to an *in vitro* culture contributes to the induction of a CPC population [25,27]. Here, we demonstrate that the addition of a 3D element further enhances that induction.

Many factors are known to regulate cell fate decisions, including growth factors, components of the ECM, neighboring cells, and the physical characteristics of the niche. The idea of a stem cell niche as a specialized microenvironment was first introduced by Scholfield almost 35 years ago [24]. The stem cell niche is defined as an *in vivo* microenvironment that regulates stem cell survival, self-renewal, and differentiation. The niche also regulates interactions between stem cells and growth factors, cell-cell contacts, and cell-matrix adhesions [32]. These interactions are extremely important to understand not only how stem cells terminally differentiate, but also maintain their multipotent state while residing within the confines of the niche. The hematopoietic stem cell niche has been widely studied for many years [32]. One way to induce differentiation is to add growth factors to the culture medium, additionally growth factors can be added to culture substrates [33]. The use of feeder cells in human ES cell cultures suggests that paracrine effects are equally important.

Recently, researchers have begun to examine the physical characteristics of the niche environment [30]. The ECM of the niche mediates cell-cell and cell-matrix interactions, which are extremely important to sell-fate regulation. Various ECM proteins have been used in ES cell culture. Notably, Matrigel is used commonly, which is a milieu of common ECM proteins. We have previously identified the importance of collagen IV to induce a CPC population from a murine ES cell population [25].

The stem cell niche also provides a 3D structure to the microenvironment. Within this environment, different forces are imposed on the cells. In efforts to replicate these forces, substrates have been made of varying stiffness. Harder surfaces promote a terminal differentiation towards an osteogenic lineage [34,35]. Softer surfaces promote differentiation down a soft tissue lineage. Neurons, in particular, seem to respond favorably to softer surfaces with the addition of the appropriate chemical cues [36]. It has also been shown that simply incorporating a mechanistic strain to the cell culture can induce a smooth muscle differentiation pathway [37]. This type of stiffness has been observed in the cardiovascular field. Fibrotic scars that develop after myocardial infarction create local rigid surface. This can create a signal to surrounding cells and has been shown to induce bone formation in the heart [38-40]. Future work will including examining the effects of the modulus of the 3D hydrogel on the cardiovascular commitment of mES cells.

Research has turned to synthetic materials to attempt to recapitulate the native stem cell niche using tissue engineering approaches. Cell shape has been indicated as a regulator of cell fate. In an effort to control shape, researchers have modified cell culture surfaces with various nanotopography. Cell alignment has been observed on highly porous 3D polystyrene substrates as compared to traditional 2D surfaces [41]. Alignment has also been observed along the

direction of grooves formed in laminin [42]. We have also shown that incorporating nanostructures into a culture can influence cellular behavior [43]. Additionally, cellular morphology is greatly different between *in vitro* 2D culture and *in vivo* 3D native tissue. The addition of a 3D component has become more widespread in many research groups. Study of ES cells often leads to the development of embryoid bodies, which are a 3D structure that spontaneously forms. This is further evidence of the importance of incorporating a 3D aspect into the study of stem cells.

In an effort to study the 3D effects of the niche microenvironment, we have opted to use the Hystem-C hydrogel. Previously we have worked with nanofibrous scaffolds. However, we observed that cells will take on average seven to 10 days to migrate into the interior of the scaffold. As we wanted to evaluate a shorter time point and a true 3D microenvironment, we decided to use a hydrogel system. In particular, this hydrogel system has been used in many stem cell studies, including a recent study to determine the effects of progenitor cells delivered *in vivo* following a cardiovascular insult.

In this study, we demonstrate the ability of a hyaluronan-based 3D hydrogel to potently induce a Flk-1^{+} CPC population. We have shown that not only does the addition of a ECM protein known to be present within the endogenous CPC niche enhances the development of a CPC population, but incorporating a 3D aspect to the culture model further augments the CPC population. With the rise of stem cell therapies, developing a useful multipotent progenitor cell for potential treatments of cardiovascular disease remains elusive. Such progenitor cell populations exist in very small populations endogenously and *in vitro* work yields low differentiation potential. This study presents an opportunity to scale up the induction of cardiovascular progenitor cells for potential therapeutic use. Additionally, this study highlights

the importance of three-dimensionality when studying not stem cell niches. The addition of a 3D element presents a more *in vivo*-like cell culture model for the laboratory setting. Future studies will include further characterization of the contributing factors of the 3D hydrogel to both maintaining multipotency of the progenitor cell population and external factors that lead to further cell differentiation.

C5. Conclusion

We show that 3D of mES cells greatly enhances induction of Flk-1^{+} CPCs. We have shown that cells encapsulated in a 3D system exhibit significantly higher expression of CPC markers than cells maintained in traditional 2D cell culture systems. This evidence provides important understanding the impact of the ECM on the stem cell niche.

D. Stem cell extracellular matrix interactions in three-dimensional system via integrins

D1. Introduction

Cells of all type interact with the ECM via integrins. Integrin receptors are the primary receptors for ECM adhesion and provide a transmembrane link between the ECM and actin cytoskeleton [44]. Integrins are non-covalently linked, heterodimeric molecules containing both an α and β subunit. To date, 19 α-integrin and 8 β-integrin subunits have been identified, leading to 25 $\alpha\beta$ heterodimers, which have been seen in almost every cell type [45]. Integrins are known to control many cellular processes, including mediating the attachment of cells to the ECM. They can act both directly and indirectly on signal transduction pathways, activating signals from both inside and outside of the cell [46].

Adhesion of ES cells to ECM proteins is essential for differentiation [47-49]. Undifferentiated ES cells express a subset of integrins, some of which may be up- or down-regulated during differentiation, indicating the potential importance of integrins in maintaining an undifferentiated ES cell state [50-52]. Different ES cell lines have reported high expression levels of integrin subunits $\alpha5$, $\alpha6$, αv, $\beta1$, and $\beta5$ [47,53]. Additionally, it has been shown that $\beta1$-associated subunits $\alpha1$, $\alpha2$, $\alpha3$, $\alpha6A$, and $\alpha7$ are regulated developmentally [54,55]. Collagen IV is known to associate with $\alpha1$, $\alpha2$, $\alpha3$, αV, $\beta1$ and $\beta8$ while laminin is known to associate with $\alpha1$, $\alpha2$, $\alpha3$, $\alpha6$, $\alpha7$, $\alpha10$, αV, $\beta1$, $\beta3$, $\beta4$ and $\beta8$. The following integrin subunits have been identified to interaction with fibronectin: $\alpha2$, $\alpha3$, $\alpha4$, $\alpha5$, $\alpha8$, $\alpha9$, αV, $\beta1$, $\beta3$, $\beta5$ and $\beta7$. Vitronectin is known to associate with $\alpha8$, αV, $\beta1$, $\beta3$, and $\beta5$ integrin subunits [56-60]. Not a lot is known about integrin expression in stem cells. Integrin expression in undifferentiated and

partially differentiated stem cells has not been well characterized, nor has the integrin contribution to differentiation.

In vivo, endogenous stem cells reside in tissue-specific anatomically defined clusters called "niches" [24]. Within the stem cell niche, cell fate is thought to be controlled both spatially and temporally, as well as through cell-cell and cell-matrix interactions [61]. Those cell-matrix interactions are in turn mediated via integrins. CPCs from fetal heart samples are thought to reside in niches found in the developing right atria, ventricle and outflow tract [62-65]. CPCs from ES cell models have been shown to further differentiate into the main cardiovascular cell lineages: vascular endothelial cells, vascular smooth muscle cells, and cardiomyocytes. CPCs from an mES cell model can be identified by various markers, specifically Isl-1, Nkx2.5, and Flk-1 (also known as KDR) [62,66,67]. Currently, the limitations in this field of study include understanding what keeps progenitor cells to remain in the niche and what causes those cells to leave the niche and continue differentiation?

In order to recreate the three-dimensionality of the CPC niche, we have fabricated electrospun scaffolds. Electrospinning in particular has been an effective method to create biomimetic scaffolds [68]. Electrospun scaffolds are nonwoven fibrous meshes consisting of a large network of interconnected pores that is conducive to tissue ingrowth. The small diameter of the fibers and the high surface area to volume ratio in electrospun scaffold promote cell adhesion and migration [12,69]. Electrospun scaffolds can be created from a variety of both synthetic and natural polymers, including poly(ε-caprolactone) (PCL), poly(lactic acid), poly(glycolic acid), poly(lactide-co-glycolide), poly(urethane), collagen, elastin, fibronectin, chitosan, and alginate [9,10,12,25,27,69-72]. Electrospun scaffolds have been used successfully in a variety of tissue engineering applications.

In particular, recent studies have demonstrated the ability of ECM proteins to recapitulate the cardiovascular stem cell niche. We have shown that collagen IV induces a cardiovascular progenitor cell (CPC) population [25] and that adding a vitronectin 3D microenvironment further induces a CPC population [27]. We have previously developed a biomaterial scaffold system to mimic a 3D microenvironment [27,72]. In this study, we have characterized how both a 3D microenvironment and ECM proteins affect integrin expression. We found that integrin expression changes significantly as mES cells begin to differentiate and causes significant differences in cell adhesion in 2D and 3D culture when exposed to different ligands (ECM proteins).

D2. Materials and Methods

D2.1 Mouse ES cell cultures and *in vitro* differentiation

Murine Flk-1 GFP-labeled embryonic stem cells (mES) were a kind gift from Dr. W. Robb MacLellan's laboratory at the Department of Medicine/Cardiology at the University of California, Los Angeles. mES cells were maintained in a feeder-free condition in ESGRO CompleteTM medium (Chemicon, Temecula, CA USA) in a humidified incubator at 37C and 5% CO_2. Cells were expanded for two passages before being used in experiments.

For differentiation assays, mES cells were introduced to a 2D or 3D culture environment. Conventional monolayer culture techniques in a standard tissue culture dish is further denoted as '2D' while cultures with the inclusion of an electrospun scaffold are denoted as '3D' culture conditions. 2D culture included mES cells being cultured on plates coated with collagen type IV (ColIV, 5µg/cm², BD Biosciences, San Jose, CA USA), vitronectin (50ng/cm², Chemicon), fibronectin (5µg/cm², Sigma), laminin (5µg/cm², BD Biosciences), Matrigel (4µg/cm², BD

Biosciences), or gelatin (0.1% gelatin in PBS). Coating concentrations were based upon manufacturer's recommendation and what we have used previously [25,27]. Undifferentiated mES cells were detached from the culture dishes and transferred to protein-coated dishes for 2D culture or protein-coated scaffolds for 3D culture. Cells were maintained in differentiation media, α-Minimum Essential Medium (α-MEM, Invitrogen, Carlsbad, CA USA) supplemented with 10% ES-FBS (Invitrogen), 0.1mM β-mercaptoethanol, 2mM L-glutamine (Invitrogen), 2mM HEPES (Invitrogen), and 0.1mM nonessential amino acids (Invitrogen). After four days, the cells were either harvested for cell adhesion assays or FACS analysis.

D2.2 Fluorescence-activated cell sorting (FACS)

Cells were harvested from 2D and 3D culture systems using Accutase (Chemicon), pelleted by centrifugation, washed in PBS, and stained with various primary antibodies (supplemental table 2-1). Secondary antibodies of fluorescein isothiocyanate (FITC) or phycoerythrin (PE) were used. Nonspecific fluorochrome- and isotype matched IgGs (BD Pharmingen) served as controls. Staining with 7-aminoactinomycin D (BD Pharmingen) was performed to exclude dead cells according to the manufacturer's instructions. Cells were gated by forward scatter (FSC) versus side scatter (SSC) to eliminate debris. A minimum of 10,000 events was counted for each analysis. All analyses were performed using a Becton Dickinson FACScan analytic flow cytometer (BD Bioscience, San Jose, CA USA) with FCS Express software (DeNovo Software, Thornhill, Ontario, Canada) at the UCLA Flow Cytometry Laboratory.

D2.3 Immunofluorescent staining

mES cells in both an undifferentiated and differentiated state were fixed with 4% paraformaldehyde (Sigma-Aldrich) in PBS for 20minutes and rinsed in PBS. All samples were blocked with a 2% goat serum, 1% bovine serum albumin (BSA, Sigma-Aldrich), 0.1% cold fish skin gelatin, 0.1% Triton X-100, and 0.05% Tween-20 in PBS for 30minutes, followed by incubation with primary antibodies overnight at 4°C. After several washes with PBS, Alexa Fluor (Invitrogen) 488 or 546 secondary antibodies were used and incubated at room temperature for 30min. Cells were counterstained with 4'-6'-diamidino-2-phenylindole (DAPI) followed by adding ProLong Gold antifade mounting medium (Molecular Probes, Carlsbad, CA USA). Staining without primary antibodies served as controls. Digital images were acquired using a Leica DM IRB inverted microscope system equipped with 20x (0.40 numerical aperture (NA)) and 40x (0.75 NA) objective lenses (Leica Microsystems Inc, Bannockburn, IL USA).

D2.4 Scaffold fabrication, cell culture, and *in vitro* differentiation in 3D culture

Electrospinning has been used to produce scaffolds with nano- to microdiameter fibers with similar structural properties to the ECM as described before [72]. Briefly, gelatin type B (bovine skin 10% w/v, Sigma-Aldrich) and ε-polycaprolactone (PCL, 10% w/v, Sigma-Aldrich) were mixed together and dissolved in 1,1,1,3,3,3-hexafluoro-2-propanol (HFP, Sigma-Aldrich). The solution was then loaded into a 10mL syringe to which an 18-gauge blunt-ended needle was attached. A core solution of polyurethane (PU, 5% w/v, Sigma-Aldrich) was dissolved in HFP and loaded into a 3mL syringe to which a 25-gauge needle was attached. This syringe and needle system was then loaded into a modified syringe pump. The positive output lead of a high voltage supply (28kV; Glassman High Voltage Inc, NJ USA) was attached to the 10mL syringe needle.

In the created electric field, a thin jet was ejected from the polymer solution in the syringe at a flow rate of 70μL/min. The grounded copper target (5cm x 5cm) was placed approximately 17cm under the needle tip and upon introduction of the electric field Taylor cone formation was observed at the base of the needle tip. A dry fibrous scaffold was collected in the form a 3D mat (100-200μm thick). The electrospun scaffolds were then sterilized by soaking the scaffolds in 70% ethanol for 30min at room temperature. After 3 washes of sterile PBS, the scaffolds were aseptically cut into 1cm x 1cm squares and coated with colIV, fibronectin, laminin, vitronectin, Matrigel, and gelatin as described previously in section D2.1.

D2.5 Proliferation Assay

mES cells were detached from the culture dish and seeded in a flat-bottom 96-well plate for 2D experiments and on the scaffold (scaffold covered the surface area of the bottom of the wells of a flat-bottom 96-well plate) for 3D experiments. The culture plates and scaffolds were coated with collagen IV, laminin, fibronectin, and vitronectin as described previously in section D2.1. Approximately 35,000 cells/well in triplicate per condition were seeded in each well in a mixture of α-MEM, (Invitrogen, Carlsbad, CA USA) supplemented with 10% ES-FBS (Invitrogen), 0.1mM β-mercaptoethanol, 2mM L-glutamine (Invitrogen), 2mM HEPES (Invitrogen), 0.1mM nonessential amino acids (Invitrogen), and AlamarBlue (Serotec, Raleigh, NC; in an amount equal to 10% of the total culture volume). Samples were incubated with α-MEM-AlamarBlue mix for at least 24hrs and up to 96hrs. The metabolism levels were evaluated on a Benchmark Plus Microplate Spectrofluorometer (BioRad, Hercules, CA) at wavelengths of 570 and 600nm (the amount of reduced AlamarBlue is Absorbance 570nm—Absorbance 600nm).

<u>D2.6 Cell Adhesion Assay</u>

mES cells were detached from the culture dish, counted, and incubated for 30 minutes in the presence or absence of integrin antibodies in culture medium (Supplemental Table 2-1) or bovine serum albumin (BSA, Sigma). Isotype control antibodies were used at the same concentration as functional antibodies. mES cells were subsequently seeded into flat-bottom 96-well plates, which were previously coated with ColIV, Fibronectin, Laminin, and Vitronectin as previously described, at 50,000 cells/well in triplicate per condition, in α-MEM supplemented media (as described previously). Cells were allowed to adhere for 60 minutes then washed with PBS three times, fixed with 4% paraformaldehyde, counterstained with DAPI and visualized using fluorescent microscopy. Three images at 10x and 20x magnification were taken of each well with three internal replicates and later stained nuclei per field area were quantified using ImageJ software (free download, NIH). Briefly, nuclei were counted for each image and then averaged.

<u>D2.7 Statistical analysis</u>

All results are presented as mean values $\pm$ standard error of mean (SEM). Statistical significance was assessed by student's t-test or ANOVA with Tukey's multiple comparison tests. $P < 0.05$ was defined as statistically significant. N=5 for all experiments.

D3. Results

<u>D3.1 Integrin expression in undifferentiated mES cells</u>

In order to investigate the presence of various integrin subunits in undifferentiated mES cells, we performed immunohistochemistry and FACS analysis. Figure 2-14A-F illustrates
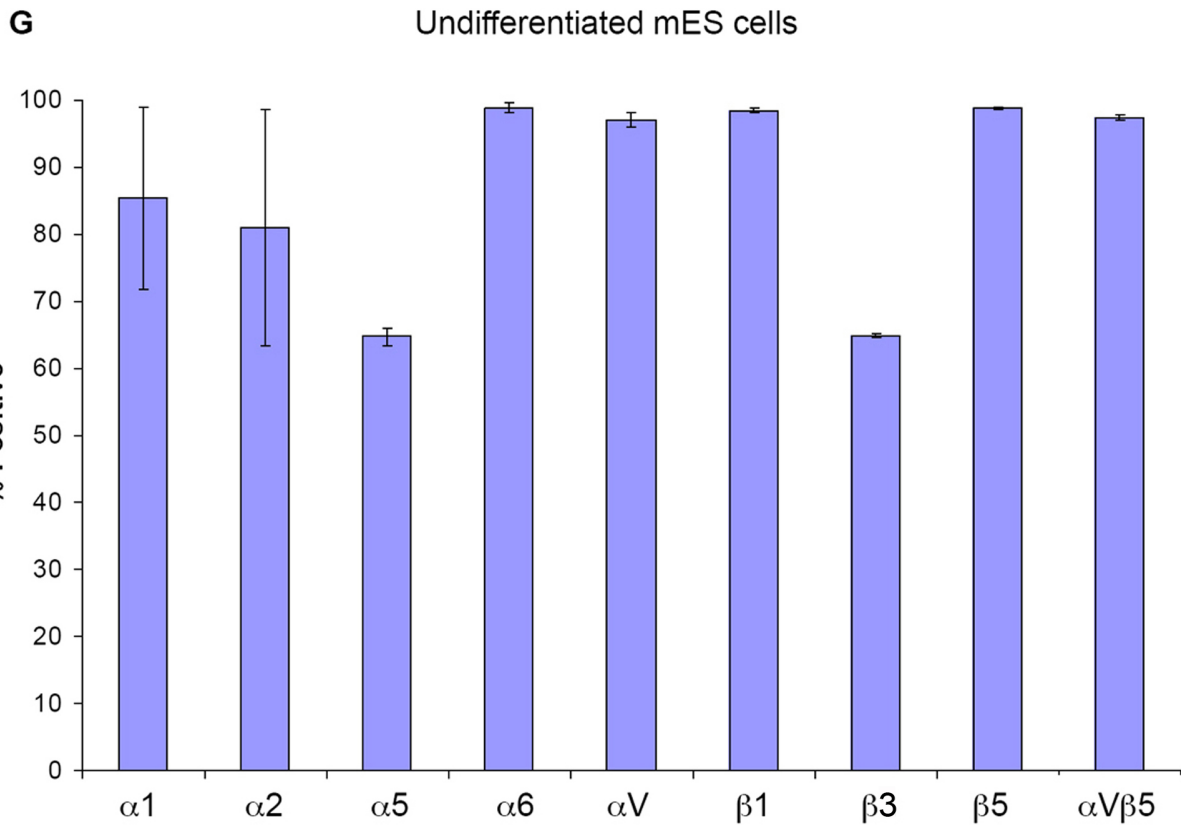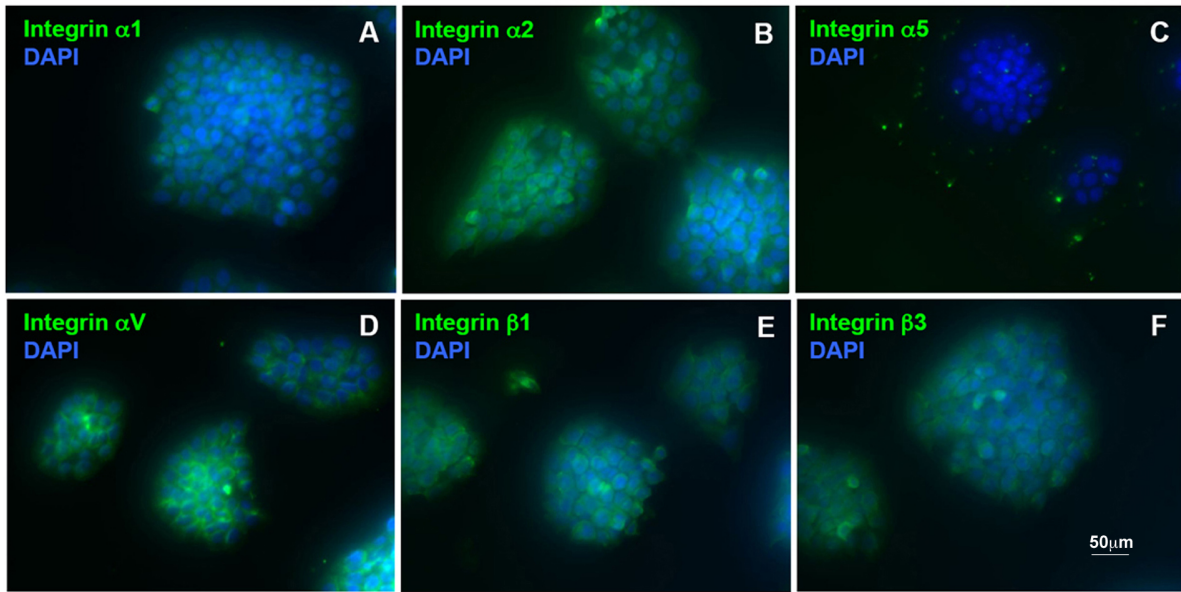
Figure 2-14: Integrin expression in undifferentiated mES cells. Immunofluorescence of undifferentiated mES cells and selected integrin subunits, α1 (A), α2 (B), α5 (C), αV (D), β1 (E), and β3 (F). FACS analysis of integrin expression of undifferentiated mES cells (G) shows relatively high expression for all integrin subunits.

integrin expression in undifferentiated mES cells. To further investigate ECM-mES cell interaction at a molecular level, we determined the baseline integrin expression of

undifferentiated mES cells through cell surface markers of α1, α2, α5, α6, αv, β1, β3, β5 and

αVβ5 via FACS analysis (Figure 2-14G). As seen in Figure 2-14B and 2-14D, integrin subunits

α2 and αV are strongly present through immunofluorescence. This is further confirmed by

FACS analysis in Figure 2-14G. There is a high level of all integrins expressed. α5 has the

lowest expression (64.75 $\pm$1.25%) as compared the other α-subunits (α1 85.45 $\pm$13.63%, α2

80.97 $\pm$17.58%, α6 98.81 $\pm$0.70%, αV 97.07 $\pm$1.05%). Likewise β3 has a lower expression

(64.89 $\pm$0.36%) than the other β integrin subunits (β1 98.50 $\pm$0.34%, β5 98.81 $\pm$0.15%). αVβ5

exhibited a similarly high expression level at 97.48$\pm$0.38%.

D3.2 Integrin expression in 2D and 3D culture

We performed FACS analysis of integrin surface marker expression of mES cells

maintained in both 2D and 3D culture conditions with the addition of our ECM proteins of

interest. We exposed the cells to ECM proteins, namely collagen IV, laminin, fibronectin, and

vitronectin. Figure 2-15 illustrates the various differences between 2D culture conditions (further

denoted as '2D') (Figure 2-15A) and 3D culture conditions (further denoted as '3D') (Figure 2-

15B). Supplemental table 2-2 gives the exact values of those represented in Figure 2-15. The

main differences are highlighted in a significantly lower α2 subunit expression in 2D culture

compared to 3D culture for all ECM proteins (ColIV $p<0.001$, laminin (LM) $p<0.005$,

fibronectin (FN) $p<0.00$, vitronectin (VN) $p<0.001$). The expression of the integrin α6 subunit is

significantly lower in 3D culture on vitronectin compared to other 3D ECM proteins ($p<0.001$).

The expression of the integrin αv subunit exhibits the greatest difference—there is a significantly

lower expression in 2D for both collagen IV and vitronectin, compared to expression in 3D

culture conditions (colIV $p<0.001$; VN $p<0.001$). Additionally, there is a significant difference

A 2D

B 3D
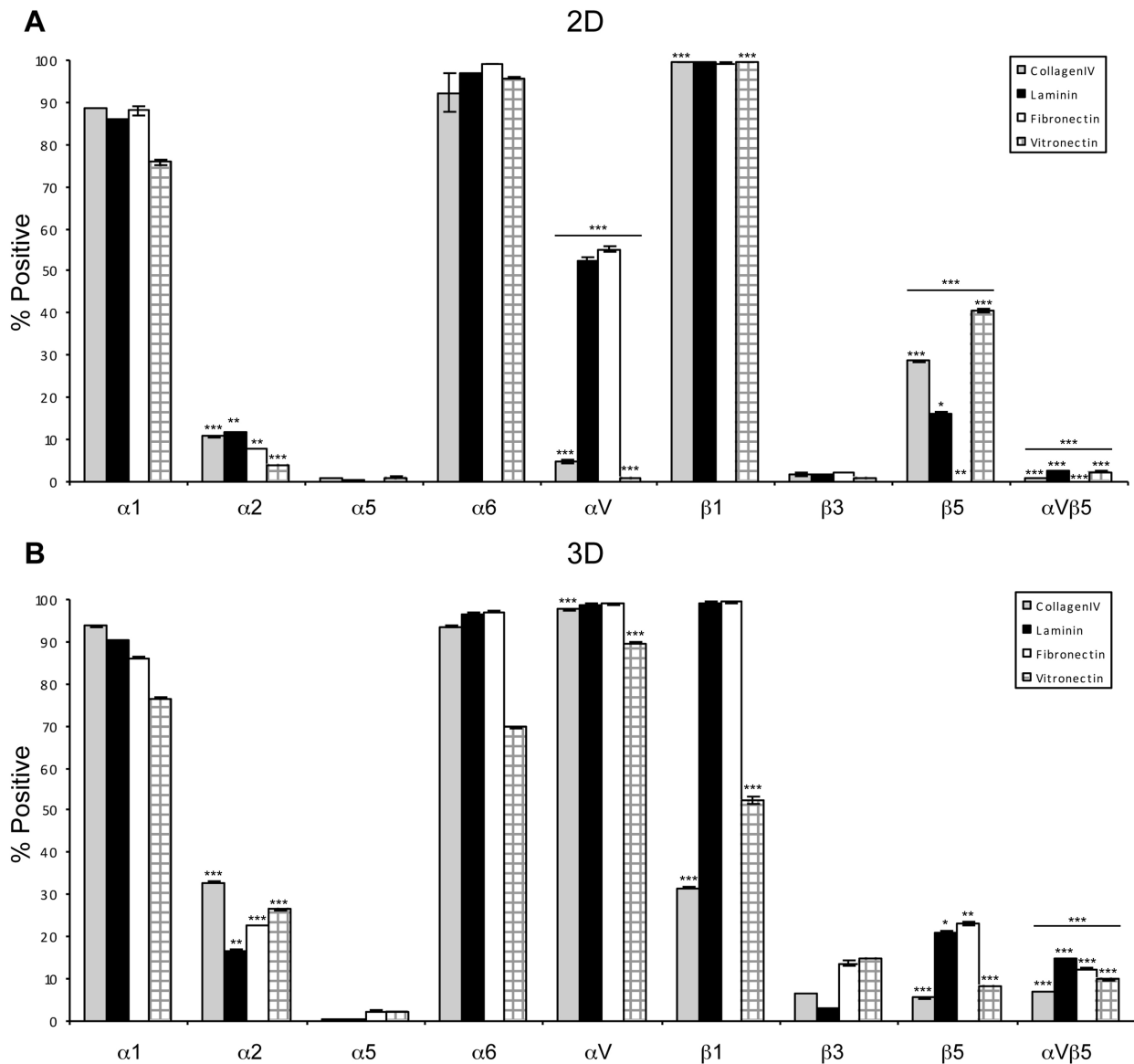
Figure 2-15: FACS analysis of integrin expression of differentiated mES cells in 2D and 3D culture. mES cells were exposed to differentiation media, ECM proteins, and 2D/3D culture conditions for 4 days. Integrin expression was analyzed for 2D (A) and 3D (B) culture conditions exposed to collagen IV, laminin, fibronectin and vitronectin. N=5 *P<0.05, **P<0.005, ***P<0.001. Single * indicates a significant difference between 2D (A) and 3D (B) of the same protein <u>*</u> indicates a significant difference within the group of proteins for the integrin subunit evaluated.

between collagen IV (p<0.001) and vitronectin (p<0.001) in 2D compared to fibronectin and laminin in 2D for expression of αv integrin. The expression of β1 in the 3D condition is lower for both collagen IV (p<0.001) and vitronectin (p<0.001). There is no significant difference in expression of β1 integrin in the 2D culture for any of the proteins of interest (p=0.26). β5 expression under 2D culture conditions is significantly lower for fibronectin coating compared to the other ECM proteins (p<0.001). There is also a significant difference in the expression of β5

between 2D and 3D culture conditions for all ECM proteins of interest (ColIV p<0.001; LM p<0.05; FN p<0.005; VN p<0.001). We observed a significantly higher expression of αVβ5 on 3D culture conditions compared to 2D culture conditions for all ECM proteins (colIV p<0.001; LM p<0.001; FN p<0.001; VN p<0.001). There was also a significant difference in integrin expression of αVβ5 on 2D culture conditions between the different protein coatings (p<0.001), as well there is significant differences between the 3D culture conditions for the different protein coatings (p<0.001).

D3.3 β1 integrin and cell proliferation on 2D and 3D

In order to further understand the role of β1 integrin, a known important integrin subunit for both mES cells and 3D culture conditions [46,52,73,74], we analyzed the proliferation rates of mES cells on a variety of microenvironments when exposed to both a β1 activator and a β1 inhibitor in both 2D and 3D.

Figure 2-16 graphically represents the proliferation of mES cells in 2D and 3D culture with exposure to β1 activator and inhibitor, as based upon enzymatic activity. Supplemental Table 2-3 gives the exact values of those represented in Figure 2-16. More specifically, mES cells cultured on collagen IV in 2D (2-16A, 2-16F) show no change in proliferation rate when exposed to the β1 inhibitor as compared to the β1 activator. There is a difference in proliferation rates between exposure to the β1 activator vs. β1 inhibitor at 96 hps for mES cells cultured on collagen IV in 3D conditions. A significant difference exists in proliferation rates of mES cells cultured on 2D and 3D collagen IV conditions at 24 (p<0.05) and 96hps (p<0.05) for the β1 inhibitor and at 24 (p<0.05) and 96hps (p<0.05) for the β1 activator. Laminin (2-16B, 2-16G) exhibits similar proliferation rates for 2D culture when exposed to both the β1 inhibitor and

93

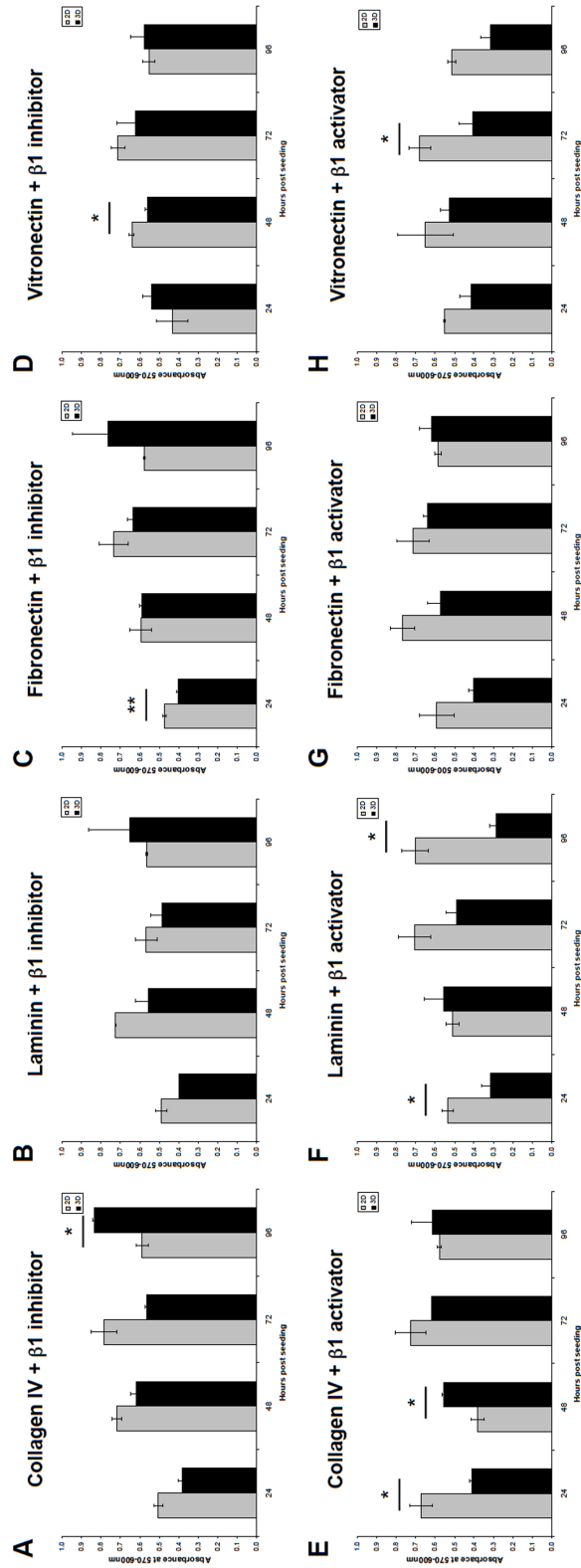***Figure 2-16: Proliferation rates of mES cells exposed to b1 integrin inhibitor and activator***. mES cells were grown on ECM proteins (ColIV: A,E; LM: B,F; FN: C,G; VN: D,H). Proliferation rates were analyzed at 24, 48, 72 and 96 hours post seeding (hps). All cultures were exposed to either a β1 integrin inhibitor (A-D) or activator (E-H). n=5 *P<0.05, **P<0.005

activator. 3D proliferation rates appear increased with the inhibitor and proliferation rates continued to increase at 96hps. When exposed to the β1 activator, overall proliferation rates for the 3D laminin conditions were decreased and peaked at 48hps. We found a significant difference in proliferation rates of mES cells culture on laminin coatings in 2D and 3D at 24 ($p<0.05$) and 96hps ($p<0.05$) when exposed to the β1 activator. However, there was no significance between 2D and 3D laminin+β1 inhibitor. Fibronectin (2-16D, 2-16H) proliferation rates of mES cells on fibronectin coatings in 3D continue an increasing trend even at 96 hps for both inhibitor and activator exposure, although the activator exposure lowers the overall proliferation rate. There appears to be difference between the activator and inhibitor exposure in the 2D culture of fibronectin. At 24hps there is a significant increase of proliferation of mES cells under 3D conditions with the addition of the β1 inhibitor ($p<0.005$), whereas there is no significant increase of proliferation of cell on 2D fibronectin with the β1 activator. The proliferation rate of mES cells on vitronectin in 2D conditions (2-16D, 2-16I) has a significant difference when exposed to the β1 inhibitor at 48hps ($p<0.05$) between 2D and 3D conditions. When exposed to the β1 activator, there is a significant decrease in proliferation rates of cells cultured in the 3D conditions at 72hps ($p<0.05$).

D3.4 Cell adhesion on 2D and 3D

To further elucidate the role of β1 and α5 integrins, we performed a cellular adhesion assay. 50,000 mES cells were added to each culture condition and allowed to adhere for 60 minutes before being analyzed. All values are relative to the baseline control condition of Matrigel. Figure 2-17 and Supplemental Table 2-4 illustrate the difference of cell adhesion of mES cells on 2D and 3D culture surfaces coated with different ECM proteins when exposed to a

β1 integrin subunit inhibitor and activator, as well as an α5 inhibitor and activator. When the β1

integrin inhibitor (2-17A) is added to the culture conditions of collagen IV (p=0.21) and

fibronectin (p=0.61), they experience a higher relative cell adhesion in 2D culture conditions

compared to their 3D counterparts, however it is not significant. Vitronectin coatings maintain a

similar level of cell adhesion in both 2D and 3D. mES cell adhesion to 2D laminin coated

surfaces is significantly decreased when exposed to the β1 inhibitor as compared to the other 2D

ECM proteins (p<0.05). Similarly, when examining the addition of the α5 integrin inhibitor to

the culture (Figure 2-17B), there is a significant increase of cell adhesion in the 2D condition of

ColIV, fibronectin, and vitronectin as compared to their 3D counterparts (ColIV p<0.05; FN
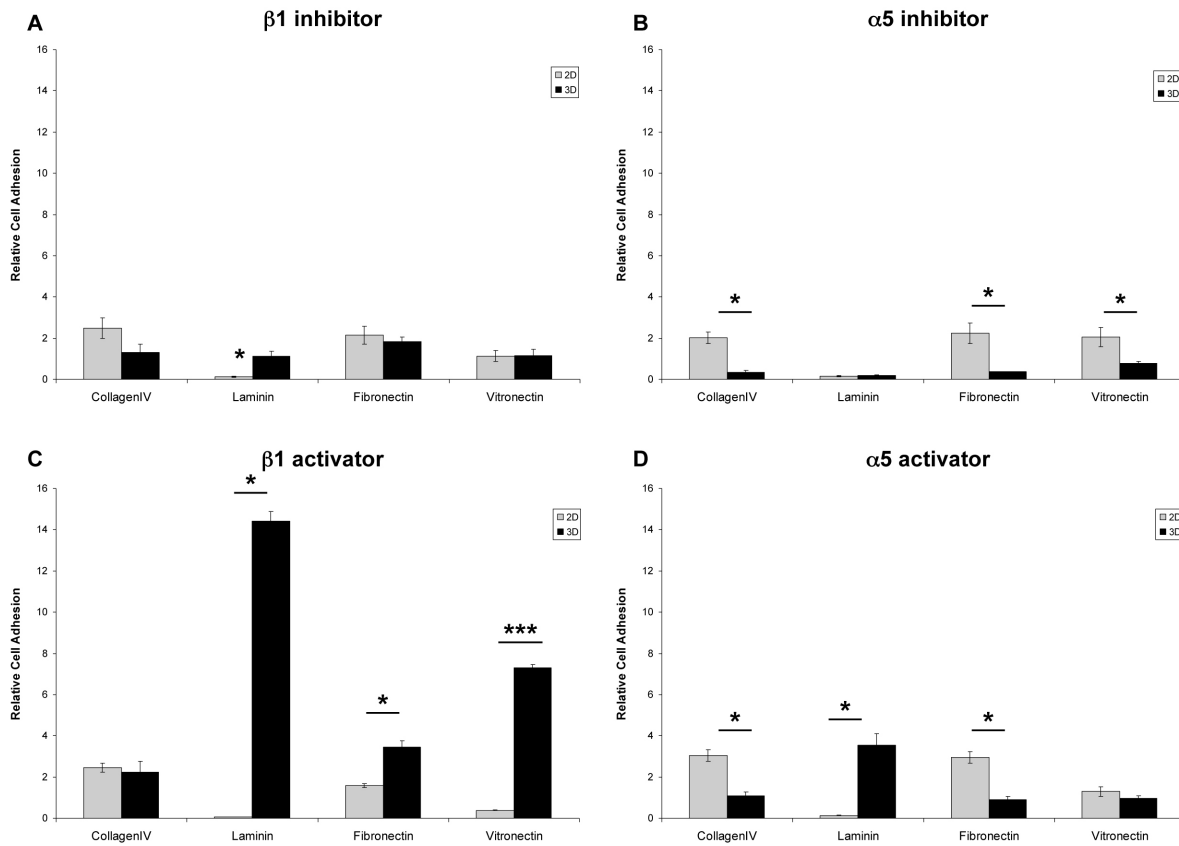
Figure 2-17: Relative cell adhesion assay with exposure to β1 and α5 inhibitor/activator. mES cells were incubated with one of the following: β1 inhibitor (A), α5 inhibitor (B), β1 activator (C), or α5 activator (D) for 30 minutes then seeded on either 2D or 3D cultures of collagen IV, laminin, fibronectin, and vitronectin. After 60 minutes, cells were fixed with 4% PFA and counted to determine the total number adhered to that surface. All cell numbers are relative to a control count of cells adhered to Matrigel after 60 minutes. N=5 * P<0.05, **P<0.005, ***P<0.001. Single * (Laminin, A) indicates a significant decrease compared to the other proteins in 2D for panel A. * indicates a significant difference comparing 2D to 3D for that protein.

p<0.05; VN 0.05). However, there is no significant difference between cell adhesion to laminin in 2D compared to 3D (p=0.48) when exposed to the α5 inhibitor.

There is a higher overall amount of cells adhered to the β1 and α5 integrin activators (Figure 2-17C and 2-17D) compared to the β1 and α5 inhibitors. Contrastingly, there is a trend of higher number of adhered cells in 3D culture when exposed to the β1 integrin activator (Figure 2-17C) as compared to the 2D culture conditions. Again, with exposure to the β1 integrin activator there is a significant decrease in cell adhesion to 2D laminin as compared to the 3D conditions (p<0.001). There is no difference between relative cell adhesion of mES cells on 2D and 3D ColIV with the addition of the β1 integrin activator (p=0.77). There is also a significant difference in relative cell adhesion between the 2D and 3D conditions for both fibronectin (p<0.005) and vitronectin (p<0.001) when exposed to the β1 activator. When examining the α5 integrin activator, there is a significant difference between the 2D laminin mES cell adhesion as compared to its 3D counterpart (p<0.05). Similar to the α5 inhibitor, there is a significantly lower amount of relative cell adhesion in 3D culture for fibronectin when exposed to the α5 integrin activator as compared to the 2D culture conditions (p<0.05). There exists a significant difference between the 2D and 3D culture conditions in the presence of the α5 integrin activator for ColIV (p<0.05). No significant differences were observed on the mES cell adhesion to vitronectin coating in 2D and 3D culture conditions in the presence of the α5 integrin activator (p=0.35).

Upon examining these cell adhesion assays, we wanted to expand our investigation to include several more integrin subunits known to interact with a 3D culture condition (Figure 2-18). In addition to examining β1/α5 activators and inhibitors, we included αV, β5, αVβ5 integrin subunits, as well as controls of BSA and no antibody. There is a low relative cell
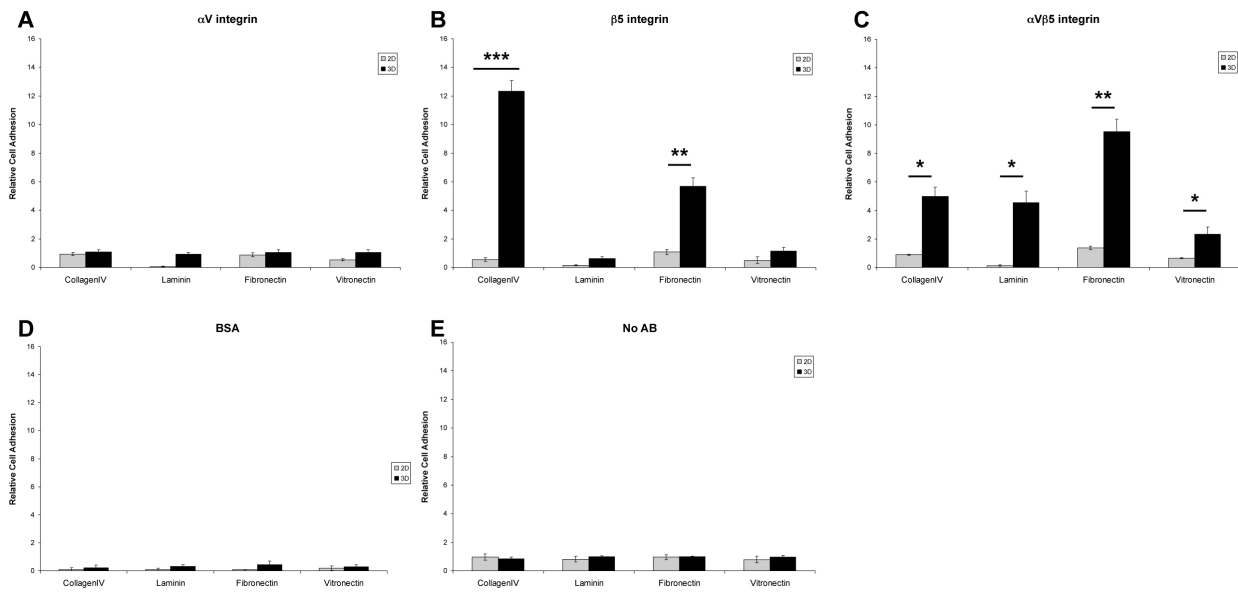
Figure 2-18: Relative cell adhesion assay with exposure to αV, β5, and αVβ5 integrins. Similar to Figure 17, mES cells were exposed to αV (A), β5 (B), αVβ5 (C), bovine serum albumin (BSA, D), and no antibody (E) to determine the total cell number adhered to the surface after 60 minutes. All cell numbers are relative to a control count of cells adhered to Matrigel. N=5
*$P<0.05$, **$P<0.005$, ***$P<0.001$

adhesion for all ECM proteins in both 2D and 3D for the αV integrin subunit assay (Figure 2-18A). When looking at the β5 integrin, there exists a significant difference in cell adhesion for the 3D culture conditions for ColIV ($p<0.001$) and fibronectin ($p<0.005$) as compared to both their 2D counterparts (Figure 2-18B). All the 3D culture conditions show a significantly increased cell adhesion for αVβ5 integrin (Figure 2-18C: colIV $p<0.05$; LM $p<0.05$; FN $p<0.005$; VN $p<0.05$). All of these known 3D interacting integrins shown in Figure 2-18A-C have shown an increase in relative cell adhesion in 3D culture compared to 2D. There is no difference between the 2D and 3D culture conditions for the control assays of BSA and No AB (Figure 2-18D, 2-18E).

D4. Discussion

Regenerative medicine is focused on the goal of repairing or replacing damaged or diseased tissue. Various strategies have been investigated such as cell-based, tissue-engineered

bioscaffolds implanted to stimulate endogenous repair mechanisms. The source and availability of cells for tissue engineering is very critical. ES cells have the capacity to differentiate into all somatic cell types.

Stem cells are maintained in niches *in vivo*. The development and normal function of endogenous stem cells is thought to be maintained by interactions through the surrounding microenvironment of the niche as well as signaling molecules found within the niche. The stem cell niche is defined as an anatomical 3D microenvironment that regulates stem cell self-renewal, cell proliferation, and differentiation through cell-cell and cell-matrix interactions [61]. Not much is known about niche matrix-cell interactions and what specifically contributes to maintaining an undifferentiated state versus what contributes to further terminal differentiation. Two major components are thought to contribute to the function of the niche, the structure of a 3D microenvironment and the inclusion of ECM proteins [61]. These microenvironment interactions are thought to be regulated through integrins.

We have previously developed a biomaterial scaffold system to mimic a 3D microenvironment [27,72]. We have previously found that the microenvironment induces as cardiovascular progenitor cell population [27]. In this study, we have characterized how both a 3D microenvironment and ECM proteins affect integrin expression using the same differentiation conditions as previously used for initial cardiovascular differentiation [27]. We found that integrin expression changes significantly as mES cells begin to differentiate. There was relatively high expression of all integrin subunits of interest in an undifferentiated state, similar to what was seen in the study by Hayashi et al [54]. This is confirmed by the fact that several knockout models of integrin subunits are embryo lethal, including $\beta1$, $\alpha5$, $\alpha6$, and αV [46]. Additionally, due to the specificity of integrin subunits to ligands, we have found that

various ECM proteins (collagen IV, fibronectin, laminin, and vitronectin) also have influence on the integrin expression of mES cells. Many integrins recognize the binding motif RGD (arginine-glycine-aspartic acid), which was originally identified as the "fibronectin receptor" [75]. It is now known that the RGD sequence is still very important for binding and many other proteins also contain the sequence, but the flanking-residues and having a 3D environment can also influence integrin specificity. Of the integrin subunits of our study, collagen IV is known to associate with $\alpha1$, $\alpha2$, and $\beta1$, while laminin is known to associate with $\alpha1$, $\alpha2$, $\alpha6$, αV, $\beta1$, and $\beta3$. Vitronectin associates with αV, $\beta1$, $\beta3$, $\beta5$, and $\alpha V\beta5$ subunits. Fibronectin associates with the most subunits of our interest: $\alpha2$, $\alpha5$, αV, $\beta1$, $\beta3$, $\beta5$, and $\alpha V\beta5$ [56-60,75].

However, as cells were exposed to differentiation media, ECM proteins and 3D culture conditions to reach a cardiovascular progenitor cell (CPC) state, as shown previously [27], integrin expression as determined by FACS analysis decreased for several subunits. Specifically, $\alpha2$, $\alpha5$, αV, $\beta3$, $\beta5$, and $\alpha V\beta5$ were all significantly decreased in 2D culture for all proteins (ColIV, laminin, fibronectin, and vitronectin), while $\alpha2$, $\alpha5$, $\beta3$, $\beta5$, and $\alpha V\beta5$ were decreased in 3D. In particular, we have found a significant difference in various integrin subunit expression of mES cells cultured in a 3D environment as compared to conventional 2D culture techniques, specifically $\alpha2$, αV, and $\alpha V\beta5$. Interestingly, we observed a decrease in integrin expression with collagen IV for $\beta1$ and $\beta5$ in 3D culture. Likewise, we saw a drop of expression for $\beta1$ with vitronectin in 3D culture. $\beta1$ and $\beta5$ integrin subunits are both known to associate with those integrins and 3D conditions. This could be due to the heterodimer configuration of integrin α and β subunits, or suggest that the 3D environment for collagen IV and vitronectin favors an alternative binding partner.

Specifically, we observed an overall trend of 2D culture conditions supporting higher proliferation rates than 3D culture conditions for almost all ECM proteins with both the β1 activator and inhibitor. This supports what other studies have seen in the past—that 2D culture conditions facilitate generally higher proliferation rates than those maintained in 3D culture conditions [71,74,76]. Specifically, we have observed a similar trend for all ECM proteins exposed to the β1 inhibitor—cell proliferation rates remain increased for 2D cultures through 72hps. However, 3D culture conditions support increased proliferation rates at 96hps. We believe this is due to the nature of 3D culture techniques. From our general observation of various studies, after cells are seeded on a 3D substrate, a group of cells adhere to the substrate, while a large amount of cells do not survive. This could account for the delay in proliferation rates. Additionally, β1 integrin inhibition has been known to lead to apoptosis [73]. We speculate that this is the reason for the decrease in proliferation rates after 72hps in 2D culture and that cells cultured in 3D adhere to the substrate via different integrin subunits, thus leading to increased proliferation in spite of the β1 integrin inhibition. Those cultures, both 2D and 3D exposed to the β1 activator show an increasing proliferation rate for all ECM proteins except for laminin and vitronectin. These two culture conditions show a significant decrease in proliferation rates at later time points for 3D cultures.

Upon further examination, we found significant differences in our cell adhesion assays. In particular, laminin demonstrated an increase 3D culture conditions compared to 2D culture for all the investigated integrin subunits. Laminin has been shown to associate with both β1 and α5 [76] integrin subunits. The significant difference between the 2D and 3D laminin cultures when exposed to the β1 inhibitor can be explained by the ability of exposure to laminin to overcome the β1 integrin deficiency [52]. β1 integrin null cells were able to adhere and survive when

exposed to exogenous laminin [52]. The lack of cell adhesion with exposure to the $\beta 1$ activator in 2D laminin conditions is surprising, yet we did expect to see a higher amount of cell adhesion in 3D which is evident. We observed a lower attachment of mES cells to 2D laminin without integrin exposure/assays (data not shown) and hypothesize a higher seeding density would be required. We did observe a higher amount of cell adhesion for all the proteins of interest in 3D culture condition when exposed to both the $\beta 1$ and $\alpha 5$ activators as compared to the inhibitors. The relatively high amount of cell adhesion under the $\beta 1$ activator for 3D laminin (14.43 ± 0.44) and vitronectin (7.29 ± 0.18) suggests the addition of the 3D microenvironment encourages adhesion through the activation of the $\beta 1$ integrin subunit. This has also been shown previously by Hayashi et al [54]. We hypothesize these two integrin subunits, $\beta 1$ and $\alpha 5$, are of particular importance for 3D culture and enhance cellular activity. Previous studies [73,74,77,78] have all observed that $\beta 1$ integrin subunit play an important role in 3D cell culture. When exposed to a 3D culture system, a high presence of $\beta 1$ integrins have been observed in various cell types. Our data is consistent with this previous observation, especially the cell adhesion assays for specific $\beta 1$ integrins. Furthermore, $\alpha 5$ integrins have been shown previously to associate with 3D culture conditions and enhance cellular attachment [76], which is again what we observed in our data with a higher adhesion in 3D when exposed to the $\alpha 5$ activator as compared to the inhibitor.

Furthermore, the αV, $\beta 5$, and $\alpha V\beta 5$ integrins all demonstrate a higher cell adhesion in 3D culture conditions for all ECM proteins. These integrin subunits have been previously identified as important for 3D culture [47,53,76]. Specifically, we observed the significantly higher amount of adhesion for the $\beta 5$ integrin in 3D collagen IV (12.34 ± 0.75) and fibronectin (5.68 ± 0.60). Additionally, the higher adhesion levels in 3D for all ECM proteins with the $\alpha v\beta 5$ integrin subunit clearly suggests its importance in cellular adhesion in 3D microenvironments.

Both the αV and β5 integrin subunits have been implicated as important mediators of cellular activity for 3D culture conditions, and have also become the targets of more specialized studies of stem cell niches [59,78-81].

In particular, activating α5, αV, β1, and β5 integrins in a 3D microenvironment have been shown to maintain a stem cell niche-like environment for mES cells [47]. We have previously found that the inclusion of a 3D collagen IV environment potently induces a cardiovascular progenitor cell population [25], which could be due in part to the high adhesion levels seen here in 3D collagen IV for β5 and αVβ5.

D5. Conclusion

We have characterized integrin expression on undifferentiated mES cells and have established a 3D system for evaluating the influence of ECM-integrin interactions on differentiation. We demonstrated a difference in proliferation rates of a 2D culture condition vs. a 3D culture system. Differences in cell adhesion in 2D and 3D culture systems with various ECM proteins have highlighted the importance of understanding the complex relationship of ECM-integrin interactions. We have also demonstrated the importance of α5, αV, β1, β5, and αVβ5 integrin subunits in 3D culture for all ECM proteins of interest. Further studies will elucidate the relationship between 3D microenvironments, ECM proteins, and integrins in the role of stem cell niches and terminal differentiation.

E. Chapter Conclusion

I have demonstrated the effects of the microenvironment on the induction of CPCs. I created a stable co-axially electrospun scaffold system for 3D culture. I provided evidence showing there is no significant immune response to the implantation of the electrospun scaffolds *in vivo*. I also demonstrated that a 3D hydrogel system potently induces CPCs as compared to conventional 2D culture systems. I also characterized the integrin expression of undifferentiated mES cells and compared the expression to partially differentiated mES cells in both 2D and 3D culture systems with various ECM proteins present.

E1. Acknowledgements

Section B is a version of "Gluck JM, Rahgozar P, Ingle NP, Rofail F, Petrosian A, Cline MG, Jordan MC, Roos KP, MacLellan WR, Shemin RJ, Heydarkhan-Hagvall S. Hybrid co-axial electrospun nanofibrous scaffolds with limited immunological response for tissue engineering. Journal of Biomedical Materials Research Part B, 2011; 99B: 180-190."

Section C is a version of "Gluck JM, Chyu J, Delman C, Heydarkhan-Hagvall S, MacLellan WR, Shemin RJ. Hyaluronan-based three-dimensional microenvironment potently

induce cardiovascular progenitor cell population. BioMed Research International, 2013, under review."

Section D is a version of "Gluck JM, Delman C, Full S, Shemin RJ, Heydarkhan-Hagvall S. Stem cell extracellular matrix interactions in three-dimensional system via integrins. Journal of Regenerative Medicine, 2013, under review"
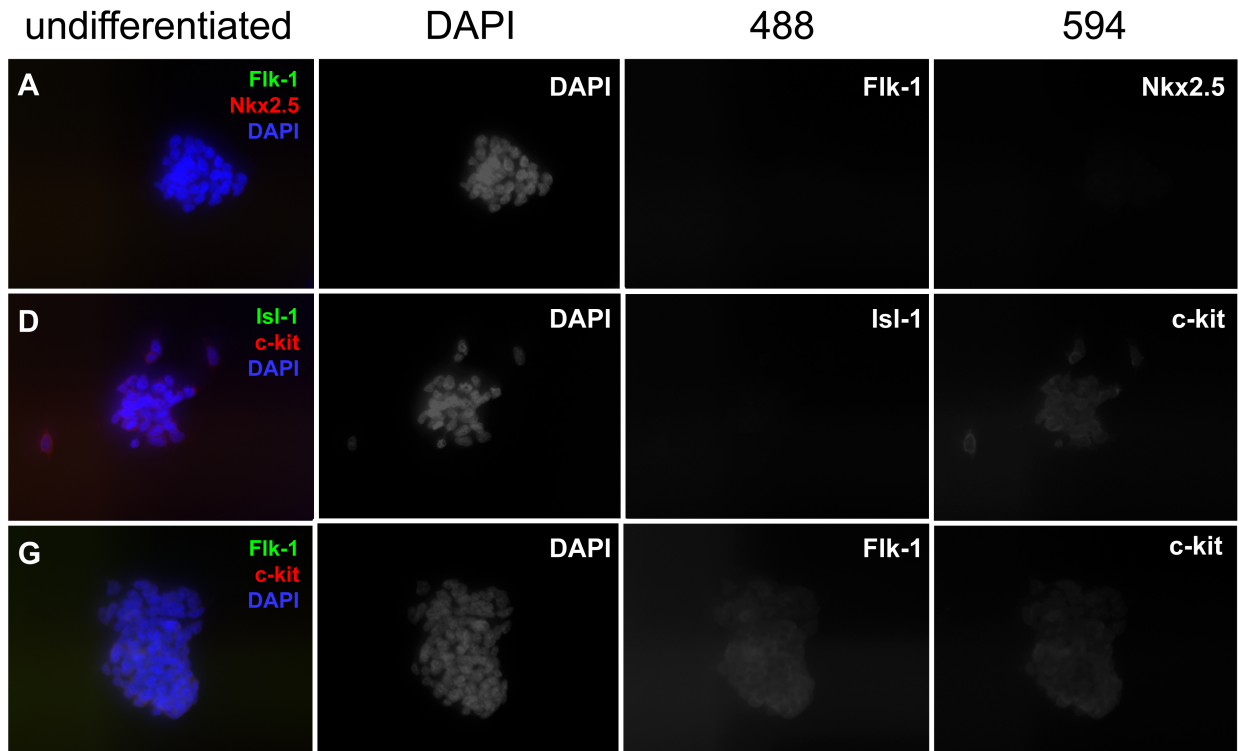
Supplemental Figure 2-1: Immunofluorescence of undifferentiated mES cells CPC markers Individual filters of immunofluorescent images from Figure 2-12 (A,D,G). Original merged images are shown in the first column. Second (DAPI), third (488), and fourth (594) columns shown their respective filters. First row shows Flk-1 and Nkx2.5. Second row shows Isl-1 and c-kit. Third row shows Flk-1 and c-kit.

| 2D collagen IV | DAPI | 488 | 594 |
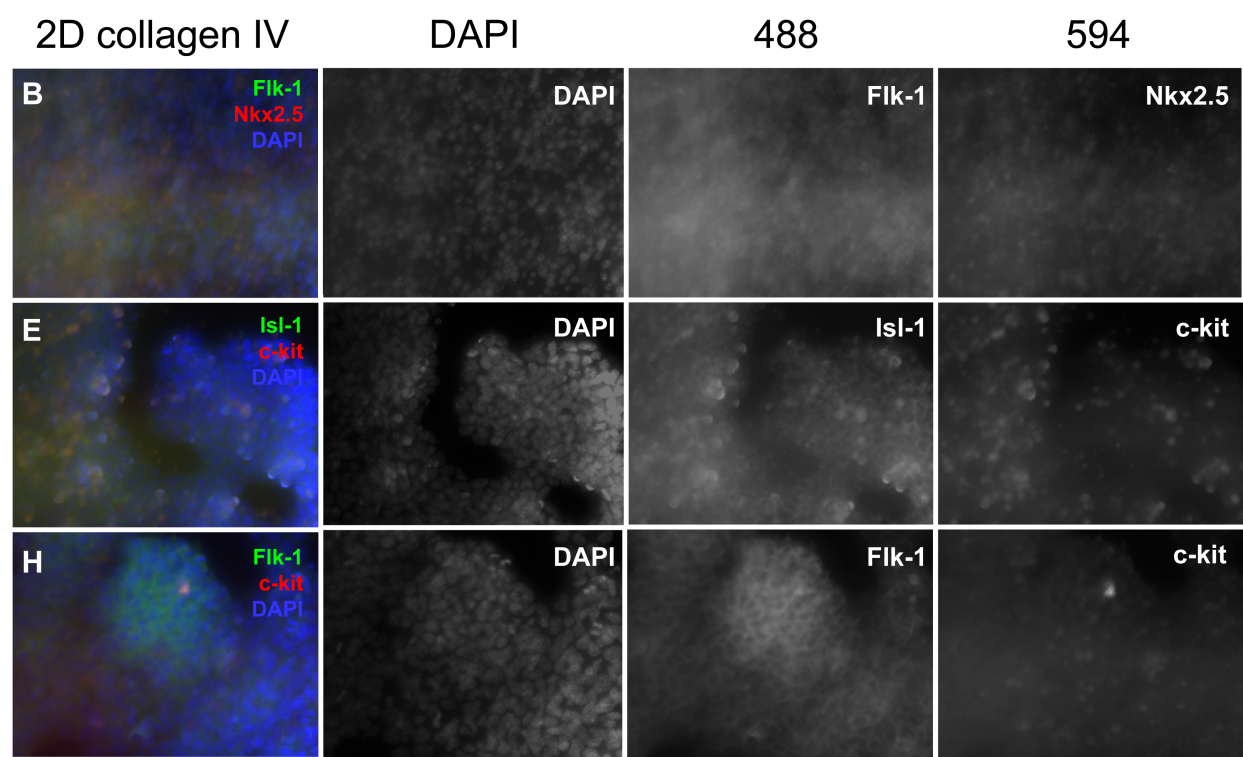
Supplemental Figure 2-2: Immunofluorescence of 2D collagen IV CPC markers Individual filters of immunofluorescent images from Figure 2-12 (B,E,H). Original merged images are shown in the first column. Second (DAPI), third (488), and fourth (594) columns shown their respective filters. First row shows Flk-1 and Nkx2.5. Second row shows Isl-1 and c-kit. Third row shows Flk-1 and c-kit.

| 3D hydrogel | DAPI | 488 | 594 |

C Flk-1 Nkx2.5 DAPI | DAPI | Flk-1 | Nkx2.5

F Isl-1 c-kit DAPI | DAPI | Isl-1 | c-kit

I Flk-1 c-kit DAPI | DAPI | Flk-1 | c-kit
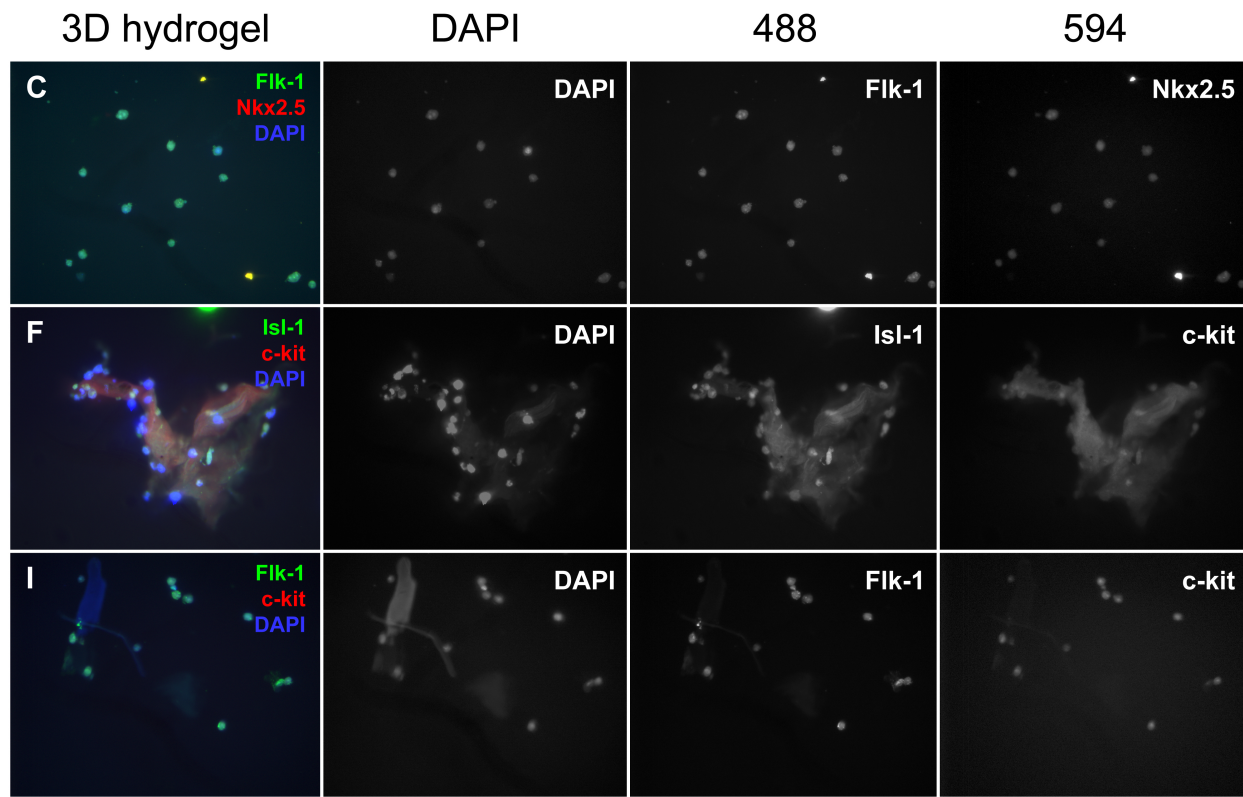
Supplemental Figure 2-3: Immunofluorescence of 3D Hydrogel CPC markers Individual filters of immunofluorescent images from Figure 2-12 (C,F,I). Original merged images are shown in the first column. Second (DAPI), third (488), and fourth (594) columns shown their respective filters. First row shows Flk-1 and Nkx2.5. Second row shows Isl-1 and c-kit. Third row shows Flk-1 and c-kit.

Supplemental Table 2-1: Antibody List

Antibody	Manufacturer
Mouse anti-a1 integrin antibody	Santa Cruz
Mouse anti- a 2 integrin antibody	Santa Cruz
Armenian hamster anti-a5 integrin antibody	Santa Cruz
Rat anti- a6 integrin antibody	R&D Systems
Rabbit anti-aV integrin antibody	Santa Cruz
Rabbit anti-b1 integrin antibody	Abcam
Mouse anti- b3 integrin antibody	BD Biosciences
Rabbit anti- b5 integrin antibody	Abcam
Mouse anti-aVb5 integrin antibody	Abcam
Mouse anti-aVb5 integrin antibody	Chemicon
Mouse anti-b1 integrin inhibiting antibody	Developmental Studies Hybridoma Bank (DSHB)
Mouse anti-b1 integrin activating antibody	DSHB
Rat anti-a5 integrin inhibiting antibody	DSHB
Mouse anti-a5 integrin activating antibody	R&D Systems

Supplemental Table 2-2: FACS analysis of integrin expression of differentiated mES cells in 2D and 3D culture (corresponding to Figure 2-15).

	a1		a2		a5		a6		aV		b1		b3		b5		aV b5	
	% positive (via FACS)																	
Protein	2D	3D	2D	3D	2D	3D	2D	3D	2D[8]	3D	2D	3D	2D	3D	2D[11]	3D	2D[20]	3D[21]
Collagen IV	88.60% ±0.12	93.71% ±0.13	10.73% ±0.26[1]	32.78% ±0.19[1]	0.88% ±0.18	0.26% ±0.02	92.26% ±4.52	93.54% ±0.27	4.88% ±0.33[6]	97.65% ±0.28[6]	99.66% ±0.04[9]	31.64% ±0.27[9]	1.86% ±0.40	6.51% ±0.02	28.65% ±0.13[12]	5.47% ±0.21[12]	1.03% ±0.06[16]	6.89% ±0.05[16]
Laminin	85.94% ±0.11	90.28% ±0.22	11.89% ±0.11[2]	16.69% ±0.35[2]	0.38% ±0.24	0.50% ±0.01	97.04% ±0.04	96.69% ±0.13	52.30% ±0.92	98.84% ±0.07	99.52% ±0.26	99.32% ±0.21	1.65% ±0.17	2.86% ±0.05	16.29% ±0.13[13]	20.85% ±0.58[13]	2.42% ±0.06[17]	14.72% ±0.12[17]
Fibronectin	88.09% ±1.09	86.23% ±0.33	7.96% ±0.10[3]	22.78% ±0.12[3]	0.06% ±0.01	2.36% ±0.19	99.05% ±0.03	97.12% ±0.10	55.10% ±0.72	99.06% ±0.19	99.19% ±0.26	99.41% ±0.19	2.30% ±0.08	13.74% ±0.55	0.04% ±0.04[14]	23.02% ±0.48[14]	0.06% ±0.06[18]	12.43% ±0.24[18]
Vitronectin	75.83% ±0.75	76.56% ±0.25	3.88% ±0.06[4]	26.48% ±0.20[4]	0.98% ±0.23	2.12% ±0.06	95.80% ±0.27	69.71% ±0.21[5]	1.04% ±0.02[7]	89.59% ±0.28[7]	99.74% ±0.02[10]	52.36% ±0.76[10]	0.73% ±0.03	15.04% ±0.02	40.75% ±0.38[15]	8.29% ±0.16[15]	2.36% ±0.07[19]	9.87% ±0.24[19]

1. p-value 8.3×10^{-6}
2. p-value 0.0045
3. p-value 2.5×10^{-7}
4. p-value 0.00010
5. p-value 1.14×10^{-12}
6. p-value 1.08×10^{-6}
7. p-value 1.27×10^{-5}
8. p-value 7.12×10^{-10}
9. p-value 2.20×10^{-5}
10. p-value 0.00038
11. p-value 7.55×10^{-15}
12. p-value 5.63×10^{-7}
13. p-value 0.019
14. p-value 0.0013
15. p-value 8.27×10^{-8}
16. p-value 2.72×10^{-6}
17. p-value 7.48×10^{-6}
18. p-value 0.00048
19. p-value 0.00065
20. p-value 3.08×10^{-7}
21. p-value 4.87×10^{-8}

Supplemental Table 2-3: Proliferation rates of mES cells exposed to β1 integrin inhibitor and activator (corresponding to Figure 2-16)

β1 inhibitor	24hps		48hps		72hps		96hps	
	2D	3D	2D	3D	2D	3D	2D	3D
Collagen IV	0.50 ±0.016[1]	0.38 ±0.016[1]	0.71 ±0.017	0.63 ±0.021	0.79 ±0.044	0.57 ±0.0064	0.58 ±0.021[2]	0.83 ±0.0080[2]
Laminin	0.48 ±0.020	0.40 ±0.0021	0.72 ±0.0064	0.56 ±0.044	0.60 ±0.045	0.49 ±0.039	0.55 ±0.023	0.58 ±0.15
Fibronectin	0.48 ±0.0057[3]	0.40 ±0.0049[3]	0.60 ±0.037	0.58 ±0.012	0.75 ±0.052	0.63 ±0.019	0.57 ±0.0043	0.80 ±0.13
Vitronectin	0.43 ±0.055	0.54 ±0.033	0.63 ±0.011[4]	0.55 ±0.0097[4]	0.71 ±0.024	0.59 ±0.071	0.55 ±0.021	0.57 ±0.046

β1 activator	24hps		48hps		72hps		96hps	
	2D	3D	2D	3D	2D	3D	2D	3D
Collagen IV	0.67 ±0.040[5]	0.41 ±0.0093[5]	0.38 ±0.022[6]	0.56 ±0.0052[6]	0.74 ±0.053	0.62 ±0.0015	0.57 ±0.012	0.63 ±0.074
Laminin	0.52 ±0.021[7]	0.30 ±0.032[7]	0.51 ±0.023	0.56 ±0.068	0.70 ±0.055	0.49 ±0.037	0.69 ±0.048[8]	0.30 ±0.024[8]
Fibronectin	0.59 ±0.046	0.40 ±0.0098	0.77 ±0.042	0.61 ±0.053	0.73 ±0.058	0.63 ±0.014	0.58 ±0.012	0.63 ±0.043
Vitronectin	0.55 ±0.0027	0.41 ±0.039	0.65 ±0.094	0.52 ±0.033	0.68 ±0.038[9]	0.41 ±0.045[9]	0.51 ±0.016	0.31 ±0.032

1. p-value 0.012
2. p-value 0.0055
3. p-value 0.0015
4. p-value 0.013
5. p-value 0.029
6. p-value 0.020
7. p-value 0.013
8. p-value 0.010
9. p-value 0.019

Supplemental Table 2-4: Relative cell adhesion assay with exposure to β1 and α5 integrin inhibitor/activator (corresponding to Figure 2-17).

	Relative cell adhesion							
	β1 inhibitor		β1 activator		α5 inhibitor		α5 activator	
Protein	**2D^3**	**3D**	**2D**	**3D**	**2D**	**3D**	**2D**	**3D**
Collagen IV	2.49 ±0.50	1.31 ±0.41	2.45 ±0.22	2.24 ±0.52	2.01 $\pm0.28^1$	0.33 $\pm0.10^1$	3.03 $\pm0.28^2$	1.08 $\pm0.18^2$
Laminin	0.12 ±0.03	1.13 ±0.23	0.06 $\pm0.01^4$	14.43 $\pm0.44^4$	0.17 ±0.03	0.20 ±0.02	0.14 $\pm0.01^5$	3.56 $\pm0.55^5$
Fibronectin	2.15 ±0.43	1.83 ±0.23	1.59 $\pm0.08^6$	3.44 $\pm0.31^6$	2.23 $\pm0.49^7$	0.36 $\pm0.02^7$	2.94 $\pm0.28^8$	0.90 $\pm0.17^8$
Vitronectin	1.13 ±0.27	1.16 ±0.29	0.38 $\pm0.01^9$	7.29 $\pm0.18^9$	2.04 $\pm0.46^{10}$	0.79 $\pm0.09^{10}$	1.30 ±0.28	0.97 ±0.10

1. p-value 0.0098
2. p-value 0.0089
3. p-value 0.019
4. p-value 1.20×10^{-5}
5. p-value 0.0071
6. p-value 0.0093
7. p-value 0.035
8. p-value 0.0069
9. p-value 5.68×10^{-6}
10. p-value 0.048

Supplemental Table 2-5: Relative cell adhesion assay with exposure to αV, β5, and αVβ5 integrins (corresponding to Figure 2-18).

Protein	Relative cell adhesion					
	αV		β5		αVb5	
	2D	3D	2D	3D	2D	3D
Collagen IV	0.94 +0.10	1.09 +0.17	0.57 +0.13[1]	12.34 +0.75[1]	0.89 +0.05[2]	4.99 +0.65[2]
Laminin	0.06 +0.02	0.94 +0.11	0.17 +0.03	0.63 +0.12	0.13 +0.05[3]	4.54 +0.81[3]
Fibronectin	0.88 +0.15	1.06 +0.19	1.09 +0.17[4]	5.68 +0.60[4]	1.37 +0.12[5]	9.53 +0.88[5]
Vitronectin	0.54 +0.08	1.07 +0.17	0.51 +0.24	1.15 +0.24	0.65 +0.03[6]	2.32 +0.50[6]

1. p-value 0.00022
2. p-value 0.0066
3. p-value 0.011
4. p-value 0.0040
5. p-value 0.0017
6. p-value 0.027

F. References

1. Langer R and Vacanti JP, Tissue engineering. Science, 1993; 260(5110): 920-926.

2. Vacanti JP, Langer R, Tissue engineering: the design and fabrication of living replacement devices for surgical reconstruction and transplantation. Lancet, 1999; 354 (suppl 1): S132-S134.

3. Narem, RM. Tissue engineering: confronting the transplantation crisis. Proc Inst Mech Eng, 2000; 214(1): 95-99.

4. Ma PX. Scaffolds for tissue fabrication. Mater Today 2004;7: 30–40.

5. Hou QP, Grijpma DW, Feijen J. Porous polymeric structures for tissue engineering prepared by a coagulation, compression molding and salt leaching technique. Biomaterials 2003;24:1937–1947.

6. Piskin E. Biodegradable polymers in medicine. In: Scott G, editor. Degradable Polymers: Principles and Applications. Kluwer: Dordrecht; 2002. p. 321

7. Fambri L, Migliaresi C, Kesenci K, Piskin E. Biodegradable polymers. In: Barbucci R, editor. Integrated Biomaterials Science. Kluwer: New York; 2002. p. 119

8. Guan J, FK, Sacks MS, Wagner WR, Preparation and characterization of highly porous, biodegradable polyurethane scaffolds for soft tissue applications. Biomaterials, 2005; 26(18): 3981-3971.

9. Khil MS, BS, Kim HY, Kim SZ, Lee KH, Novel fabricated matrix via electrospinning for tissue engineering. J Biomed Mater Res B Appl Biomater, 2005; 15(72): 117-124.

10. Li WJ, LC, Caterson EJ, Tuan RS, Ko FK, Electrospun nanofibrous structure: a novel scaffold for tissue engineering. J Biomed Mater Res, 2002; 60: 613.

11. Boland ED, MJ, Pawlowski KP, Simpson DG, Wnek GE, Bowlin GL, Electrospinning collagen and elastin: preliminary vascular tissue engineering. Frontiers in Bioscience, 2004; May(9): 1422-1432.

12. Theron SA, ZE, Yarin AL, Experimental investigation of the governing parameters in the electrospinning of polymer solutions. Polymer, 2004; 45(6):2017-2030.

13. Liang D, HB, Chu B, Functional electrospun nanofibrous scaffolds for biomedical applications. Adv Drug Deliv Rev, 2007; 59(14): 1392-1412.

14. Heydarkhan-Hagvall S, Schenke-Layland S, Dhanasopon AP, Rofail F, Smith H, Wu BM, Shemin RJ, Beygui RE, MacLellan WR, Three-dimensional electrospun ECM-based hybrid scaffolds for cardiovascular tissue engineering. Biomaterials, 2008; 29(19): 2907-2914.

15. Rose P, Encyclopedia of polymer science and engineering. 1987, New York: Wiley

16. Johns P, CA, The science and technology of gelatin. 1977, London: Academic

17. Anderson JM, Rodriguez A, Chang DT. Foreign body reaction to biomaterials. Semin Immunol 2008;20:86–100.

18. Ratner BD. Reducing capsular thickness and enhancing angiogenesis around implant drug release systems. J Control Release 2002;78:211–218.

19. Anderson JM. Biological responses to materials. Ann Rev Mater Res 2001;31:81–110.

20. Von Recum AF, Van Kooten TG. The influence of microtopography on cellular response and the implications for silicone implants. J Biomater Sci, Polym Edn 1995;7:181–198.

21. Campbell CE, Von Recum AF. Microtopography and soft tissue response. J Invest Surg 1989;2:51–74.

22. Jansen JA, von Recum AF, van der Waerden JP, De Groot K. Soft tissue response to different types of sintered metal fibreweb materials. Biomaterials 1992;13:959–968.

23. Hulbert SF, Morrison SJ, Klawitter JJ. Tissue reaction to three ceramics of porous and non-porous structures. J Biomed Mater Res 1972;6:347–374.

24. Schofield R. The relationship between the spleen colony-forming cell and the haemopoietic stem cell. Blood Cells, 1978; 4: 7-25.

25. Schenke-Layland K, Nsair A, van Handel B, Angelis E, Gluck JM, Votteler M, Goldhaber JI, Mikkola HKA, Kahn M, MacLellan WR. Recapitulation of the embryonic cardiovascular progenitor cell niche. Biomaterials, 2011; 32: 2748-2756.

26. Shu XZ, Ahmad S, Liu Y, Prestwich GD. Synthesis and evaluation of injectable in situ crosslinkable synthetic extracellular matrices for tissue engineering. J Biomed Mater Res A, 2006; 79: 902-912.

27. Heydarkhan-Hagvall S, Gluck JM, Delman C, Jung M, Ehsani N, Full S, Shemin RJ. The effect of vitronectin on the differentiation of embryonic stem cells in a 3D culture system. Biomaterials, 2012; 337(7): 2032-2040.

28. Shu XU, Liu Y, Luo Y, Roberts MC, Prestwich GD. Disulfide crosslinked hyaluronan hydrogels. Biomacromolecules, 2002 ; 3 : 1304-1311.

29. Burdick J, Prestwich GD. Hyaluronic acid hydrogels for biomedical applications. Adv Mater, 2011; 23: H41-H56.

30. Prestwich GD, Erickson I, Zarembinski TI, West M, Tew WP. The translational imperative: making cell therapy simple and effective. Acta Biomaterialia, 2012; 8: 4200-4207.

31. Cheng K, Blusztajn A, Shen D, Li TS, Sun B, Galang G, Zarembinski TI, Prestwich GD, Marban E, Smith RR, Marban L. Functional performance of human cardiosphere-derived cells delivered in an in situ polymerizable hyaluronan-gelatin hydrogel. Biomaterials, 2012; 33: 5317-5324.

32. Discher D, Mooney DJ, Zandstra PW. Growth factors, matrices, and forces combine and control stem cells. Science, 2009; 324: 1673-1677.

33. Chung BG, Flanagan LA, Rhee SQ, Schwartz PH, Lee AP, Monuki ES, Jeon NL. Human neural stem cell growth and differentiation in a gradient-generating microfluidic device. Lab Chip, 2007;5: 401-406.

34. Guilak F, Cohen DM, Estes BT, Gimble JM, Liedtke W, Chen CS. Control of stem cell fate by physical interactions with the extracellular matrix. Cell Stem Cell, 2009; 5: 17-26.

35. Engler AJ, Sen S, Sweeney HL, Discher DE. Matrix elasticity directs stem cell lineage specification. Cell, 2006; 126: 677-689.

36. Saha K, Keung AJ, Irwin EF, Li Y, Little L, Schaffer DV, Healy KE. Substrate modulus directs neural stem cell behavior. Biophys J, 2008; 95: 4426-4438.

37. Kurpinski K, Chu J, Hashi C, Li S. Anisotropic mechanosensing by mesenchymal stem cells. PNAS, 2006; 103: 16095-16100.

38. Berry MF, Engler AJ, Woo YJ, Pirolli TJ, Bish LT, Jayasankar V, Morine KJ, Gardner TJ, Discher DE, Sweeney HL. Mesenchymal stem cell injection after myocardial infarction improves myocardial compliance. Am J Physiol Heart Circ Physiol, 2006; 290: H2196-H2203.

39. Wipff PJ, Rifkin DB, Meister JJ, Hinz B. Myofibroblast contraction activates latent TGF-β1 from the extracellular matrix. J Cell Biol, 2007; 179: 1311-1323.

40. Breitbach M, Bostani T, Roell W, Xia Y, Dewald O, Nygren JM, Fries JWU, Tiemann K, Bohlen H, Hescheler J, Welz A, Bloch W, Jacobsen SEW, Fleischmann BK. Potential risks of bone marrow cell transplantation into infracted hearts. Blood, 2007; 110: 1362-1369.

41. Hayman MW, Smith KH, Cameron NR, Przyborski. Growth of human stem cell-derived neurons on solid three-dimensional polymers. J Biochem Biophys Methods, 2005; 62: 231-240.

42. Recknor JB, Sakaguchi DS, Mallapragada SK. Directed growth and selective differentiation of neural progenitor cells on micropatterned polymer substrates. Biomaterials, 2006; 27: 4098-4108.

43. Schenke-Layland K, Rofail F, Heydarkhan S, Gluck JM, Ingle NP, Angelis E, Choi C, MacLellan WR, Beygui RE, Shemin RJ, Heydarkhan-Hagvall S. The use of three-dimensional nanostructures to instruct cells to produce extracellular matrix for regenerative medicine strategies. Biomaterials, 2009; 30: 4665-4675.

44. Moiseeva EP. Adhesion receptors of vascular smooth muscle cells and their functions. Cardiovasc Res, 2001; 52: 372-386.

45. Caswell PT, Vadrevu S, Norman JC. Integrins: masters and slaves of endocytic transport. Nature Rev Mol Cell Biol, 2009; 10: 843-853.

46. Hynes RO. Integrins: bidirectional, allosteric signaling machines. Cell, 2002; 110: 673-687.

47. Lee ST, Yun JI, Jo YS, Mochizuki M, van der Vlie AJ, Kontos S, Ihm JE, Lim JM, Hubbell JA. Engineering integrin signaling for promoting embryonic stem cell self-renewal in a precisely defined niche. Biomaterials, 2010; 31: 1219-1226.

48. Danen EH, Yamada KM. Fibronectin, integrins, and growth control. J Cell Physiol, 2001; 189: 1-13.

49. Ramirez F, Rifkin DB. Cell signaling events: a view from the matrix. Matrix Biol, 2003; 22: 101-107.

50. Hata RI. Where am I? How a cell recognizes its positional information during morphogenesis. Cell Biol Int, 1996; 20: 59-65.

51. Boudreau N, Bissell MJ. Extracellular matrix signaling: integration of form and function in normal and malignant cells. Curr Opin Cell Biol, 1998; 10: 640-646.

52. Li S, Harrison D, Carbonetto S, Fassler R, Smyth N, Edgar D, Yurchenco PD. Matrix assembly, regulation, and survival functions of laminin and its receptors in embryonic stem cell differentiation. J Cell Biol, 2002; 157(7): 1279-1290.

53. Martino MM, Mochizuki M, Rothenfluh DA, Rempel SA, Hubbell JA, Barker TH. Controlling integrin specificity and stem cell differentiation in 2D and 3D environments through regulation of fibronectin domain stability. Biomaterials, 2009; 30: 1089-1097.

54. Hayashi Y, Furue M, Okamoto T, Ohnuma K, Myoishi Y, Fukuhara Y, Abe T, Sato JD, Hata RI, Asashima. Integrins regulate mouse embryonic stem cell self-renewal. Stem Cells, 2007;25: 3005-3015.

55. Sutherland AE, Calarco PG, Damsky CH. Developmental regulation of integrin expression at the time of implantation in the mouse embryo. Development, 1993; 119: 1175-1186.

56. Humphries MJ. The molecular basis and specificity of integrin-ligand interactions. J Cell Sci, 1990; 97: 585-592.

57. Avraamides CJ, Garmy-Susini B, Varner JA. Integrins in angiogenesis and lymphangiogenesis. Nature Reviews, 2008; 8: 604-617.

58. Humphries JD, Byron A, Humphries MJ. Integrin ligands at a glance. J Cell Sci, 2006; 119: 3901-3903.

59. Braam SF, Zeinstra L, Litjens S, Ward-van Oostwaard D, van den Brink S, van Laake L, Lebrin F, Kats P, Hochstenbach R, Passier R, Sonnenberg A, Mummery CL. Recombinant vitronectin is a functionally defined substrate that supports human embryonic stem cell self-renewal via $\alpha V\beta 5$ integrin. Stem Cells, 2008; 26: 2257-2265.

60. Heino J. The collagen receptor integrins have distinct ligand recognition and signaling functions. Matrix Biol, 2000; 19: 319-323.

61. Scadden DT. The stem-cell niche as an entity of action. Nature, 2006; 441: 1075-1079.

62. Moretti A, Caron L, Nakano A, Lam JT, Bernshausen A, Chen Y, Qyang Y, Bu L, Sasaki M, Martin-Puig S, Sun Y, Evans SM, Laugwitz KL, Chien KR. Multipotent embryonic isl1+ progenitor cells lead to cardiac, smooth muscle, and endothelial cell diversification. Cell, 2006; 127: 1151-1165.

63. Wu SM, Fujiwara Y, Cibulsky SM, Clapham DE, Lien CL, Schultheiss TM, Orkin SH. Developmental origin of a bipotential myocardial and smooth muscle cell precursor in the mammalian heart. Cell, 2006; 127: 1137-1150.

64. Schenke-Layland K, Rhodes KE, Angelis E, Butylkova Y, Heydarkhan-Hagvall S, Gekas C, Zhang R, Goldhaber JI, Mikkola HK, Plath K, MacLellan WR. Reprogrammed mouse fibroblasts differentiate into cells of the cardiovascular and hematopoietic lineages. Stem Cells, 2008; 26: 1537-1546.

65. Bu L, Jiang X, Martin-Puig S, Caron L, Zhu S, Shao Y, Roberts DJ, Huang PL, Domain IJ, Chien KR. Human isl1 heart progenitors generate diverse multipotent cardiovascular cell lineages. Nature, 2009; 460: 113-117.

66. Kattman SJ, Huber TL, Keller GM. Multipotent Flk-1+ cardiovascular progenitor cells give rise to the cardiomyocyte, endothelial, and vascular smooth muscle lineages. Dev Cell, 2006; 11: 723-732.

67. Laugwitz KL, Moretti A, Lam J, Gruber P, Chen Y, Woodard S, Lin LZ, Cai CL, Lu MM, Reth M, Platoshyn O, Yuan JXJ, Evans S, Chien KR. Postnatal isl1+ cardioblasts enter fully differentiated cardiomyocyte lineages. Nature, 2005; 433: 647-653.

68. Formhals A. US Patent 1,975,5042; 1934.

69. Reneker DH, Kataphinan W, Theron A, Zussman E, Yarin AL. Nanofiber garlands of polycaprolactone by electrospinning. Polymer, 2002; 43: 6785-6794.

70. Bhattarai SR, Yi HK, Hwang PH, Cha DI, Kim HY. Novel biodegradable electrospun membrane: scaffold for tissue engineering. Biomaterials, 2004;25:2595.

71. Chew SY, Yim EKF, Leon KW. Sustained release of proteins from electrospun biodegradable fibers. Biomacromolecules, 2005;6:2017-2024.

72. Gluck JM, Rahgozar P, Ingle NP, Rofail F, Petrosian A, Cline MG, Jordan MC, Roos KP, MacLellan WR, Shemin RJ, Heydarkhan-Hagvall S. Hybrid co-axial electrospun nanofibrous scaffolds with limited immunological response created for tissue engineering. J Biomed Mater Res Part B, 2011; 99B, 180-190.

73. Fassler R, Meyer M. Consequences of lack of beta1 integrin gene expression in mice. Genes Dev, 1995; 9: 1896-1908.

74. Cukierman E, Pankov R, Stevens D, Yamada KM. Taking cell-matrix adhesions to the third dimension. Science, 2001; 294: 1708-1712.

75. Plow EF, Haas TA, Zhang L, Loftus J, Smith JW. Ligand binding to integrins. J Biol Chem, 2000; 275(29): 21785-21788.

76. Vuoristo S, Virtanen I, Takkunen M, Palgi J, Kikkawa Y, Rousselle P, Sekiguchi K, Tuuri T, Otonkoski T. Laminin isoforms in human embryonic stem cells: synthesis, receptor usage and growth support. J Cell Mol Med, 2009; 13: 2622-2633.

77. Abraham S, Kogata N, Fassler R, Adams RH. Integrin B1 subunit controls mural cell adhesion, spreading, and blood vessel wall stability. Circ Res, 2008; 102: 562-570.

78. Larsen M, Artym VV, Green JA, Yamada KM. The matrix reorganized: extracellular matrix remodeling and integrin signaling. Curr Opin Cell Biol, 2006; 18: 463-471.

79. Prowse ABJ, Chong F, Gray PP, Munro TP. Stem cell integrins: implications for ex-vivo culture and cellular therapies. Stem Cell Res, 2011; 6: 1-12.

80. Rowland TJ, Miller LM, Blaschke AJ, Doss EL, Bonham AJ, Hikita ST, Johnson LV, Clegg DO. Roles of integrins in human induced pluripotent stem cell growth on matrigel and vitronectin. Stem Cells Dev, 2009; 19: 1231-1240.

81. Prowse AB, Doran MR, Cooper-White JJ, Chong F, Munro T, Fitzpatrick J, Chung TL, Haylock DN, Gray PP, Wolvetang EJ. Long term culture of human embryonic stem cells on recombinant vitronectin in ascorbate free media. Biomaterials, 2010; 31: 8281-8288.

CHAPTER THREE

Microenvironment influences cardiovascular differentiation of murine cardiovascular progenitor cells

A. Introduction

In vivo, endogenous stem cells reside in tissue-specific anatomically defined clusters called "niches." The idea of the stem cell niche was first proposed by Schofield almost 35 years ago as he studied mammalian haematology [1]. Within the stem cell niche, cell fate is thought to be controlled both spatially and temporally, as well as through cell-cell and cell-matrix interactions. Paracrine and autocrine effects are also thought to regulate cell fate within the niche—there is mounting evidence that stem cells secrete a variety of growth factors, cytokines, chemokines and bioactive lipids which regulate biology and interactions within the surrounding microenvironment. These factors are thought to inhibit apoptosis, stimulate proliferation, and promote vascularization [2]. Additionally, interactions with resident niche cells or the surrounding niche ECM are thought to play an equally important role.

Cardiovascular progenitor cells (CPCs) are thought to reside in niches found in the developing right atria, ventricle and outflow tract. A small endogenous population of CPCs in the adult myocardium exists which are able to repair small damages [3]. Stem cells are able to initially differentiate to this CPC state [4,5]. These progenitor cells are at one of the earliest stages in mesodermal differentiation towards a cardiovascular lineage. Because the ECM contributes to cell-fate decision it makes the native CPC niche ECM's role in cardiac development very important to understand. In the absence of signals coming from the ECM, cells

can undergo apoptosis. Various studies have shown the importance of ECM support necessary for angiogenesis and cardiovascular physiology [6]. However, the exact nature of the ECM's role during cardiac development is still unknown.

Cardiovascular tissue engineering presents an opportunity to not only attempt to recreate native tissue *in vitro*, but also gain a better understanding of how the tissue develops [7-9]. Tissue engineered structures could also be used to create bioengineered myocardial patches to reinforce a weakened tissue and promote endogenous healing properties, as well as potentially replace damaged/diseased tissues [10-12]. Development of 3D scaffolds that mimic the natural fibrous ECM can allow for diffusion of nutrients, metabolites and soluble factors necessary to the seeded cells until they are able to produce their own functional ECM [12,13]. Electrospinning technology can be utilized to create customized electrospun nonwoven mats consisting of essentially any polymer and create microenvironments upon which different cell types have been known to proliferate and thrive [13-18].

More specific to the CPC niche environment, we have shown that CPC commitment and further differentiation can be directed by the microenvironment and that an *in vitro* 3D culture model can be used to promote cardiac differentiation in a mouse ES model by adding both ECM proteins and a 3D electrospun scaffold [19]. Further studies demonstrated that laminin- or vitronectin-coated 3D scaffolds induced an even higher population of Flk-1^{+} CPCs as compared to 2D culture conditions [20].

We aim to determine the role of the microenvironment on further committed cardiovascular differentiation of mouse CPCs using electrospun scaffolds and ECM proteins to create an *in vitro* 3D culture system. Additionally, we will bioengineer a CPC-derived vascular graft.

B. Materials and Methods

B1. Mouse ES cell culture

Murine ES v6.5 cells were purchased from Open Biosystems. mES cells were maintained in an undifferentiated, feeder-free state in leukemia inhibitory factor (LIF) supplemented medium (Knockout Dulbecco's modified Eagle's medium, Invitrogen, Carlsbad, CA USA) with 15% ES-FBS (Invitrogen), 0.1mM β-mercaptoethanol, 2mM L-glutamine (Invitrogen), 0.1mM nonessential amino acids (Invitrogen), 1000U/mL recombinant LIF (Chemicon, Temecula CA USA), and 2mM HEPES (Invitrogen). Cells were cultured on gelatin-coated (0.1% gelatin in PBS, coated for 2h at 37°C) T-75 flasks at 37C, 5% CO_2 in a humidified incubator. Cells were passaged every 2-3 days to maintain an undifferentiated state.

For initial differentiation assays, mES cells were introduced to collagen IV flasks (BD Biosciences, San Jose, CA USA) and maintained in α-minimum essential medium (α-MEM) (Invitrogen) supplemented with 10% ES-FBS (Invitrogen), 0.1mM β-mercaptoethanol, 2mM L-glutamine (Invitrogen), 0.1mM nonessential amino acids (Invitrogen), and 2mM HEPES (Invitrogen). Media was refreshed daily. After five days, cells were isolated for Magnetic-Activated Cell Sorting (MACS).

B2. Magnetic-Activated Cell Sorting (MACS)

To induce differentiation into Flk-1$^+$ cardiovascular progenitors, undifferentiated mES cells were detached from the collagen IV flasks using TrypLE Select (Invitrogen) after five days as described previously [19,20]. To purify a Flk-1$^+$ population, indirect magnetic-activated cell sorting (MACS, Miltenyi Biotec, Auburn CA) was used. Cells were pelleted via centrifugation and resuspended in MACS rinsing buffer supplemented with 2% ES-FBS and incubated with rat

anti-mouse Flk1 antibody (1:200, BD Pharmingen, San Diego, CA) at 4°C for 20 minutes. Cells were then washed, pelleted and resuspended in rinsing buffer with magnetic microbeads (20μL beads + 80μL buffer per 10^6 cells, Miltenyi Biotec) and incubated at 4°C for 15 minutes. Cells were again washed, pelleted and resuspended in 500μL rinsing buffer. The cell suspension was run through an MS-column and MiniMACS separator to purify the Flk-1^+ population per manufacturer's instructions. Cells were then used for differentiation experiments.

For differentiation assays, the mES cells were either cultured on 2D plates coated with collagen IV (ColIV, 5μg/cm^2, BD Biosciences, San Jose CA), laminin (5μg/cm^2, BD Biosciences), fibronectin (5μg/cm^2, Sigma), vitronectin (50nm/cm^2, Chemicon), and gelatin (0.1% w/v in sterile PBS) or 3D electrospun scaffolds coated with collagen IV, laminin, fibronectin, vitronectin, and gelatin following the same protocol as 2D dishes. Cells were maintained in smooth muscle growth medium (SmGM-2; Lonza, Walkersville, MD) supplemented with 10ng/mL platelet-derived growth factor-BB (PDGF, R&D Systems Inc, Minneapolis, MN) for SMC differentiation or endothelial growth medium (EGM-2; Lonza) supplemented with 50ng/mL vascular endothelial growth factor (VEGF, R&D Systems, Inc) for EC differentiation for up to 14 days at 37°C and 5% CO^2.

B3. Electrospun scaffold and tubular structure fabrication

Electrospinning has been used to produce scaffolds with nano- to microdiameter fibers with a similar 3D nature to the ECM as described before [21]. Briefly, gelatin type B (bovine skin 10% w/v, Sigma-Aldrich) and ε-polycaprolactone (PCL, 10% w/v, Sigma-Aldrich) were mixed together and dissolved in 1,1,1,3,3,3-hexafluoro-2-propanol (HFP, Sigma-Aldrich). The solution was then loaded into a 10mL syringe to which an 18-gauge blunt-ended needle was

attached. A co-axial electrospinning system was used to provide mechanical integrity as previous scaffolds lacked the ability to be cultured for more than two to three days [21]. A core solution of polyurethane (PU, 5% w/v, Sigma-Aldrich) was dissolved in HFP and loaded into a 3mL syringe to which a 25-gauge needle was attached. This syringe and needle system was then loaded into a modified syringe pump. The positive output lead of a high voltage supply (28kV; Glassman High Voltage Inc, NJ USA) was attached to the 10mL syringe needle. In the created electric field, a thin jet was ejected from the polymer solution in the syringe at a flow rate of 70µL/min. The grounded copper target (5cm x 5cm) was placed approximately 17cm under the needle tip and upon introduction of the electric field Taylor cone formation was observed at the base of the needle tip. A dry fibrous scaffold was collected in the form a 3D mat (100-200µm thick). The electrospun scaffolds were then sterilized by soaking the scaffolds in 70% ethanol for 30min at room temperature. After 3 washes of sterile PBS, the scaffolds were aseptically cut into 1cm x 1cm squares and statically coated with colIV, fibronectin, laminin, and vitronectin as described previously in section B2. Cells were then seeded statically.

Tubular structures were fabricated by collecting randomly aligned nanofibers on a grounded rotating mandrel in lieu of a flat copper collection plate, as seen in Figure 3-1A. The tubular structures were approximately 2cm in diameter and 300-500µm in thickness. They were sterilized with 70% ethanol and placed in a bioreactor system, LumeGen V60 (Tissue Growth Technologies, Minnetonka, MN, USA). A pump source was used to introduce a flow of media through the lumen of the electrospun tubular scaffold at a constant pressure of 120mmHg (as seen in Figure 3-1B). Flk-1$^+$ CPCs were isolated as described and $5x10^6$ were seeded in the lumen of the tubular scaffold and maintained in smooth muscle cell growth media. The exterior of the scaffold was also maintained in smooth muscle cell growth media. The entire bioreactor

system was rotated 90 degrees approximately every 12hrs for the first 3-4 days, then the media

flow was applied for about 2 week. A second cell seeding of 5×10^6 Flk-1^+ CPCs was then seeded

in the lumen of the same scaffold and maintained in endothelial cell growth media. The media

reservoir was also changed to endothelial cell growth media to supply the media flow in the

lumen of the scaffold. The exterior of the scaffold remained maintained with smooth muscle cell
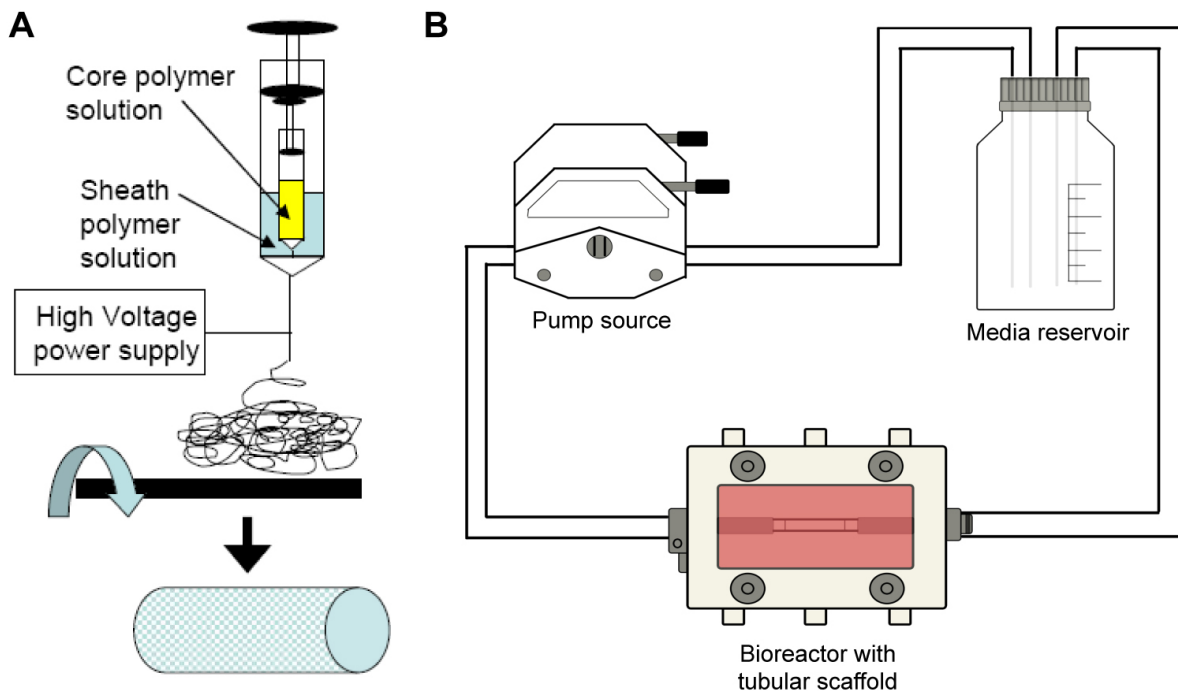
growth media.

Figure 3-1 Electrospun tubular scaffold fabrication Electrospun fibers were collecting on a rotating mandrel (A). The electrospun tubular scaffolds were placed in a bioreactor chamber and seeded with Flk-1^+ CPCs. Media from the reservoir was pumped through the lumen of the tubular scaffold at a controlled pressure of 120mmHg.

B4. Immunofluorescence

The mES cells plated on ECM-coated culture slides as well as undifferentiated mES cells

were washed and fixed with 4% paraformaldehyde, for 20 min and rinsed with PBS. Slides were

then blocked with 1% bovine serum albumin (BSA) and 2% goat serum in PBS for 1hr at room

temperature. Slides were then incubated with primary antibodies (smooth muscle specific markers: SM-α-actin (Dako, Carpinteria, CA), h-caldesmon (Dako), basic calponin (Dako), SM-myosin (Sigma); endothelial specific markers: CD31 (Pecam, Dako), VE-cadherin (CD144, Santa Cruz Biotechnology, Santa Cruz, CA) and von Willebrand Factor (vWF, Dako); cardiomyocyte specific markers: troponin (Santa Cruz), MF20 (Developmental Hybridoma Bank, Iowa, CA), connexin 43 (Santa Cruz)) for 1hr at room temperature or overnight at 4°C followed by several washes with PBS. Alexa Fluor 488- or 546-conjugated secondary antibodies (Molecular Probes, Eugene, OR) were applied to the samples and incubated for 30 minutes at room temperature. After several washes, the cells were counterstained with 4'-6-diamidino-2-phenylindole (DAPI) followed by mounting ProLong Gold antifade mounting medium (Molecular Probes, Carlsbad, CA). Staining without primary antibodies served as controls. Digital images were acquired using a Leica DM IRB inverted microscope system equipped with 20x (0.40 numerical aperture (NA)) and 40x (0.75 NA) objectives (Leica Microsystems Inc., Bannockburn, IL).

B5. Fluorescence-activated cell sorter analysis (FACS)

Cells were harvested from both 2D (conventional culture) and 3D (scaffold) culture, pelleted via centrifugation, washed in FACS buffer (sterile PBS supplemented with 1% ES-FBS, 2% BSA and 0.25% saponin) and stained with primary antibodies (smooth muscle marker: SM-myosin; endothelial cell marker: CD31). The cells were gated by forward scatter (FSC) versus side scatter (SSC) to eliminate debris. A minimum of 10,000 events were counted for each analysis. All analyses were performed using a Becton Dickinson FACScan analytic flow

126

cytometer (BD Biosciences) with FCS Express software (DeNovo Software, Thornhill, Ontario, Canada) at the UCLA Flow Cytometery Laboratory.

B6. Quantitative real time-PCR analysis (RT-PCR)

Total RNA was extracted from cells using the Qiagen RNeasy Kit (Qiagen) according to the manufacturer's instructions. First-strand cDNA was generated from RNA by using the Quantitect Reverse Transcription kit (Omniscript; Qiagen). Real-time quantitative PCR was conducted using the ABI PRISM 7900 Sequence Detection System (TaqMan; Applied Biosystems) with the UCLA GenoSeq Core. PCR amplicons were detected by fluorescent detection of SYBR green (QuantiTect SYBR green PCR kit; Qiagen). Data was analyzed using the $\Delta\Delta Ct$ method, using ribosomal protein S26 as a stable reference gene for normalization control. Primers used were purchased from Qiagen (QuantiTect Primer Assay).

B7. Bioreactor Analysis

For ultrastructural analysis, unseeded tubular scaffold samples were processed for characterization by scanning electron microscopy (SEM) as described previously [21]. Fiber samples were cut from different, randomly selected locations on the tubular scaffold to obtain representative fibers from both the inner and outer circumferences. The samples were mounted onto stubs and sputter coated with gold/palladium (Au/Pd to a thickness of ~10µm) using Denton Desk II before scanning with a JEOL 6610 Low-Vacuum SEM (JEOL, Ltd, Tokyo, Japan). Fiber diameters in the electrospun scaffolds were measured on scanning electron micrographs. Average fiber diameter was determined from measurements taken perpendicular to the long axis of the fibers within representative microscopic fields (50 measurements per field). The pores

formed at the interstices of the fibers were measured using ImageJ software (free download available at http://rsbweb.nih.gov/ij/). For each sample, at least 5 scanning electron micrographs at 2000x magnification were used for image analysis and pore size measurement.

After 30 days, the electrospun tubular scaffolds were removed from the bioreactor chamber and fixed in 4% PFA. The tubular scaffolds were cut perpendicular to the lumen as well as parallel to obtain a representative sample of both the cross-section of the cell-seeded tubular scaffold and the inner and outer cell layers. Samples were then paraffin-embedded and prepared for immunofluorescence staining as previously described in section B4.

B8. Statistical Analyses

All results are presented as mean values $\pm$ standard error of mean (SEM). Statistical significance was assessed by a general linear model, which was fit with main effects for time points (day 7 or day 14), environment (2D or 3D) and protein (ECM proteins of interest: gelatin, collagen IV, laminin, fibronectin, or vitronectin) and two-way interaction terms (environment x protein, environment x day, and day x protein). The interaction terms were left in the model even if they were not statistically significant as these terms helped to explain some of the total variability and consumed a relatively small number of degrees of freedom. $P < 0.05$ were defined as statistically significant.
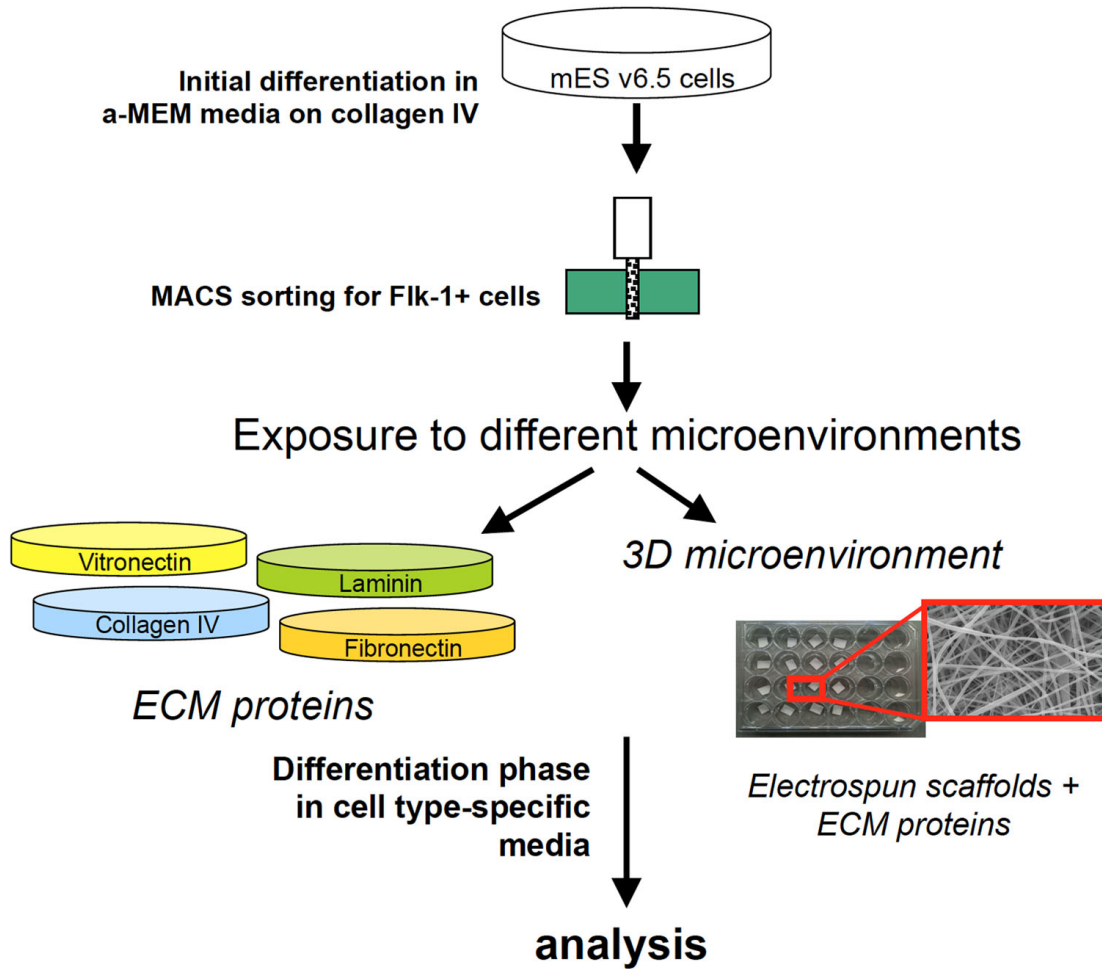
C. Results

Figure 3-2: Experimental Design Schematic depicting experimental design. mES cells were expanded in initial differentiation media and then sorted for Flk-1⁺ CPCs. Isolated CPCs were then exposed to various microenvironments in both 2D and 3D and analyzed at day 7 or 14.

As depicted in Figure 3-2, we first expanded mES v6.5 cells then exposed them to initial

differentiation conditions in α-MEM media. After five days, we isolated Flk-1⁺ CPCs using the

MACS system and then seeded the CPCs in both 2D and 3D microenvironments for either seven

or 14 days in both endothelial and smooth muscle cell specific culture media.
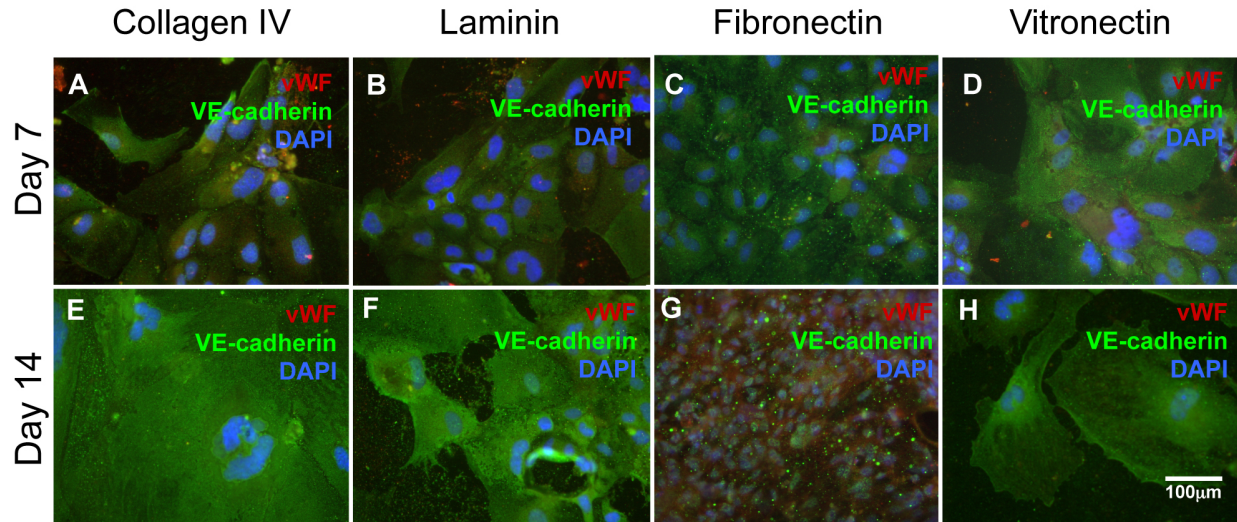
C1. Immunofluorescence Imaging

Figure 3-3: Vascular endothelial cell differentiation mES cell-derived Flk-1$^+$ CPCs were exposed to different microenvironments for both 7 and 14 days. Cells were analyzed for vWF (red) and VE-cadherin (green).

We were able to successfully differentiate the isolated CPCs into all three main cardiovascular lineages—endothelial cells (Figure 3-3), smooth muscle cells (Figure 3-4) and cardiomyocytes (Figure 3-5) as shown by immunofluorescence. Examining the endothelial cells in Figure 3-3, we see that all four ECM proteins of interest (collagen IV, laminin, fibronectin, and vitronectin) are able to support vascular endothelial cell differentiation. It appears that laminin (Fig 3-3B,F) and vitronectin (Fig 3-3D,H) cultures exhibit a slightly delayed differentiation pattern, as the signal for vWF, a marker of more mature endothelial cells, is faint at both day7 and day14. Collagen IV cultures exhibit both VE-cadherin and vWF at both time points (Fig 3-3A,E), while fibronectin appears to support the most robust differentiation, as evidenced by the strong positive signal of vWF at day14 (Fig 3-3G). Figure 3-4 examines the smooth muscle cell differentiation of the CPCs. All four ECM proteins supported smooth muscle cell differentiation with no significant difference between the two time points evaluated (Figure 3-4). Cardiomyocyte differentiation is analyzed in Figure 3-5.
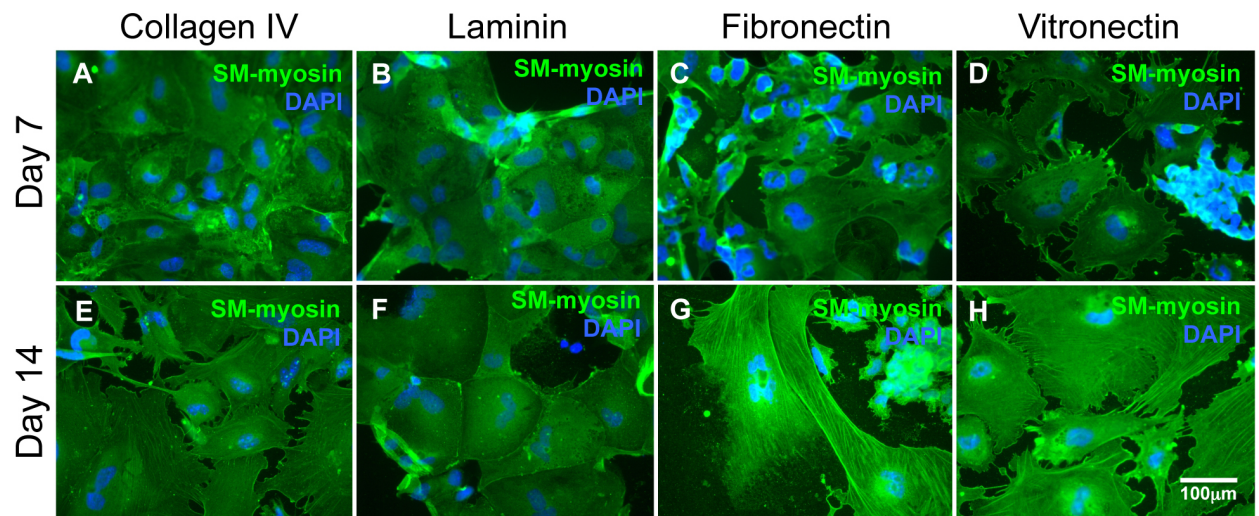
Figure 3-4: Vascular smooth muscle cell differentiation mES cell-derived Flk-1^{+} CPCs were exposed to different microenvironments for both 7 and 14 days. Cells were analyzed for SM-myosin (green).

We demonstrated that cardiomyocyte differentiation is possible from the isolated CPCs and all four ECM proteins of interest support differentiation. Collagen IV (Fig 3-5A,E) and vitronectin (Fig 3-5D,H) support early differentiation as evidence by the increased MF-20 signal present at day 7 while the later time points do not demonstrate any significant increase. There appears to be little difference in any time points for laminin cultures (Fig 3-5B, F). Fibronectin is the only protein that exhibits increasingly differentiation over time, as there is a progressive increase in
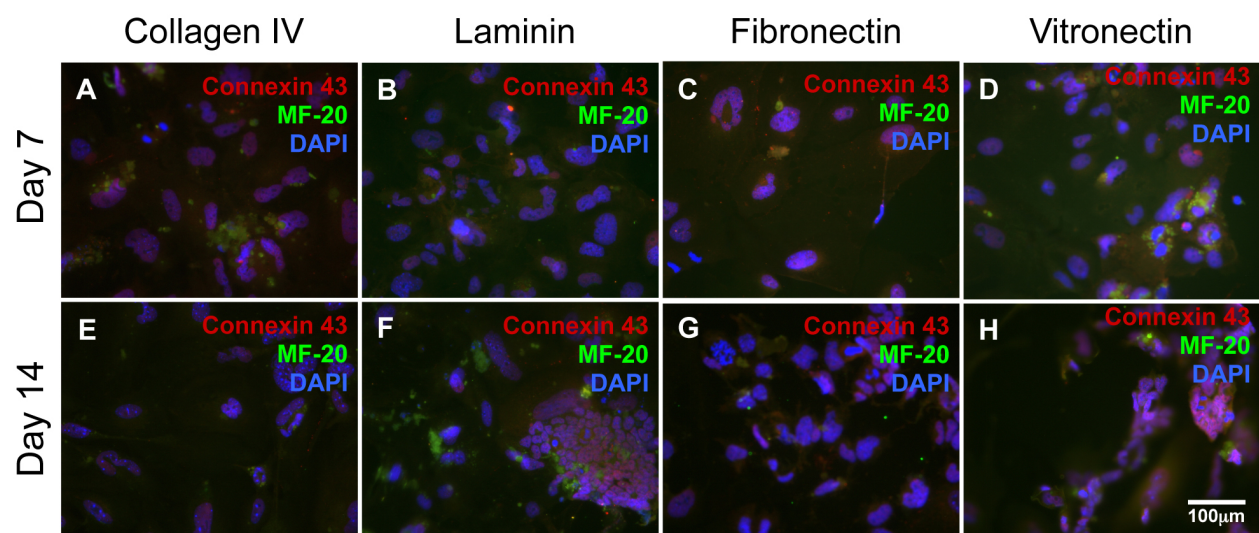

Figure 3-5: Cardiomyocyte differentiation mES cell-derived Flk-1^{+} CPCs were exposed to different microenvironments for both 7 and 14 days. Cells were analyzed for connexin43 (red) and MF-20 (green).

MF-20 signal (Fig 3-5C, G). Further physiological phenotyping including a matrigel vessel assay, as well as carbachol-induced contraction was conducted previously [20]. Thus isolated CPCs differentiate to cardiomyocytes, vascular endothelial, and smooth muscle cells.

C2. FACS

We analyzed the percentage of endothelial and smooth muscle cells via FACS analysis at day 7 and day 14. Figure 3-6 shows the expression of CD31 (also known as Pecam), a well-known vascular endothelial marker in both 2D and 3D culture. At day 7, the only culture that exhibits a higher expression of CD31 in 3D is laminin (2D 52.61±9.04% 3D 60.38±3.57%). A significant increase was observed in percentage of cells expressing CD31 at day 14 compared to day 7 ($p < 0.05$), as well as a significant difference amongst the ECM proteins evaluated ($p < 0.0001$). We observed increased differentiation on 3D cultures at the later time point (day14) for gelatin (d7: 3D 34.61±0.49%, d14: 3D 77.62±1.51%) and fibronectin (d7: 3D 17.62±3.48%, d14: 3D 60.17±9.26%). We also observed an increased differentiation on laminin in 2D at the later time point (d7: 2D 52.61±9.04%, d14: 2D 95.81±0.37%). There was a slight increase in CD31 expression for collagen IV in 3D culture at the later time point, but no real change in 2D
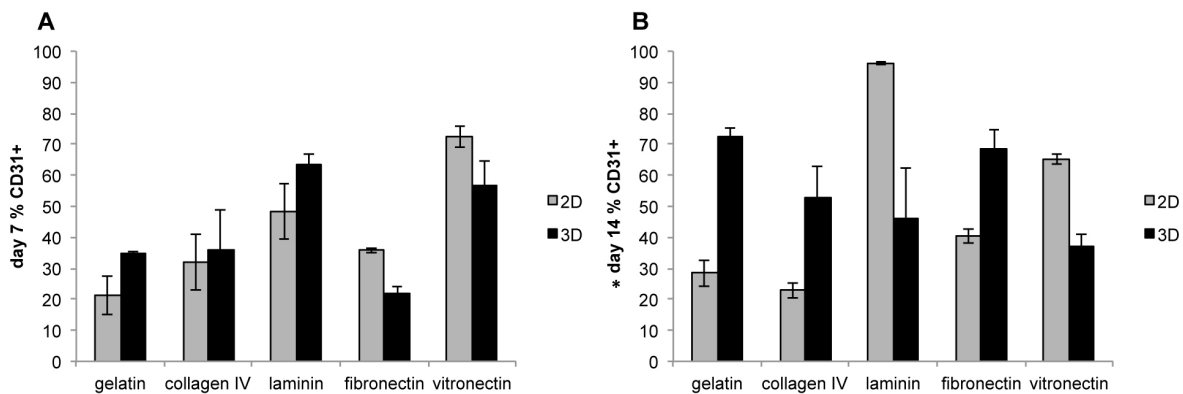

Figure 3-6: FACS analysis of vascular endothelial cells Flk-1^{+} CPCs were exposed to different microenvironments in both 2D (grey bars) and 3D (black bars) for both 7 (A) and 14 (14) days. CD31 was used as a cell surface marker for endothelial cells for FACS analysis. N=3 *P<0.05

culture (d7: 3D 31.36+12.76%, d14: 3D 47.83+23.15%). Vitronectin in 3D culture experienced a decrease in CD31 expression at day 14 (d7: 3D 51.02+7.98%, d14: 3D 30.03+1.19%) while the expression in 2D cultures remained relatively constant. Overall, we observed little difference in CD31 expression between the time points for 2D cultures (except for laminin). We did observe an increase in differentiation at the later time points for three of the ECM proteins (gelatin, collagen IV and fibronectin).

We evaluated smooth muscle cell differentiation via FACS analysis using smooth muscle-myosin (SM-myosin) as a marker as seen in Figure 3-7. Unlike the endothelial cells, we observed a clear trend in differentiation patterns. We see significantly higher SM-myosin expression in 3D cultures as compared to 2D cultures (p<0.0001), as well as a significant difference between the mean effect of day 7 compared to day 14 (p<0.0001) and all the ECM proteins evaluated (p<0.0001). Both 2D and 3D cultures for gelatin exhibited comparable SM-myosin expression at day 7 (d7: 2D 38.38+0.36% 3D 27.78+1.44%) and there was an increase in expression for 3D culture at day 14 (d14: 2D 9.22+0.3%, 3D 36.04+4.24%) but a decrease for expression in 2D culture. Collagen IV and laminin also demonstrated a similar pattern—an increase in expression in 3D at the later time point, but a decrease in 2D culture (Collagen IV d7: 2D 20.53+0.88%, 3D 11.89+1.102%; d14: 2D 7.93+0.10%, 3D 23.04+0.80%; Laminin d7: 2D 17.33+1.69%, 3D 36.52+0.65%; d14: 2D 8.13+0.15%, 3D 32.75+0.64%). Fibronectin exhibited the highest expression of SM-myosin of all cultures at day 7 (d7: 2D 73.57+2.20%, 3D 82.57+0.56%), while there was still a higher level of expression for 3D cultures compared to 2D cultures at day 14 it was a lower level expression compared to the earlier time point (d14: 2D 46.69+1.34%, 3D 70.79+2.27%). Vitronectin remained relatively constant for both time points, with expression of SM-myosin remaining higher for 3D cultures than 2D cultures (d7: 2D

28.63$\pm$7.67%, 3D 39.89$\pm$6.66%, d14: 2D 18.71$\pm$0.35%, 44.69$\pm$1.18%). Overall, we see a trend of progressive differentiation over time for 3D cultures compared to 2D cultures and the robust differentiation for fibronectin cultures.
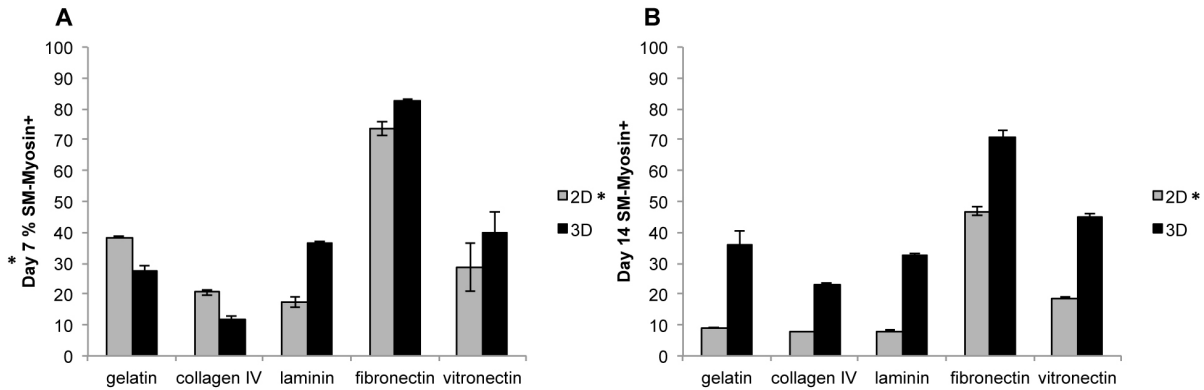

Figure 3-7: FACS analysis of vascular smooth muscle cells Flk-1^{+} CPCs were exposed to different microenvironments in both 2D (grey bars) and 3D (black bars) for both 7 (A) and 14 (B) days. SM-myosin was used as a marker for FACS analysis. N=3
*P<0.0001

C3. RT-PCR analysis

In order to more closely examine the expression of endothelial and smooth muscle cell markers expressed in the differentiated CPCs, we performed quantitative RT-PCR analysis. We evaluated endothelial markers: von Willebrand's Factor (vWF), CD31, Flk-1, and Tie-2 (Figure 3-8); as well as smooth muscle cell markers: α-smooth muscle actin, connexin43, SM-myosin, and myosin light chain (Figure 3-9).

Examining the vascular endothelial cell gene expression in Figure 3-8, we did not observe a clear trend in data. 3D culture conditions enhanced vWF expression at the later time point (day 14, Figure 3-8B) for collagen IV, fibronectin and vitronectin. The expression of vWF was decreased for the 2D culture conditions for all the ECM proteins evaluated (Figure 3-8A). There was a significant difference amongst all the ECM proteins evaluated (p<0.01), however there is no significant difference in vWF expression in 2D vs. 3D cultures or day 7 vs. day 14.

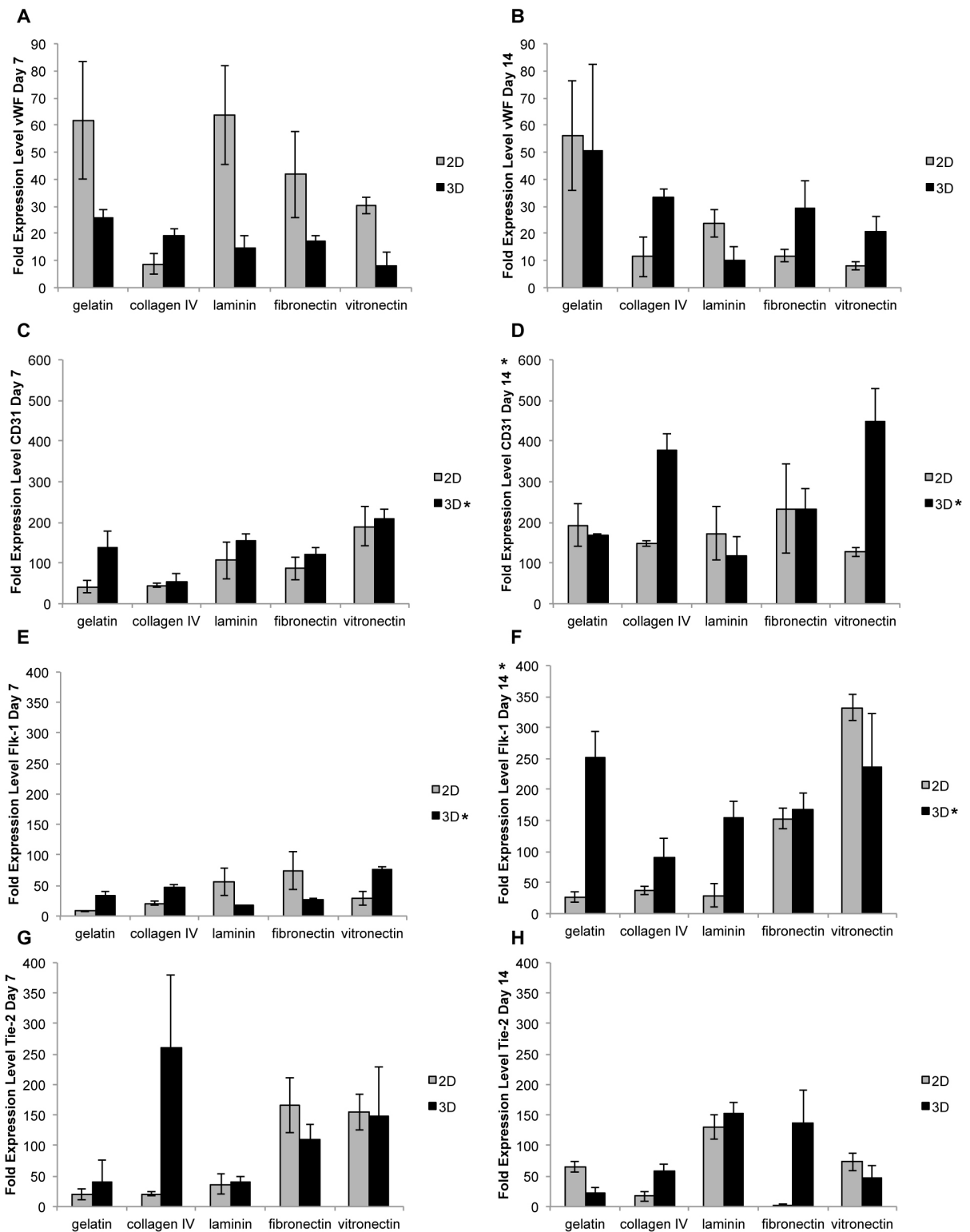***Figure 3-8: qPCR analysis of CPC-derived vascular endothelial cells*** Flk-1^{+} CPCs were exposed to different microenvironments in both 2D (grey bars) and 3D (black bars) for both 7 (A,C,E,G) and 14 (B,D,F,H) days. We examined the following markers: vWF (A,B), CD31 (C,D), Flk-1 (E,F), and Tie2 (G,H). N=3, *P<0.05

CD31 gene expression was significantly increased at the later time point (day 14, Figure 3-8D,

p<0.0001) for all conditions. While, we did observe a decrease in expression for only 3D laminin, there was a significantly larger mean effect of 3D cultures compared to 2D cultures (p<0.01). There was also a significant difference of CD31 expression amongst all the ECM proteins evaluated. There was increased expression for 3D culture conditions for collagen IV, fibronectin, and vitronectin, with both 2D and 3D vitronectin having significantly more expression than the other ECM proteins. We observed a significant increase in Flk-1 expression at day 14 compared to day 7 (Figure 3-8E,F, p<0.0001). Additionally, there was a significantly higher mean effect of Flk-1 expression in 3D culture conditions compared to 2D culture conditions (Figure 3-8E,F, p<0.01). However, we saw a decrease in expression at day 14 (Figure 3-8E) for gelatin and collagen IV and relatively no change for vitronectin in 3D culture conditions. Again, we observed a significant difference in Flk-1 expression amongst all the proteins we evaluated. We observed slight increases in Flk-1 expression in 2D culture conditions for gelatin, collagen IV and vitronectin. There was an increase in 2D fibronectin at day 14 compared to day 7. Tie-2, an early vascular endothelial cell marker, had high expression at day 7 (Figure 3-8G) for 3D collagen IV, fibronectin and vitronectin, which then decreased at day 14 (Figure 3-8H). Laminin in both 2D and 3D saw increased Tie-2 expression at day 14.

When we evaluated the smooth muscle cell markers in Figure 3-9, we first examined α-smooth muscle actin. A significant difference in SM-actin expression was present when comparing day 7 to day 14 (p<0.0001), as well as when comparing the 5 ECM proteins evaluated (p<0.0001). We observed an increase in expression at the later time point (day 14, Figure 3-9B) for both 2D and 3D culture conditions for collagen IV, laminin, fibronectin, and vitronectin. The only decrease we observed was in a-SM actin for 3D gelatin. We also found that expression levels were higher in 3D compared to 2D for laminin, fibronectin, and vitronectin at day 14
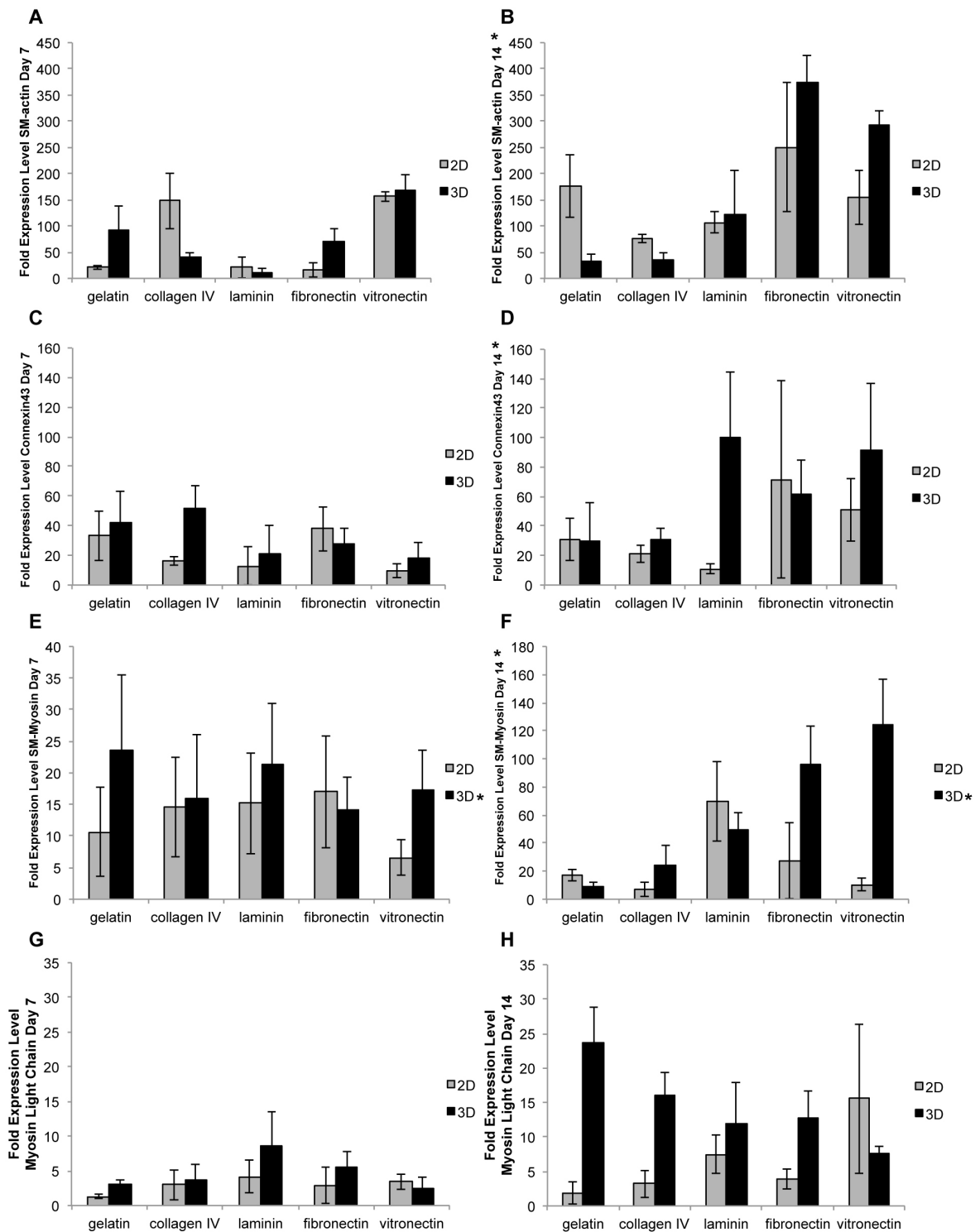
Figure 3-9: qPCR analysis of CPC-derived vascular smooth muscle cells Flk-1^{+} CPCs were exposed to different microenvironments in both 2D (grey bars) and 3D (black bars) for both 7 (A,C,E,G) and 14 (B,D,F,H) days. We examined the following markers: α-smooth muscle actin (A,B), connexin43 (C,D), myosin (E,F), and myosin light chain (G,H). N=3, *$P<0.05$

(Figure 3-9A,B). There was also an significantly increased level of expression of connexin43 day

14 (Figure 3-9C,D, p<0.05). There was little difference between 2D and 3D culture conditions for fibronectin. We continued to observe a significant increase in expression of myosin at day 14 compared to day 7 (Figure 3-9E,F, p<0.0005)). Additionally, we saw significantly increased myosin expression in 3D culture conditions compared to 2D culture conditions (p<0.05). We observed slight increases in myosin expression in 2D laminin for both day 7 and day 14. When examining myosin light chain expression, we again found increased levels of expression at day 14 compared to day 7 for gelatin, collagen IV, fibronectin, and vitronectin, although these differences were not significant. We did not see much change in expression for cells cultured on 2D laminin between the two time points, and observed a significant decrease in expression for cells cultured on 3D laminin. There was a significantly higher expression of myosin light chain in 3D culture conditions compared to 2D at day 14 for gelatin, collagen IV, fibronectin and vitronectin.

C4. Bioreactor analysis

We analyzed the physical properties of the electrospun tubular scaffold in Figure 3-10. We observed a significant difference in the fiber size and fiber diameter of the fibers found on the lumen (Figure 3-10D,E,F) of the tubular scaffold compared to the outer circumference (Figure 3-10A,B,C). We found significantly smaller fibers on the outer most layer, with an average fiber size of 0.47+0.05μm and an average pore size of 1.78+0.25μm^2 (Figure 3-10A,B,C). The fibers in the lumen were larger with an average fiber size of 6.38+0.92μm and an average pore size of 55.36+11.07μm^2 (Figure 3-10D,E,F).

Immunofluorescence staining was performed on the sections of the Flk-1$^+$ CPC seeded electrospun tubular scaffolds. A cross-section of the tubular scaffold shows cells distributed
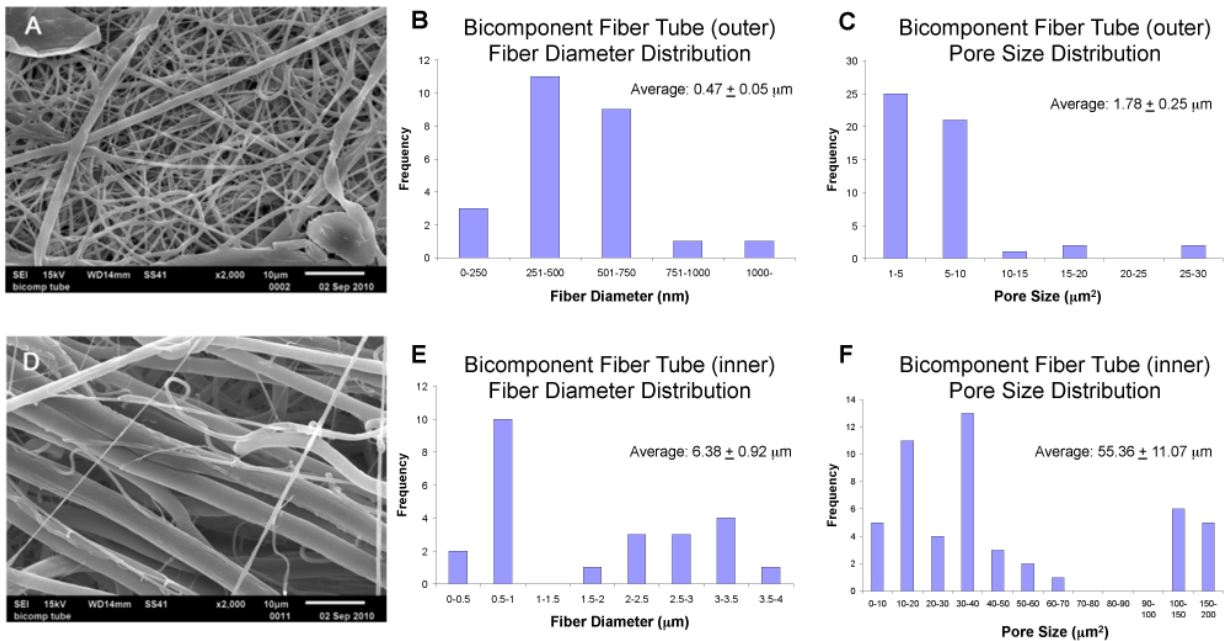
Figure 3-10: Physical properties of electrospun tubular scaffold Representative SEM micrographs show the fiber morphology of the outer most layer of fibers (A) and inner most layer (D). Fiber diameter distributions were calculated for the outer most layer of fibers (B) and the inner most layer (E). Pore size distributions were also calculated for the outer fibers (C) and the inner fibers (F).

throughout the tubular scaffold after 30 days of culture and flow through the lumen of the scaffold in the bioreactor chamber (Figure 3-11A, lumen is denoted as 'L' with lines indicating the borders of the scaffold). We then analyzed the scaffolds for evidence of the endothelial and smooth muscle cell layers. By seeding the CPCs at staggered time points under cell-specific culture media conditions, we hoped to create a layer of smooth muscle cells on the outer most circumference of the scaffold by maintaining the first CPCs seeded in smooth muscle cell growth media. The second set of CPCs was maintained in endothelial cell growth media in efforts to create a endothelial layer on the inner lumen of the tubular scaffold. The second CPCs seeded were labeled with GFP for the first experiment to establish the existence of cell layers. Further studies did not use GFP-labeled cells so they could be immunostained without GFP interference. We can see in Figure 3-11B that there is a higher concentration of green fluorescence found in the inner lumen of the tubular scaffold (concentration of GFP^{+} cells is shown with *). It is a

subtle observation as the fibers of the scaffold absorb any fluorochrome or dye, but the GFP-labeled CPCs are found in the lower right corner of panel 3-11B, which confirms the existence of cell layers. There is evidence of GFP$^+$ cells throughout the tubular scaffold, however the greatest concentration is found on the inner most area (lumen). We also performed cell type specific immunofluorescence staining for endothelial cells (CD31) and smooth muscle cells (SM-myosin). Again, there is a subtle distinction between the presence of marker-positive cells compared to the fibers. However, we are able to see a higher fluorescence for CD31$^+$ cells on the lumen (inner most circumference of the tubular scaffold, labeled 'I' and concentration of CD31$^+$ cells is shown with *) in Figure 3-11C. In Figure 3-11D, we are able to detect the subtle distinction of a concentration area of SM-myosin$^+$ cells on the outer most circumference of the tubular scaffold (labeled 'O' and concentration of SM-myosin$^+$ cells is shown with *). This is further evidence of the creation of CPC-derived layers.
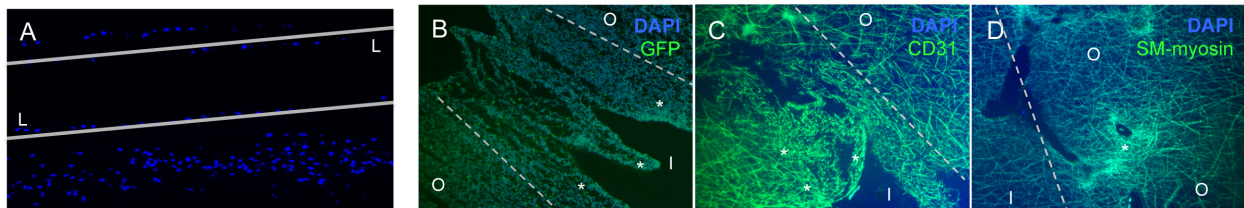

Figure 3-11: Immunofluorescent imagining of the electrospun tubular scaffold after 30 days in the bioreactor chamber Cells were found even distributed throughout the cross-section of tubular scaffold. The lumen of the scaffold is denoted by 'L' and the lines represent the boundaries of the scaffold (A). The existence of CPC-derived cell layers is found by the higher concentration of green fluorescence—more GFP$^+$ cells (shown with *) which were seeded second are found in the inner most circumference (denoted as 'I') of the tubular scaffold (B); more CD31$^+$ cells (shown with *), which were seeded second are found in the inner most circumference or lumen; more SM-myosin$^+$ cells (shown with *) which were seeded first are found on the outer most circumference of the tubular scaffold (denoted as 'O') (D).

D. Discussion

A major barrier to developing new treatment strategies for cardiovascular disease is the lack of understanding of the development of the native tissue. In order to elucidate the complicated role of the stem cell niche in cell fate decisions, we used a 3D culture system in

conjunction with known vascular ECM proteins. Matrigel has been used previously as a 3D substrate, but is ill-defined and inconsistent in composition, making it difficult to determine the exact microenvironment contributions [22]. In this study, we attempted to recapitulate the niche microenvironment to understand the role it plays in more committed vascular differentiation.

We have determined that native ECM proteins contribute to the induction of a CPC population previously [19,20,23]. We next wanted to determine the effects of the microenvironment on continued differentiation. By creating nanofibrous scaffolds and coating them with various ECM proteins, we are able to isolate individual protein contributions as well as determine the impact of a 3D environment on committed differentiation. We focused on the differentiation of endothelial and smooth muscle cells to ultimately create a tissue engineered small diameter vascular graft.

Native vessels consist of a layer of vascular endothelial cells on the lumen side of the vessel and several layers of vascular smooth muscle cells on tunica adventitia [24]. The endothelial layer is meant to prevent thrombosis, while the smooth muscle layer is to provide mechanical integrity and contraction. Previous studies have shown the ability to create artificial blood vessels or tissue engineered vascular grafts with limited capabilities. Heparin has been used to promote endothelial cell proliferation, but failed to support smooth muscle cell growth [25]. PCL has been used to create scaffolds to use for vascular tissue engineering, with success when immobilized VEGF has also been incorporated [26].

Our PCL scaffolds have previously been shown to withstand prolonged cell culture but require additional mechanical integrity for use in tissue engineering applications [21]. We have demonstrated that the microenvironment does have an effect on continued committed differentiation. We observed that laminin and vitronectin enhance endothelial cell growth.

141

Laminin has been shown to exist in myocardium, while vitronectin has been found in native blood vessels [27]. Both of these proteins were used in composite scaffolds, which have been used successfully as cardiac repair platforms [27]. Additionally, laminin has been shown to assist in endothelial cell growth in the retina [28]. Vitronectin was previously shown to enhance CPC populations [20]. Fibronectin was observed to enhance vascular smooth muscle cell growth. This was expected as fibronectin has a close, well-documented relationship with VEGF and vasculogenesis [29-31]. Scaffolds consisting of a fibronectin component have been shown to enhance endothelialization and vascular differentiation for vascular grafts or artificial vessels [32-35]. We were surprised to see that fibronectin did not have as great of an effect on endothelial cell differentiation as it did on the vascular smooth muscle cells.

The addition of a 3D microenvironment did not seem to greatly enhance endothelial cell differentiation. There were minor differences in Tie-2 gene expression at day 7 for 3D collagen IV, Flk-1 at day 14 for 3D laminin, and CD31 at day 7 for 3D vitronectin. However, an overall trend was not obvious. We suspect this is due to the nature of endothelialization and the process of vasculogenesis creating its own 3D structure. Perhaps our scaffold was too constricting to the natural process of vasculogenesis. There was a significant improvement of differentiation into smooth muscle cells that were cultured on the 3D scaffolds. We observed the improvement at the later time point (day 14), which is due to the amount of time required for cells to migrate to the interior of the scaffold and for the 3D microenvironment to have its effect. The addition of a 3D microenvironment or scaffold improves differentiation for vascular grafts [33,35], which our results confirm.

Through our studies for optimizing vascular differentiation, we were able to create a layered vascular graft using a bioreactor system. Small diameter vascular grafts with long-term

functionality have been extremely hard to create. Synthetic grafts for large vessels have shown great success, however the "gold standard" for replacement for a small vessel is to use an autologous graft [36]. Synthetic small diameter vascular grafts have problems with the lack of endothelialization on the luminal surface, which can lead to intimal hyperplasia formation and thrombosis [37-39]. Previous studies have focused on improving endothelialization through the addition of fibronectin and other factors, including the Flameng group [33] which created knitted polyester grafts that were coated with fibronectin and a stem cell homing factor SDF-1α. These grafts had marked success with improved endothelialization in a sheep model. Mun et al [40] created electrospun scaffolds to use for small diameter vascular grafts. The group was able to electrospin a PCL-PLA co-polymer to use *in vitro* with successful results. Zhao et al [41] created cellular sheets from mesenchymal stem cells, which they then fabricated into a tubular structure and implanted in a rabbit model. These constructs showed complete endothelialization after four weeks. This study is one of the few that combines synthetic scaffolds with ES cell-derived progenitors to create a layered structure. We have only demonstrated the proof of concept for this system—that we are able to create an ES cell-derived layered vascular graft, which is a novel development. This relatively simple system can be used in the future to recreate physiologically relevant situations, such as hypertension or chronic overload to examine the cellular effects.

E. Conclusions

We have characterized the effects of the microenvironment on differentiation of CPCs. After determining that the addition of a 3D microenvironment greatly enhances the induction of a CPC population, we aimed to determine if those effects were translated to later stages of differentiation as the CPCs continued to differentiate down a vascular pathway. We found that

laminin and vitronectin enhanced vascular endothelial cell growth in a traditional 2D cell culture system, while fibronectin enhanced vascular smooth muscle cell growth in a 3D system. The 3D system exhibited greater effects on differentiation at later time points, which is due to the longer amount of time necessary for cells to migrate to the interior of the scaffold. We have also created a layered tissue engineered vascular graft using our 3D scaffolds and time dependent cell-seeding protocol. Overall, we have enhanced our understanding the contributions of the microenvironment to vascular differentiation and how to apply that knowledge to develop new treatment strategies.

F. Acknowledgments

G. References

1. Schofield R. The relationship between the spleen colony-forming cell and the haemopoietic stem cell. Blood Cell, 1978, 4: 7-25.

2. Ratajczak MZ, Kucia M, Jadczyk T, Greco NJ, Wojakowski W, Tendera M, Ratajczak. Pivotal role of paracrine effects in stem cell therapies in regenerative medicine: can we translate stem cell-secreted paracrine factors and microvesicles into better therapeutic strategies? Leukemia, 2012; 26: 1166-1173.

3. Mouquet F, Pfister O, Jain M, Oikonomopouls A, Ngoy S, Summer R, Fine A, Liao R. Restoration of cardiac progenitor cells after myocardial infarction by self-proliferation and selective homing of bone marrow-derived stem cells. Cir Res 2005;97:1090-1092.

4. Heydarkhan-Hagvall S, Schenke-Layland K, Yang JQ, Heydarkhan S, Xu Y, Zuk Pa, MacLellan WR, Beygui RE. Human adipose stem cells: a potential source for cardiovascular tissue engineering. Cells Tissues Organs, 2008;187:263-274.

5. Schenke-Layland K, Rhodes KE, Angelis E, Butylkova Y, Heydarkhan-Hagvall S, Gekas C, Zhang R, Goldhaber JI, Mikkola HK, Plath K, MacLellan WR. Reprogrammed mouse fibroblast differentiate into cells of the cardiovascular and hematopoietic lineages. Stem Cells, 2008; 26: 1537-1546.

6. Ingber, DE. Mechanical signaling and the cellular response to extracellular matrix in angiogenesis and cardiovascular physiology. Circ Res. 2002; 91: 877-887.

7. Malik S, Wong ND, Franklin SS, Kamath TV, L'Italien GJ, Pio JR, Williams GR. Impact of the metabolic syndrome on mortality from coronary heart disease, cardiovascular disease, and all causes in United States adults. Circulation. 2004;110:1245-1250.

8. Hunt SA, Baker DW, Chin MH, et al. ACC/AHA Guidelines for the evaluation and management of chronic heart failure in the adult: Executive Summary; A report of the American College of Cardiology/American Heart Association Task Force on practice guidelines (committee to revise the 1995 guidelines for the evaluation and management of heart failure): Developed in collaboration with the International Society for Heart and Lung Transplantation, Endorsed by the Heart Failure Society of America. Circulation. 2001;104:2996-3007.

9. Ornish D, Brown SE, Scherwitz LW, et al. Can lifestyle changes reverse coronary heart disease? Lancet 1990;336:129-133.

10. Nerem RM. Tissue engineering: confronting the transplantation crisis. Proc Inst Mech Eng [H], 2000;214(1): 95-99.

11. Vacanti JP. Tissue engineering: the design and fabrication of living replacement devices for surgical reconstruction and transplantation. Lancet, 1999;354(supp 1): S132-S134.

12. Zong X, Chung CY, Yin L, Fang D, Hsiao BS, Chu B, Entcheva E. Electrospun fine-textured scaffolds for heart tissue constructs. Biomaterials, 2005; 26(26): 5330-5338.

13. Khil MS, Kim KY, Kim SZ, Lee KH, Novel fabricated matrix via electrospinning for tissue engineering. J Biomed Mater Res B Appl Biomater, 2005; 15(72): 117-124.

14. Formhals A. US Patent 1,975,5042; 1934.

15. Theron SA, Zussman E, Yarin AL. Experimental investigation of the governing parameters in electrospinning of polymer solutions. Polymer, 2004; 45:217-230.

16. Reneker DH, Kataphinan W, Theron A, Zussman E, Yarin AL. Nanofiber garlands of polycaprolactone by electrospinning. Polymer, 2002; 43: 6785-6794.

17. Bhattarai SR, Yi HK, Hwang PH, Cha DI, Kim HY. Novel biodegradable electrospun membrane: scaffold for tissue engineering. Biomaterials, 2004;25:2595.

18. Li WJ, Caterson EJ, Tuan RS, Ko FK. Electrospun nanofibrous structure: a novel scaffold for tissue engineering. J Biomed Mater Res, 2002;60:613.

19. Schenke-Layland K, Nsair A, van Handel B, Angelis E, Gluck JM, Votteler M, Goldhaber JI, Mikkola HKA, Kahn M, MacLellan WR. Recapitulation of the embryonic cardiovascular progenitor cell niche. Biomaterials, 2011; 32: 2748-2756

20. Heydarkhan-Hagvall S, Gluck JM, Delman C, Jung M, Ehsani N, Full S, Shemin RJ. The effect of vitronectin on the differentiation of embryonic stem cells in a 3D culture system. Biomaterials, 2012; 33 (7), 2032-2040.

21. Gluck JM, Rahgozar P, Ingle NP, Rofail F, Petrosian A, Cline MG, Jordan MC, Roos KP, MacLellan WR, Shemin RJ, Heydarkhan-Hagvall S. Journal Biomedical Materials Research Part B, 2011; 99B: 180-190.

22. Cushing MC, Anseth KS. Hydrogel cell cultures. Science, 2007; 316: 1133-1134.

23. Chapter 2, section C: Hyaluronan-based three-dimensional microenvironment potently induce cardiovascular progenitor cell population.

24. L'Heureux N, Dusserre N, Konig G, Victor B, Keire P, Wight TN, Chronos NAF, Kyles AE, Gregory CR, Hoyt G, Robbins RC, McAllister TN. Human tissue-engineered blood vessels for adult arterial revascularization. Nat Med, 2006; 12: 361-365.

25. Chiu LL, Radisic M. Scaffolds with covalently immobilized VEGF and angiopoietin-1 for vascularization of engineered tissues. Biomaterials, 2010; 31: 226-241.

26. Du F, Wang H, Zhao W, Li D, Kong D, Yang J, Zhang Y. Gradient nanofibrous chitosan/poly-e-caprolactone scaffolds as extracellular microenvironment for vascular tissue engineering. Biomaterials, 2012; 33: 762-770.

27. Godier-Furnemont AFG, Martens TP, Koeckert MS, Wan L, Parks J, Arai K, Zhang G, Hudson B, Homma S, Vunjak-Novakovic G. Composite scaffold provides a cell delivery platform for cardiovascular repair. PNAS, 2011; 108: 7974-7979.

28. Aizawa Y, Shoichet MS. The role of endothelial cells in the retinal stem and progenitor cell niche within a 3D engineered hydrogel matrix. Biomaterials, 2012; 33: 5198-5205.

29. Wijelath ES, Rahman S, Murray J, Patel Y, Savidge G, Sobel M. Fibronectin promotes VEGF-induced CD34+ cell differentiation into endothelial cells. Journal of Vascular Surgery, 2004; 39: 655-660.

30. Wijelath ES, Murray J, Rahman S, Patel Y, Ishida A, Stand K, Aziz S, Cardona C, Hammond WP, Savidge GF, Rafii S, Sobel M. Novel vascular endothelial growth factor binding domains of fibronectin enhance vascular endothelial growth factor biological activity. Circ Res, 2002; 91: 25-31.

31. Risau W, Flamme I. Vasculogenesis. Annu Rev Cell Dev Biol, 1995; 11: 73-91.

32. Krawiec JT, Vorp DA. Adult stem cell-based tissue engineered blood vessels: A review. Biomaterials, 2012; 33: 3388-3400.

33. De Visscher G, Mesure L, Meuris B, Ivanova A, Flameng W. Improved endothelialization and reduced thrombosis by coating a synthetic vascular graft with fibronectin and stem cell homing factor SDF-1α. Acta Biomaterialia, 2012; 8: 1330-1338.

34. Pimton P, Sarker S, Sheth N, Perets A, Marcinkiewicz C, Lazarovici P, Lelkes P. Fibronectin-mediated upregulation of a5b1 integrin and cell adhesion during differentiation of mouse embryonic stem cells. Cell Adhesion and Migration, 2011; 5: 73-82.

35. Ferreira LS, Gerecht S, Fuller J, Shieh HF, Vunjak-Novakovic G, Langer R. Bioactive hydrogel scaffolds for controllable vascular differentiation of human embryonic stem cells. Biomaterials, 2007; 28: 2706-2717.

36. Davies MG, Hagen PO. Pathophysiology of vein graft failure: a review. Eur J Vasc Endovasc Surg, 1995; 9: 7-18.

37. Rotmans JI, Heyligers JMM, Stroes ESG, Pasterkamp G. Endothelial progenitor cell-seeded grafts: rash and risky. Can J Cardiol, 2006; 22: 1113-1116.

38. Welch M, Durrans D, Carr HM, Vohra R, Rooney OB, Walker MG. Endothelial cell seeding: a review. Ann Vasc Surg, 1992; 6: 473-484.

39. Davie EW. Biochemical and molecular aspects of the coagulation cascade. Thromb Haemost, 1995; 74: 1-6.

40. Mun CH, Jung Y, Kim SH, Lee SH, Kim HC, Kwon IK, Kim SH. Three-dimensional electrospun poly(lactide-co-e-caprolactone) for small-diameter vascular grafts. Tissue Engineering Part A, 2012; 18: 1608-1616.

41. Zhao J, Liu L, Wei J, Ma D, Gen W, Yan X, Zhu J, Du H, Liu Y, Li L, Chen F. A novel strategy to engineer small-diameter vascular grafts from marrow-derived mesenchymal stem cells. Artif Organs, 2012; 36: 93-101.

CHAPTER FOUR

Extracellular matrix proteins in the microenvironment enhance cardiac differentiation of human induced pluripotent stem cells

A. Introduction

Stem cell biology has become a major focus of recent cardiovascular research. Many therapeutic approaches using mouse ES cell models have been reported and we have also demonstrated successful murine cardiovascular differentiation [1-3]. However, translating this work to a human model has proven difficult. Directing human ES or iPS cell differentiation down a cardiovascular lineage is more challenging and the contribution from the microenvironment to cell fate decisions poorly understood. Cell fate is thought to be controlled both spatially and temporally, as well as through cell-cell and cell-matrix interactions. Paracrine and autocrine effects are also thought to regulate cell fate—there is mounting evidence that stem cells secrete a variety of growth factors, cytokines, chemokines and bioactive lipids which regulate biology and interactions within the surrounding microenvironment. These factors inhibit apoptosis, stimulate proliferation, and promote vascularization [4]. The surrounding microenvironment is 3D in nature and regulates self-renewal, proliferation, and differentiation through cell-cell and cell-matrix interactions. This makes understanding the role of ECM in cardiac development very important to understand.

Our previous work demonstrated that stem cell-derived CPC commitment and further cardiovascular differentiation is influenced by the microenvironment and that an in vitro 3D culture model can be used to promote cardiac differentiation in a mouse ES cell model. We

established that collagen IV and laminin are present within the endogenous mouse and human CPC niche, while collagen I and fibronectin are found outside the niche. Collagen IV was identified as an ECM component with the ability to induce trophoectoderm differentiation in mES cells [5]. Collagen IV, which can be detected in the mouse embryo as early as the 32-64-cell stage [6] induced expression of haematopoietic, endothelial, and smooth muscle genes specific to the mesoderm, as well as a panel of trophoectoderm-markers. Adding ECM proteins to mES cells can induce a CPC population [2]. The addition of collagen IV with a synthetic 3D electrospun matrix made of a co-axial nanofibers containing a PCL-gelatin sheath and PU core induced the highest CPC population of the study [7]. Additional studies demonstrated that laminin- or vitronectin-coated 3D scaffolds induced an even higher population of Flk-1$^+$ CPCs as compared to 2D culture conditions [3].

We aim to translate our work with microenvironment studies to a human iPS cell model and try to understand the contributions of both a 3D microenvironment and ECM proteins present in native tissue have on human cardiac differentiation.

B. Materials and Methods

B1. Human iPS cell culture and differentiation

hiPS cells (hiPS2 line) were obtained from the UCLA Embryonic Stem Cell Bank. Cells were maintained in an undifferentiated state in Dulbecco's modified Eagle's medium/F12 (DMEM/F12, Invitrogen, Carlsbad, CA USA) with 10% Knockout Serum Replacement (KSR, Invitrogen), 0.1mM β-mercaptoethanol, 2mM Glutamax (Invitrogen), 0.1mM nonessential amino acids (Invitrogen), and 10ng/mL bFGF (PeproTech, Rocky Hill, NJ USA). No antibacterial agents were added. Cells were cultured on irradiated murine embryonic fibroblast

(MEF, Applied StemCell Inc, Menlo Park, CA USA) feeder layers which were plated at a density of about 35,000 MEFs/cm² at 37C, 5% CO2 in a humidified incubator. Media was refreshed daily.

A modified version of Willems et al [8] protocol was used to induce cardiomyocyte differentiation. Briefly, hiPS cells were used directly from MEFs and detached using TrypLE Select. Cells were collected and put through a 100μm cell strainer before being pelleted via centrifugation at 1200rpm for 5minutes. Cells were resuspended to 600,000 cells/mL in mTeSR media supplemented with a ROCK Inhibitor (Y-27632, Sigma, final concentration is 0.01μM) and 10ng/ml BMP4 (R&D Systems). 50μl of the cell suspension was added to each well of a conical-bottom 96-well plate (Fisher Sci, USA). The plates are then centrifuged at 1200rpm for 5min and left overnight in the incubator to create uniformly formed embryoid bodies (EBs). The following day, EBs are transferred to a 6-well low-attachment dish (Corning) and the media is changed to StemPro 34 (Invitrogen) media supplemented with 3ng/mL Activin A (R&D Systems), 5ng/mL bFGF (R&D Systems), and 10ng/mL BMP4 (R&D Systems) (called 'Stage 1' media). One well of the 6-well dish can hold approximately 100-150 EBs. The media is refreshed every 2-3 days as necessary. On day 4, the floating EBs are transferred to an ECM-treated dish with 2mL of Stage 1 media with IWR-1 (at a final concentration of 5μM, Sigma). The following day, the media is changed to StemPro 34 (Invitrogen) supplemented with 5ng/mL VEGF, 10ng/mL bFGF, 5μM IWR-1. Media is refreshed every other day.

ECM-treated dishes are prepared in 2D and 3D conditions. 2D dishes are coated with collagen IV (ColIV, 5μg/cm^2, BD Biosciences, San Jose CA), laminin (5μg/cm^2, BD Biosciences), fibronectin (5μg/cm^2, Sigma), vitronectin (50nm/cm^2, Chemicon), and gelatin (0.1% w/v in sterile PBS) or 3D electrospun scaffolds coated with collagen IV, laminin, fibronectin,

vitronectin, and gelatin (0.1% gelatin w/v in sterile PBS) following the same protocol as 2D dishes.

B2. Scaffold fabrication and in vitro differentiation in 3D culture

We have utilized electrospinning to produce scaffolds with nano- to microdiameter fibers with similar structural properties to the ECM as described before [9]. Briefly, gelatin type B (bovine skin 10% w/v, Sigma-Aldrich) and ε-polycaprolactone (PCL, 10% w/v, Sigma-Aldrich) were mixed together and dissolved in 1,1,1,3,3,3-hexafluoro-2-propanol (HFP, Sigma-Aldrich). The solution was then loaded into a 10mL syringe to which an 18-gauge blunt-ended needle was attached. A core solution of polyurethane (PU, 5% w/v, Sigma-Aldrich) was dissolved in HFP and loaded into a 3mL syringe to which a 25-gauge needle was attached. This syringe and needle system was then loaded into a modified syringe pump. The positive output lead of a high voltage supply (28kV; Glassman High Voltage Inc, NJ USA) was attached to the 10mL syringe needle. In the created electric field, a thin jet was ejected from the polymer solution in the syringe at a flow rate of 70μL/min. The grounded copper target (5cm x 5cm) was placed approximately 17cm under the needle tip and upon introduction of the electric field Taylor cone formation was observed at the base of the needle tip. A dry fibrous scaffold was collected in the form a 3D mat (100-200μm thick). The electrospun scaffolds were then sterilized by soaking the scaffolds in 70% ethanol for 30min at room temperature. After 3 washes of sterile PBS, the scaffolds were aseptically cut into 1cm x 1cm squares and coated with colIV, fibronectin, laminin, vitronectin, and gelatin as described previously in section B1.

B3. Immunofluorescent staining

The hiPS cells plated on ECM-coated culture slides as well as undifferentiated hiPS cells were washed and fixed with 4% paraformaldehyde, for 20 min and rinsed with PBS. Slides were then blocked with 1% bovine serum albumin (BSA) and 2% goat serum in PBS for 1 h at room temperature. Slides were then incubated with primary antibodies (basic calponin (Dako), troponinT (R&D systems), MF-20 (Developmental Studies Hybridoma Bank), connexin 43 (Santa Cruz), and troponinI (R&D systems)) or one hour at room temperature or overnight at 4°C followed by several washes with PBS. Alexa Fluor 488- or 546-conjugated secondary antibodies (Molecular Probes, Eugene, OR) were applied to the samples and incubated for 30 minutes at room temperature. After several washes, the cells were counterstained with 4'-6-diamidino-2-phenylindole (DAPI) followed by mounting ProLong Gold antifade mounting medium (Molecular Probes, Carlsbad, CA). Staining without primary antibodies served as controls. Digital images were acquired using a Leica DM IRB inverted microscope system equipped with 20x (0.40 numerical aperture (NA)) and 40x (0.75 NA) objectives (Leica Microsystems Inc., Bannockburn, IL).

B4. Fluorescence-activated cell sorter analysis (FACS)

Cells were harvested from both 2D (conventional culture) and 3D (scaffold) culture at day 10, pelleted via centrifugation, washed in FACS buffer (sterile PBS supplemented with 1% ES-FBS and 0.25% saponin) and incubated with the primary antibody (cardiac Troponin-T, 1:350, R&D Systems) at 4°C for at least 45minutes. The secondary antibody (Alexa Fluor 488, 1:400, Molecular Probes) was added following a washing step and centrifugation. The cells were gated by forward scatter (FSC) versus side scatter (SSC) to eliminate debris. A minimum of

10,000 events were counted for each analysis. All analyses were performed using a Becton Dickinson FACScan analytic flow cytometer (BD Biosciences) with FCS Express software (DeNovo Software, Thornhill, Ontario, Canada) at the UCLA Flow Cytometery Laboratory.

B5. Quantitative Real time-PCR analysis (RT-PCR)

Total RNA was extracted from cells using Qiagen mini RNAeasy kits according to the manufacturer's instructions. First-strand cDNA was generated from RNA by using the Quantitect Reverse Transcription kit (Omniscript; Qiagen). Real-time quantitative PCR was conducted using the ABI PRISM 7900 Sequence Detection System (TaqMan; Applied Biosystems) with the UCLA GenoSeq Core. PCR amplicons were detected by fluorescent detection of SYBR green (QuantiTect SYBR green PCR kit; Qiagen). Data was analyzed using the ΔΔCt method, using ribosomal protein S26 as a stable reference gene for normalization control. Primers used were purchased from Qiagen (QuantiTect Primer Assay).

B6. Statistical Analyses

All results are presented as mean values $\pm$ standard error of mean (SEM). Statistical significance was determined using a general linear model fit with the main effects for protein (gelatin, collagen IV, laminin, fibronectin, and vitronectin) and environment (2D and 3D) and an interaction term (protein x environment). $P < 0.05$ were defined as statistically significant.
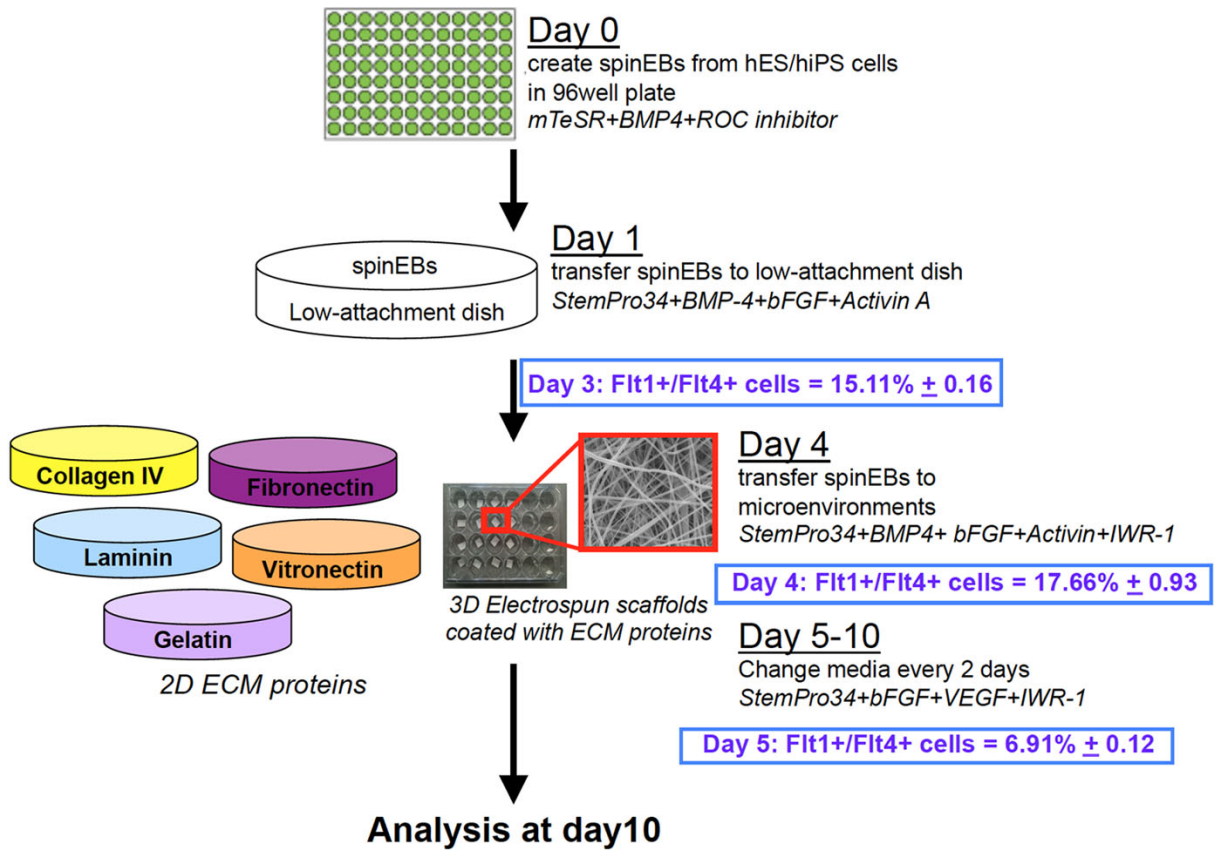
C. Results

Figure 4-1: Experimental Design Schematic depicting experimental design. EBs are created on Day 0 and transferred to a low attachment dish on Day1. At Day 3, 15.11% of cells are expressing CPC markers Flt1 and Flt4. At Day4, EBs are transferred to different microenvironments, with 17.66% CPCs. On Day 5, only 6.91% of cells still express CPC markers. Analysis was performed on day 10.

We were successfully able to differentiate hiPS cells towards a cardiac lineage using a spinEB method adapted from Willems et al [8]. As shown in Figure 4-1, we created uniformly sized EBs at day 0 and transferred them to a low-attachment dish at day 1. On day 4, we transferred the EBs to the various ECM microenvironments, in both 2D and 3D culture conditions. We analyzed the number of cardiac progenitor cells present in the cell population at the early stages of the protocol. Using the cell surface markers Flt1 and Flt4 as previously shown are markers of human CPCs [10], we found that there was a $15.11 \pm 0.16\%$ at day 3. Day 4 showed an increase in CPCs with $17.66 \pm 0.93\%$ Flt1$^+$/Flt4$^+$ expression. Day 5 saw a decrease in

CPC population with only 6.91 $\pm$ 0.12% exhibiting both CPC markers. This confirms that day 4 is the day with the highest cardiac differentiation potential for the transfer to the microenvironment. The progression of the size of EBs throughout the course of the differentiation protocol can be seen in Figure 4-2.
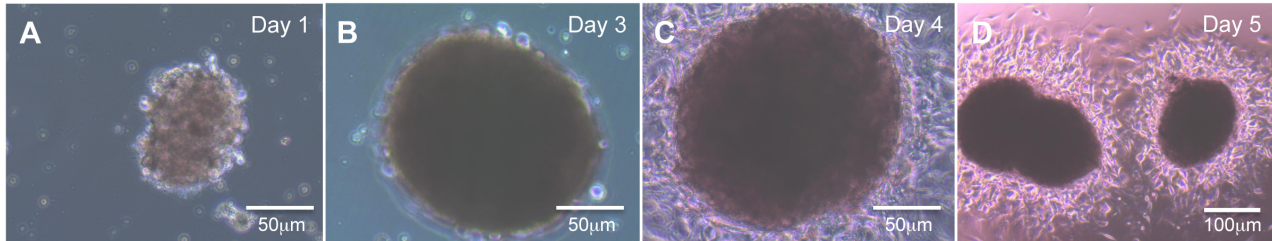

Figure 4-2: SpinEB creation and progression EBs are created on Day0 and transferred to a low attachment dish on Day1. On Day4, the EBs are transferred to the different microenvironment.

C1. Immunofluorescence

Our cardiac differentiation protocol is shown to be successful as cells exhibited cardiac markers Nkx2.5, MF-20, troponinT, connexin43, calponin, and troponinI (Figure 4-3). We observed large EB formation, followed by individual differentiating cells migrating out of the EB after being transferred to the microenvironment on day 4. In particular, cells cultured on collagen IV (Figure 4-3A,E,I,M) show positive signal for all cardiac markers. The large EB with migrating cells is evident in Figure 4-3A and 4-3E. Laminin (Figure 4-3B,F,J,N) also exhibits positive signal for all the cardiac markers. A large EB is present with cells migrating out of the EB positive for troponinT and connexin43 (Figure 4-3B). Laminin cultures support monolayer cell confluence as seen in panel 4-3J. These cells all exhibit a strong signal for calponin. Similar to collagen IV and laminin, fibronectin also exhibits positive signal for all cardiac markers of interest. Vitronectin is shown to have a weaker signal for the cardiac markers of interest. We
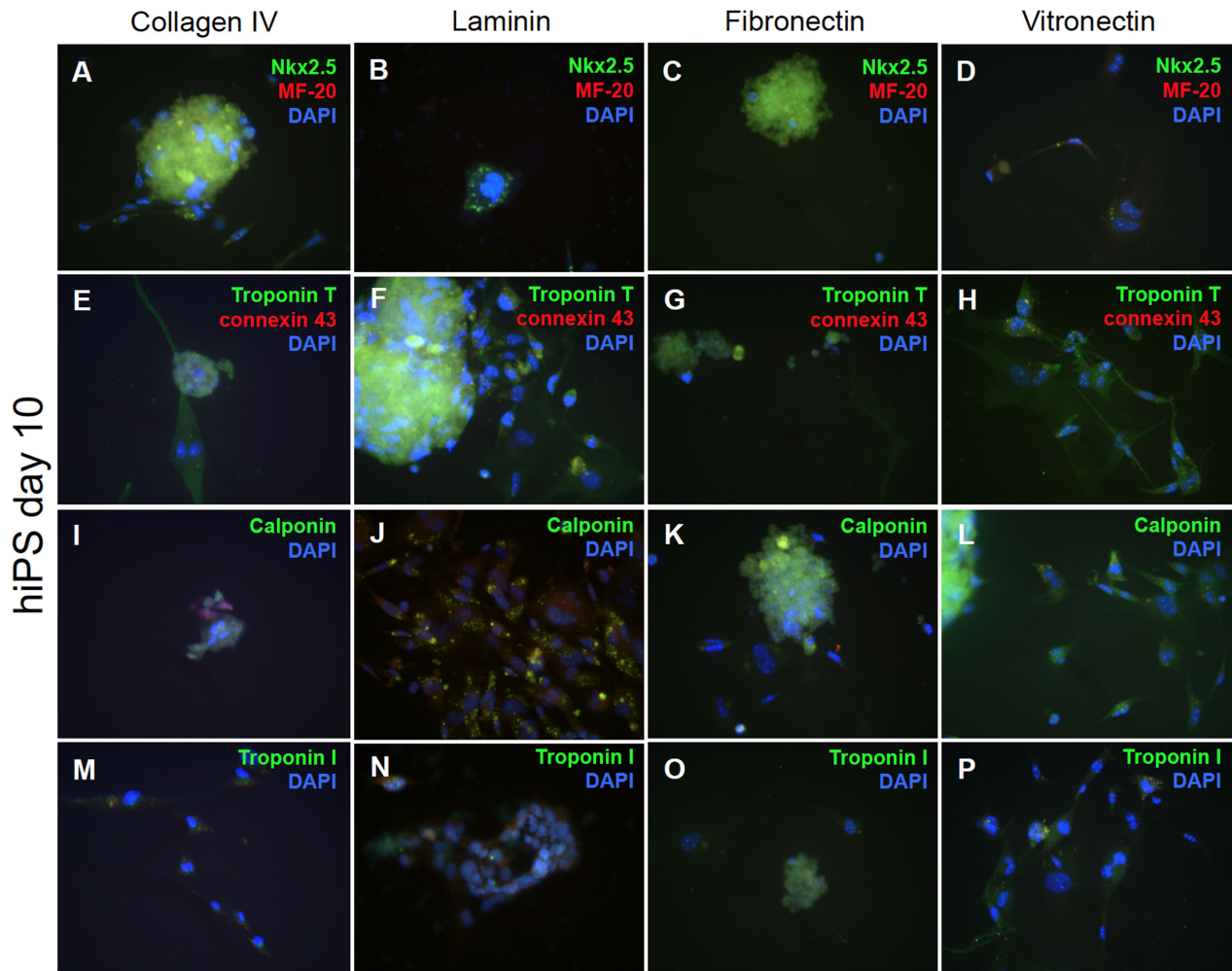
Figure 4-3: Cardiac differentiation of hiPS cells Cells exposed to different microenvironments are analyzed for cardiac differentiation: first row (A-D) Nkx2.5 (green) MF-20 (red); second row (E-H) TroponinT (green) connexin43 (red); third row (I-L) Calponin (green); fourth row (M-P) TroponinI (green)

observed that the EBs once transferred to the vitronectin environment did not adhere as well as the other ECMs (data not shown).

C2. FACS analysis

At day 10 of the cardiac differentiation protocol, we harvested cells for FACS analysis to evaluate troponinT expression for both 2D and 3D culture systems. We observed that the effect of the 2D culture system was significantly higher than that of the 3D system. More specifically, we observed significantly higher expression for troponinT in 2D cultures as compared to 3D

culture systems across all five ECM proteins of interest (p<0.0001). In particular, there was a significant difference between 2D and 3D cultures for gelatin (2D: 49.47±2.17%, 3D: 16.02±2.23%), laminin (2D: 64.09±0.75%, 3D: 43.51±0.41%), and fibronectin (2D: 68.51±0.92%, 3D: 30.36±0.92%). We observed little difference between 2D and 3D cultures for collagen IV (2D: 61.33±2.67%, 3D: 59.25±0.71%) and vitronectin (2D: 34.10±3.41%, 3D: 30.43±0.60%). Collagen IV (both 2D and 3D cultures), laminin (2D culture) and fibronectin (2D culture) exhibited the highest levels of troponinT, over 60%. Gelatin and fibronectin in 3D culture as well as both 2D and 3D culture of vitronectin showed the lowest levels of troponinT expression, with about 30%. We found a significant difference between gelatin vs. collagen IV (p<0.0001), laminin (p<0.0001) and fibronectin (p<0.0001), with the gelatin mean effect being significantly smaller. The collagen IV mean effect compared to fibronectin (p<0.01) and
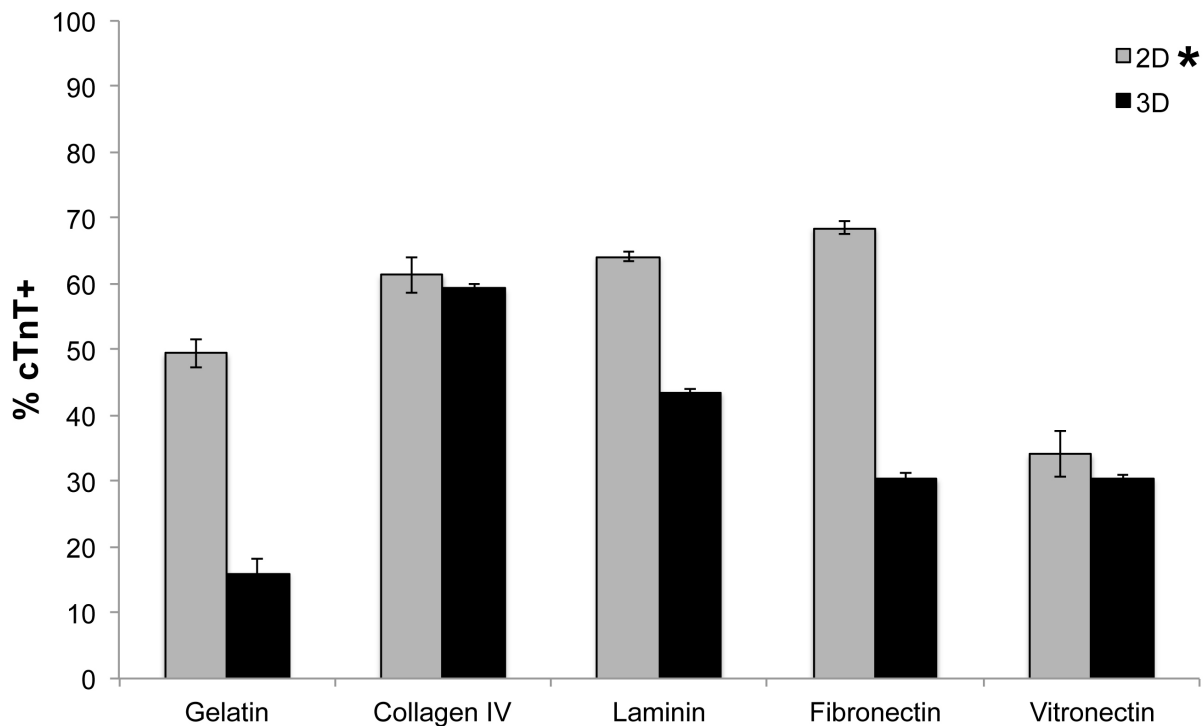

Figure 4-4: FACS analysis of cardiac differentiation hiPS cells at day 10 exposed to both 2D (grey bars) and 3D (black bars) microenvironments were evaluated for cardiac TroponinT expression via FACS analysis.
N=3, *p<0.0001 (2D vs. 3D)

vitronectin (p<0.0001) was significantly larger. Also, the laminin mean effect compared to vitronectin (p<0.0001) was significantly larger, similar to the fibronectin mean effect compared to vitronectin (p<0.0001). Overall, we observed that the ECM proteins have a large impact on increased cardiac differentiation, while the 3D environment seems to inhibit or delay cardiac differentiation.

C3. RT-PCR analysis

At day 10, we harvested RNA from both 2D and 3D cultures for all proteins of interest. We then performed quantitative real-time PCR analysis to examine the mRNA levels of the markers of interest. We included analysis for endothelial and smooth muscle markers to determine if the microenvironments promoted endothelial or smooth muscle differentiation in lieu of or in addition to cardiac differentiation (Figure 4-5). We observed low levels of expression for the early endothelial cell marker Tie2 (4-5A). We found a significant difference between the contributions of the five proteins examined. Specifically, we observed relatively similar expression of Tie2 for gelatin (2D: 3.18 ± 0.59; 3D 1.01 ± 0.49), and collagen IV (2D: 3.81 ± 1.70; 3D 0.70 ± 0.53), and vitronectin (2D: 1.11 ± 0.56; 3D 0.45 ± 0.30)—all three proteins demonstrated a similar pattern of slightly higher expression in 2D culture as compared to 3D culture. Laminin (2D: 1.93 ± 0.82; 3D 6.11 ± 2.01) and fibronectin (2D: 2.80 ± 1.51; 3D 18.51 ± 8.85) both exhibited a pattern of higher expression in 3D cultured compared to 2D cultures. We did see a significantly higher expression of Tie2 for fibronectin in 3D (p<0.05 compared to all ECM proteins). Similarly, we observed high expression of the other more mature vascular endothelial markers we evaluated, vWF (Figure 4-5B) and VE-Cadherin (Figure 4-5C), for the 2D and 3D fibronectin (vWF 2D: 6.05 ± 3.66; 3D 12.25 ± 2.50; VE-cadherin 2D: 27.30 ± 9.57; 3D 36.26 ± 17.16)
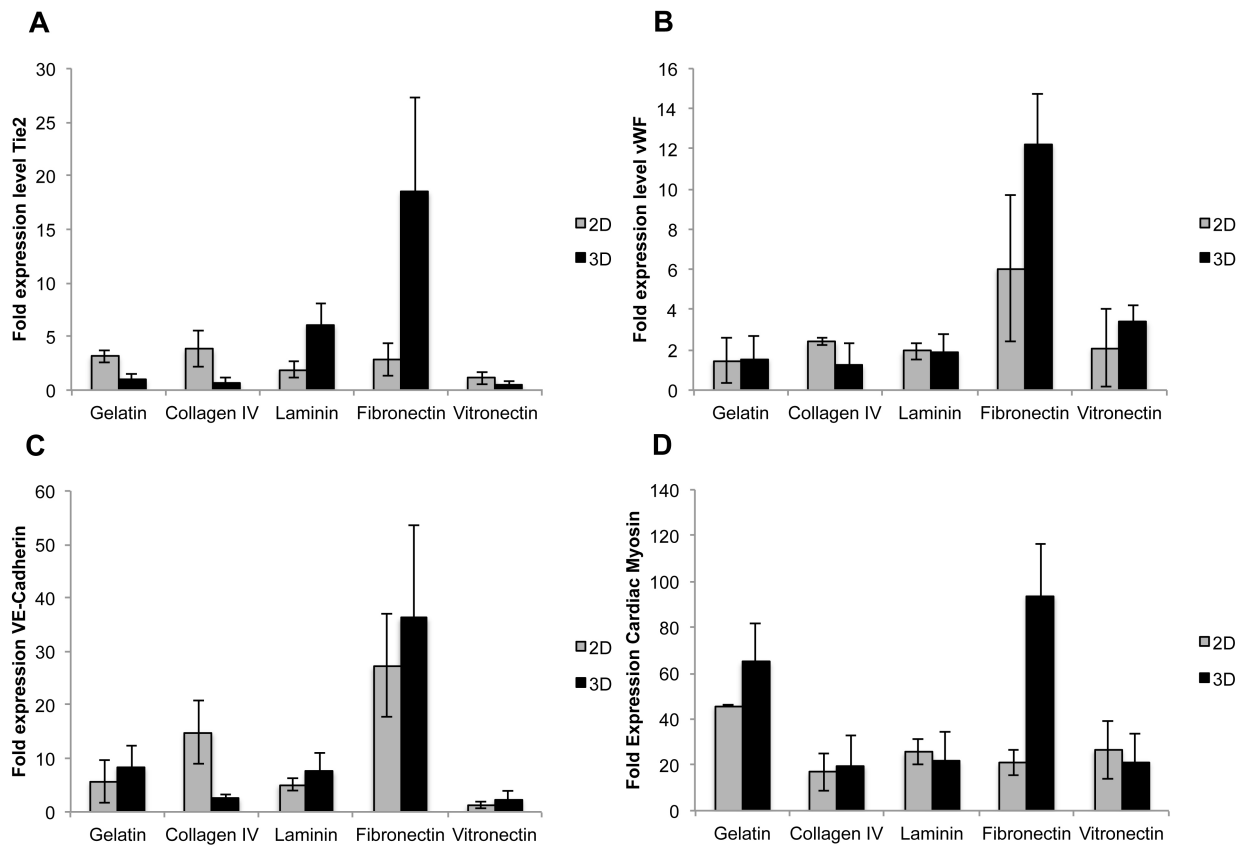
Figure 4-5: qPCR analysis of vascular endothelial and smooth muscle markers hiPS cell subjected to cardiac differentiation and exposed to microenvironments in both 2D (grey bars) and 3D (black bars) were analyzed at day 10 for endothelial markers: Tie2 (A), vWF (B) and VE-Cadherin (C); and smooth muscle marker myosin (D). n=3

culture conditions. Fibronectin elicited a significantly higher expression of vWF ($p<0.0010$) and VE-Cadherin ($p<0.005$) compared to the other ECM proteins of interest. The other proteins maintained relatively similar lower levels of expression of vWF as compared to fibronectin (gelatin 2D: 1.47 ± 1.12; 3D 1.57 ± 1.10; collagen IV 2D: 2.39 ± 0.18; 3D 1.23 ± 1.27; laminin 2D: 1.93 ± 0.42; 3D 1.87 ± 0.91; vitronectin 2D: 2.08 ± 1.93; 3D 3.43 ± 0.83). Likewise, a similar pattern of expression exists for VE-Cadherin. Gelatin (2D: 5.69 ± 3.96; 3D 8.38 ± 3.88), laminin (2D: 5.10 ± 1.10; 3D 7.57 ± 3.53), and vitronectin (2D: 1.27 ± 0.59; 3D 2.35 ± 1.56) exhibit similar levels of expression of VE-Cadherin. We see higher levels of expression of smooth muscle markers for cells cultured in certain 3D microenvironments. In particular, 3D gelatin (65.01 ± 16.39) and fibronectin (93.86 ± 22.37) appear to enhance the expression levels of myosin as seen in Figure 4-

5D. 2D gelatin (45.78+0.47) exhibits a similar expression to its 3D counterpart, while we observe a minimal difference between 2D and 3D environments for collagen IV (2D: 16.97+8.25; 3D 19.67+13.36), laminin (2D: 25.60+5.60; 3D: 21.67+12.70), and vitronectin (2D: 26.70+12.80; 3D: 21.29+12.06). There was a significant difference between 2D (20.94+5.51) and 3D (93.86+22.37) culture conditions for fibronectin. Again we found a significant difference among the five proteins examined (p<0.01).

In Figure 4-6, we determined expression levels of cardiac-specific genes. We observed significantly higher expression of actinin (figure 4-6A) in 2D laminin (17.39+4.84) and 3D

A

B

C

D
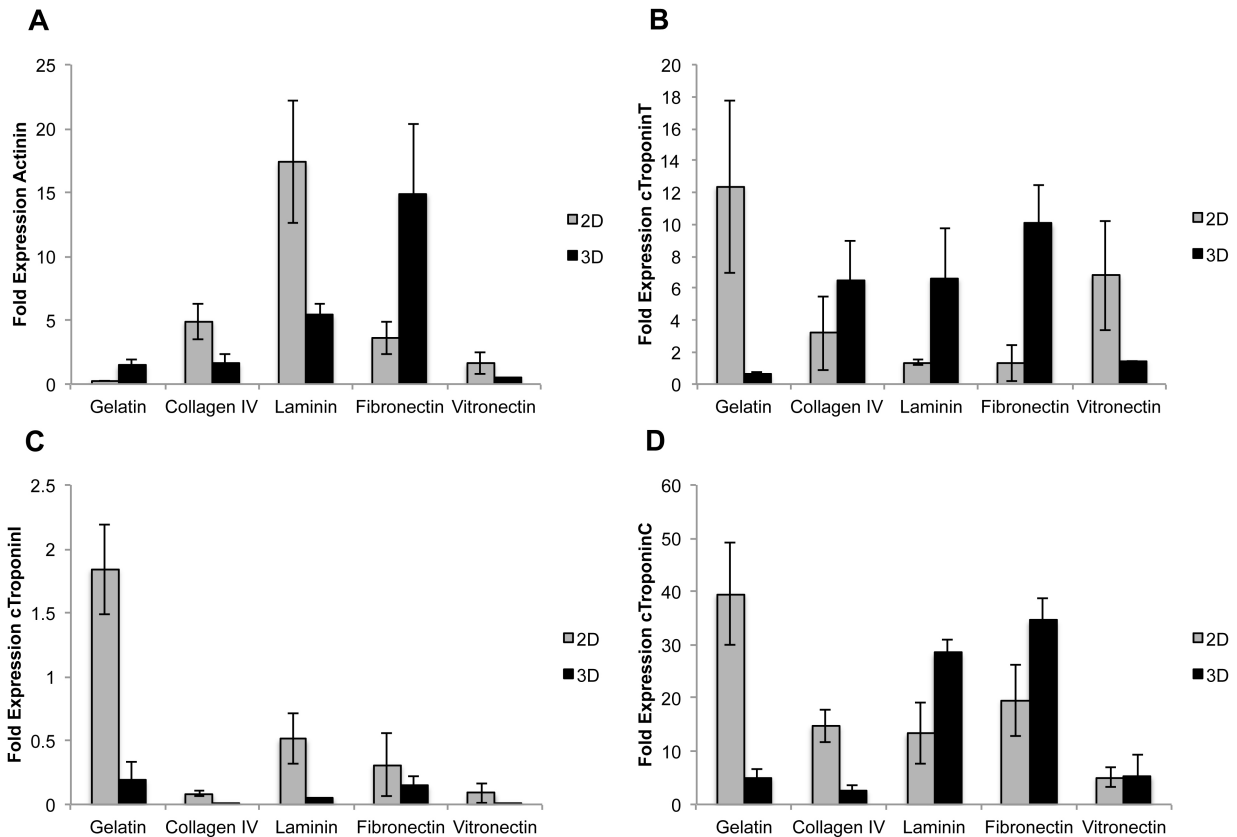
Figure 4-6: qPCR analysis of cardiac differentiation. hIPS cells were subjected to cardiac differentiation and exposed to different microenvironments in both 2D (grey bars) and 3D (black bars). Cardiac markers evaluated were actinin (A), Troponin T (B), Troponin I (C), and Troponin C (D). RNA was isolated on day 10, n=3

fibronectin (14.92+5.45). These levels of expression were significantly higher than their counterparts (3D laminin: 5.42+0.89; 2D fibronectin: 3.59+1.30). The other proteins expressed

similar low levels of actinin: gelatin (2D: 0.26 ± 0.01; 3D: 1.47 ± 0.41), collagen IV (2D: 4.91 ± 1.41; 3D: 1.59 ± 0.72), and vitronectin (2D: 1.62 ± 0.82; 3D: 0.52 ± 0.04). We observed a significant difference between the five proteins ($p<0.005$), as well as a significant interaction between the 2D/3D environment and the ECM proteins ($p<0.01$), namely 2D laminin and 3D fibronectin. The troponin complex is an important mediator of cardiac contractility and made up of 3 components: TroponinT, TroponinI, and TroponinC. We examined levels of TroponinT expression (Figure 4-6B) and found that expression was enhanced by collagen IV (6.54 ± 2.39), laminin (6.62 ± 3.18), and fibronectin (10.04 ± 2.46) in 3D compared to their 2D counterparts (2D collagen IV: 3.20 ± 2.33; 2D laminin: 1.35 ± 0.18; 2D fibronectin: 1.311 ± 1.17). Standard 2D conditions of gelatin (12.37 ± 5.40) and vitronectin (6.80 ± 3.42) also enhanced troponinT expression compared to the same proteins in 3D conditions (3D gelatin: 0.58 ± 0.17; 3D vitronectin: 1.45 ± 0.01). Figure 4-6C shows the expression levels of TroponinI, which were increased in the 2D cultures compared to the 3D cultures ($p<0.0001$), as well as significant difference between the proteins ($p<0.0001$). There was also a significant interaction between the 2D/3D environment and the ECM proteins ($p<0.0005$). The expression levels are shown to be relatively similar for all the conditions, except 2D gelatin, which is observed to promote TroponinI (Gelatin 2D: 1.84 ± 0.35, 3D: 0.19 ± 0.14; collagen IV 2D: 0.08 ± 0.02, 3D: 0.004 ± 0.0006; laminin 2D: 0.51 ± 0.20, 3D: 0.05 ± 0.01; fibronectin 2D: 0.31 ± 0.25, 3D: 0.14 ± 0.07; vitronectin 2D: 0.09 ± 0.08, 3D: 0.002 ± 0.0002). Similar to TroponinT, we observed higher expression levels of TroponinC in 3D for laminin (28.43 ± 2.37) and fibronectin (34.53 ± 4.18), as well as gelatin in 2D (19.13 ± 9.56). However, there is not a significant difference between 2D and 3D culture conditions. Again, we observe a significant difference between the expression levels of TroponinC between the ECM proteins ($p<0.0005$). We saw slightly higher expression

of troponinC in collagen IV for 2D (14.74+3.04) compared to 3D (2.58+1.13). 2D culture conditions of laminin (13.30+5.79) and fibronectin (19.60+6.75) were lower than their 3D counterparts. Culture conditions in 3D for gelatin (5.11+1.37) and collagen IV (2.58+1.13) were lower than standard 2D and similar to the expression levels seen in both conditions for vitronectin (2D: 5.11+1.82; 3D: 5.25+4.01).

D. Discussion

We have demonstrated our ability to successfully differentiate hiPS cells down a cardiovascular pathway. By creating uniformly sized EBs we can successfully modulate differentiation of hiPS cells by altering the microenvironment in which they are cultured (Figure 4-1 and 4-2). While previous studies [11,12] have focused on manipulating signaling pathways to optimize cardiac differentiate, we have focused on understanding the role of the microenvironment on differentiation as well as exploiting that knowledge to guide differentiation. Here, we have shown the influence of specific ECM proteins on differentiation in both 2D and 3D microenvironments in an effort to capitalize on manipulating the native signals from the cardiovascular stem cell niche. We have shown that at day 10 cells exhibit many cardiac specific markers, including Nkx2.5, calponin, troponinT and troponinI (Figure 4-3). In some cases, we observed spontaneously beating cells (data not shown). Immunostaining alone did not specify or characterize the ability of specific proteins or dimensionality of the culture conditions for cardiac differentiation. FACS analysis of cardiac troponinT showed that we were able to achieve at least 30% differentiation in 2D culture conditions, and at least 16% differentiation on 3D scaffolds (Figure 4-4). We found that collagen IV and vitronectin had similar differentiation efficiency in both 2D and 3D, while the other proteins we evaluated show higher differentiation

in 2D compared to 3D. Many other cardiac differentiation protocols have demonstrated lower differentiation efficiencies, about 20% to 40% of cells expressing a similar cardiac marker at a comparable time of analysis via FACS [12-14]. One study from Murry's lab [12] in 2007 used an Activin/BMP protocol that yielded about 30% cardiomyocytes from ES cells, which they then purified and used for functional studies. Zhang's study [13] examined various hES cell lines and found that about 15% of the H9 hES cells expressed MF20 at day 10, while Carpenter's study [14] found that about 40% of the hiPS cells differentiated to express troponinI and α-actinin. In particular, Keller's lab [11] used a hypoxic differentiation protocol in conjunction with small molecules (Nodal inhibitor SB and BMP4 inhibitor dorsomorphin) to target the Activin/Nodal pathway, which resulted in almost 60% cardiac troponinT$^+$ cells at day 14. Our study yielded similar differentiation potential. As FACS analysis only tells us the percentage of cells evaluated that express the protein of interest (troponinT), we performed further quantitative analysis of real time-PCR.

Gene expression of a full panel of differentiation markers gives us a more complete picture. We found that fibronectin enhanced vascular endothelial and smooth muscle cell marker expression, especially in a 3D microenvironment. It is known that proteins enhance vascularization, with fibronectin in particular being used to promote induction of vascular endothelial cells [15]. The processes of vascularization include both vasculogenesis and angiogenesis. Fibronectin has been used in conjunction with VEGF to induce/enhance both processes [16-18]. Our results confirm these findings. We found that fibronectin in a 3D scaffold significantly increased the amount of cells expressing endothelial markers Tie2, vWF, and VE-cadherin (Figure 4-5A-C). Vasculogenesis and angiogenesis create 3D structured tubes as precursors for vessel formation, we were not surprised to see that the fibronectin in 3D promoted

the most vascular endothelial cell induction. Protein coating of vascular grafts to improve endothelialization has been tested, with fibronectin being the protein of choice [16]. Fibronectin is known to enhance and direct vascular differentiation of ES cells [17,18], which our results also confirm (Figure 4-5A-C). We observed a similar pattern of expression amongst the proteins of interest in both 2D and 3D culture conditions. Myosin was also promoted when cultured in 3D scaffolds, specifically for gelatin and fibronectin (Figure 4-5D).

Cardiac differentiation was evaluated by examining RNA levels of actinin and the components of the troponin complex (Figure 4-6). Little is known about the timing of the expression of the individual components of the troponin complex. Our data would suggest that troponinT and troponinC are expressed at an earlier time point than troponinI. The tropomyosin-troponin complex is comprised of the three troponins (T,C,I) and as well as tropomyosin and regulates the development of force by the contractile apparatus. When calcium is released from the sarcoplasmic reticulum, it binds to troponinC causing a conformational change allowing for movement of tropomyosin away from the myosin binding sites on actin [19,20]. TroponinT and I are thought to influence Ca^{2+} sensitivity, while troponinC is thought to act as a switch for Ca^{2+} activation. During development, there is thought to be a transition from fetal to adult isoforms of troponinT and I. Some of these have been studied in animal models [21,22], but little is known about the early expression profile. Overall, we saw higher expression of actinin in 2D laminin and 3D fibronectin culture conditions. We observed similar expression patterns for troponinT and C—with 3D culture conditions for laminin and fibronectin showing enhanced expression compared to 2D. As these results are somewhat contradictory of our FACS analysis data, we believe this is due to the relatively early time point of our study as well as the difference between protein (FACS) and RNA (qPCR). We believe if we were to examine a later time (about 14days

compared to 10 days) we would see a higher percentage of cells expressing troponinT through FACS analysis. We saw relatively low expression of troponinI of all proteins of interests in both 2D and 3D, although 2D gelatin is significantly higher than the rest (Figure 4-6B). The gelatin in 2D culture condition consistently enhanced all our cardiac markers.

Our studies suggest that troponinT and C are expressed early during differentiation in immature cardiomyocytes, while troponinI is expressed later. As little characterization exists on the expression profile and timing of the troponin complex in an iPS or ES cell model, it is an area of research we intend to investigate further.

E. Conclusions

We demonstrated our ability to successfully differentiate hiPS cells into cardiac cells. We have also characterized the effects of ECM proteins and the microenvironment on that differentiation. We found that fibronectin in 3D culture conditions enhances vascular differentiation, while 2D culture conditions with gelatin and 3D laminin and fibronectin promote cardiomyocyte differentiation. We believe the results of our investigations can be used for further tissue engineering studies as well as provide a better understanding of the role of the microenvironment in cardiovascular differentiation.

F. Acknowledgments

G. References:

1. Schenke-Layland K, Rhodes KE, Angelis E, Butylkova Y, Heydarkhan-Hagvall S, Gekas C, Zhang R, Goldhaber JI, Mikkola HK, Plath K, MacLellan WR. Reprogrammed mouse fibroblast differentiate into cells of the cardiovascular and hematopoietic lineages. Stem Cells, 2008; 26: 1537-1546.

2. Schenke-Layland K, Nsair A, Van Handel B, Angelis E, Gluck JM, Votteler M, Goldhaber JI, Mikkola HK, Kahn M, MacLellan WR. Recapitulation of the embryonic cardiovascular progenitor cell niche. Biomaterials, 2011; 32: 2748-2756.

3. Heydarkhan-Hagvall S, Gluck JM, Delman C, Jung M, Ehsani N, Full S, Shemin RJ. The effect of vitronectin on the differentiation of embryonic stem cells in a 3D culture system. Biomaterials, 2012; 33 (7), 2032-2040.

4. Ratajczak MZ, Kucia M, Jadczyk T, Greco NJ, Wojakowski W, Tendera M, Ratajczak. Pivotal role of paracrine effects in stem cell therapies in regenerative medicine: can we translate stem cell-secreted paracrine factors and microvesicles into better therapeutic strategies? Leukemia, 2012; 26: 1166-1173.

5. Schenke-Layland K, Angelis E, Rhodes KE, Heydarkhan-Hagvall S, Mikkola HK, MacLellan WR. Collagen IV induces trophoectoderm differentiation of mouse embryonic stem cells. Stem Cells, 2007; 25: 1529-1538.

6. Dziadek M, Timpl R. Expression of nidogen and laminin in basement membranes during mouse embryogenesis and in teratocarcinoma cells. Dev Biol, 1985; 111: 372-382.

7. Heydarkhan-Hagvall S, Schenke-Layland K, Dhanasopon AP, Rofail R, Smith H, Wu BM, Shemin R, Beygui RE, MacLellan WR. Three-dimensional electrospun ECM-based hybrid scaffolds for cardiovascular tissue engineering. Biomaterials. 2008;29(19):2907-2914.

8. Willems E, Spiering S, Davidovics H, Lanier M, Xia Z, Dawson M, Cashman J, Mercola M. Small-molecule inhibitors of the Wnt pathway potently promote cardiomyocytes from human embryonic stem cell-derived mesoderm. Circ Res. 2011 Aug 5;109(4):360-4.

9. Gluck JM, Rahgozar P, Ingle NP, Rofail F, Petrosian A, Cline MG, Jordan MC, Roos KP, MacLellan WR, Shemin RJ, Heydarkhan-Hagvall S. Journal Biomedical Materials Research Part B, 2011; 99B: 180-190.

10. Nsair A, Schenke-Layland K, Van Handel B, Evseenko D, Kahn M, Zhao P, Mendelis J, Heydarkhan S, Awaji O, Vottler M, Geist S, Chyu J, Gago-Lopez N, Crooks GM, Plath K, Goldhaber J, Mikkola HKA, MacLellan WR. Characterization and therapeutic potential of induced pluripotent stem cell-derived cardiovascular progenitor cells. PLoS One, 2012; 7: e45603.

11. Kattman SJ, Witty AC, Gagliardi M, Dubois NC, Niapour M, Hotta A, Ellis J, Keller G. Stage-specific optimization of activin/nodal and BMP signaling promotes cardiac differentiation of mouse and human pluripotent stem cell lines. Cell Stem Cell, 2011; 8: 228-240.

12. Laflamme MA. Chen KY, Naumova AV, Muskheli V, Fugate JA, Dupras SK, Reinecke H, Xu C, Hassanipour M, Police S, O'Sullivan C, Collins L, Chen Y, Minami E, Gill EA, Ueno S, Yuan C, Gold J, Murry CE. Cardiomyocytes derived from human embryonic stem cells in pro-survival factors enhance function of infarcted rat hearts. Nature Biotech, 2007; 25: 1015-1024.

13. Zhang J, Wilson GF, Soerens AG, Koonce CH, Yu J, Palecek SP, Thomson JA, Kamp TJ. Functional cardiomyocytes derived from human induced pluripotent stem cells. Circ Res, 2009; 104: e30-e41.

14. Carpenter L, Carr C, Yang CT, Stuckey DJ, Clarke K, Watt SM. Efficient differentiation of human induced pluripotent stem cells generates cardiac cells that provide protection following myocardial infarction in the rat. Stem Cells and Development, 2012; 21: 977-986.

15. Krawiec JT, Vorp DA. Adult stem cell-based tissue engineered blood vessels: A review. Biomaterials, 2012; 33: 3388-3400.

16. De Visscher G, Mesure L, Meuris B, Ivanova A, Flameng W. Improved endothelialization and reduced thrombosis by coating a synthetic vascular graft with fibronectin and stem cell homing factor SDF-1α. Acta Biomaterialia, 2012; 8: 1330-1338.

17. Pimton P, Sarker S, Sheth N, Perets A, Marcinkiewicz C, Lazarovici P, Lelkes P. Fibronectin-mediated upregulation of a5b1 integrin and cell adhesion during differentiation of mouse embryonic stem cells. Cell Adhesion and Migration, 2011; 5: 73-82.

18. Ferreira LS, Gerecht S, Fuller J, Shieh HF, Vunjak-Novakovic G, Langer R. Bioactive hydrogel scaffolds for controllable vascular differentiation of human embryonic stem cells. Biomaterials, 2007; 28: 2706-2717.

19. Posterino GS, Dunn SL, Botting KJ, Wang W, Gentili S, Morrison JL. Changes in cardiac troponins with gestational age explain changes in cardiac muscle contractility in the sheep fetus. J Appl Physiol, 2011; 111: 236-243.

20. Asumda FZ, Chase PB. Nuclear cardiac troponin and tropomyosin are expressed early in cardiac differentiation of rat mesenchymal stem cells. Differentiation, 2012; 83: 106-115.

21. Kruger M, Kohl T, Linkel WA. Developmental changes in passive stiffness and myofilament Ca2+ sensitivity due to titin and troponin-I isoform switching are not critically triggered by birth. Am J Physiol Heart Circ Physiol, 2006; 291: H496-H506.

22. Siedner S, Kruger M, Schroeter M, Metzler D, Roell W, Fleischmann BK, Hescheler J, Pfitzer G, Stehle R. Developmental changes in contractility and sarcomeric proteins from early embryonic to the adult stage in the mouse heart. J Physiol, 2003; 257: H1-H9.

CHAPTER FIVE

A. Summary and Conclusions

The goal of this dissertation was to study the effects of the microenvironment on cardiovascular differentiation. Previous work from our lab had begun to explore the role of ECM proteins found within and around the CPC niche. The research outlined here furthers our understanding of the contribution of major ECM proteins as well as to explore the effects of a 3D environment, similar to what is seen in native ECM. I first sought to determine the contribution of the microenvironment to the induction of CPCs from undifferentiated ES cells. I then asked the question, do we continue to see an effect from the microenvironment on later cardiovascular lineage commitment? Finally, do these effects translate into a human model of cardiovascular differentiation?

In the first phase of investigation, I examined the effects of the microenvironment on the induction of a CPC population. I first developed a more stable electrospun nanofibrous scaffold to use as a 3D culture system for future studies. By using a co-axial electrospinning system, I incorporated PU into our already established PCL-gelatin system. By doing so, I increased the mechanical integrity and elasticity of the scaffolds, and created a more stable system that had the capability to last more than two months in continuous culture systems. I characterized the physical and mechanical properties and demonstrated the biocompability of the scaffolds by implanting them subcutaneously in mice. The scaffolds elicited minimal immune response, and endogenous cells were shown to migrate into the scaffolds after four and seven weeks post implantation.

While I had developed a 3D scaffold that has great potential for cardiovascular tissue engineering, my original goal was to understand the effects of the 3D environment on CPC

induction. I had observed that it took cells approximately seven to ten days to migrate into the interior of the scaffold *in vitro*, which complicated analyzing early differentiation effects. Thus, in order to examine the immediate effects of a 3D environment, I used a hydrogel system, which could immediately encapsulate mES cells. The hydrogel, Hystem-C, is commercially available and approved for medical uses. I found that the hydrogel alone could potently induce a CPC population. Using standard 2D cell culture techniques, we observed about 2% CPC induction at day five. The addition of collagen IV increased the CPC population to about 5%, while the inclusion of the electrospun scaffold increased the CPC population to about 6%. The electrospun scaffold with a collagen IV coating further increased the CPC population to about 8%. The hydrogel system significantly increased CPC induction to about 11%. Further gene expression analysis confirmed these results and revealed a dramatic increase in CPC marker expression. This data demonstrates the importance of the understanding the contribution of the microenvironment to cardiovascular differentiation.

In an effort to understand the mechanism underlying the effects I had observed, I examined integrin expression of both undifferentiated and partially differentiated mES cells. Integrins are known to mediate cell-matrix interactions and were a logical target to account for the effects elicited by different ECM proteins and the addition of a 3D substrate. I characterized integrin expression and observed differences not only between undifferentiated and partially differentiated mES cells, but also between cells cultured in 2D vs. 3D and those exposed to different ECM proteins. Through a series of analyses, we found that $\alpha5$, αV, $\beta1$, $\beta5$, and $\alpha V\beta5$ integrin subunits were extremely important for cellular adhesion to a 3D substrate. To date, this was the first such study to characterize and compare integrin expression of undifferentiated and partially differentiated mES cells in both 2D and 3D culture systems. Overall, I was able to

demonstrate the importance of understanding the microenvironment on the induction of a CPC population. I found that the 3D microenvironment greatly enhances the amount of CPCs. I also developed two separate 3D culture system for *in vitro* investigation and characterized integrin expression.

In the second study, I examined the effects of the microenvironment on cardiovascular differentiation of CPCs. I isolated CPCs and seeded them in culture exposed to the same ECM proteins and 2D or 3D culture systems. I analyzed endothelial and vascular smooth muscle cell lineage differentiation. I found that laminin and vitronectin enhanced endothelial cell differentiation, while fibronectin enhanced smooth muscle cell differentiation. I also observed that the effects of the 3D electrospun scaffolds were delayed and not noticeable until the later time point (day 14), which may be due to the amount of time necessary for the cells to migrate to the interior of the scaffold. I was then able to create a tubular electrospun scaffold to use in a bioreactor system to create a layered bioengineered ES cell-derived vascular graft. By seeding isolated CPCs into the tubular scaffolds and initiating smooth muscle cell differentiation followed by a second cell seeding two weeks later with endothelial cell differentiation conditions, I demonstrated that creating a layered effect engineered construct was feasible. The study characterized the contributions of both ECM proteins and the addition of a 3D culture system to the continued cardiovascular differentiation.

In the final study, I aimed to determine if these effects could be translated to a human model. To initiate this study, I first optimized a cardiovascular differentiation protocol for human iPS cells. I found a "spinEB" method, which creates uniformly sized EBs and introduces the EBs to a controlled microenvironment at day four. I examined the effects of the same ECM proteins in both 2D and 3D culture system. Surprisingly, I found that fibronectin in 3D culture greatly

enhanced vascular endothelial and smooth muscle cell differentiation. I also observed that there was a time dependent differentiation effect for the components of the troponin complex. 3D culture systems were shown to enhance cardiac differentiation at the gene expression level, but not at the protein level. I believe this is due to the relatively early time point I examined (day 10) and that if the differentiation protocol was analyzed again at a later time point, we would see enhanced differentiation of hiPS cells exposed to the 3D scaffold system. Overall, this study found that microenvironment can direct differentiation towards various lineages of the cardiovascular system and that the effects of the microenvironment are seen in a human model, though slightly different than what was observed in the mouse model.

My dissertation has introduced a new line of study in terms of cardiovascular differentiation. I have shown the importance of studying differentiation in more physiologically relevant 3D systems. Previously, there has been limited information on stem cell differentiation in a 3D environment. Here, I have shown the importance of the 3D microenvironment to all stages of differentiation in both mouse and human stem cell models. Additionally, I have shown the contribution of the ECM proteins native to the CPC niche for late cardiovascular differentiation. I have optimized a cardiac differentiation protocol for hiPS cells as well as begun investigating the role of the microenvironment on human cardiovascular differentiation. This dissertation has implications for future research as well as possible avenues of tissue engineering. Understanding cardiac differentiation is extremely important to developing new treatment strategies.

B. Future directions in the research

This collection of studies has raised many possible avenues of future research. In terms of the CPC niche, I have developed a system to evaluate the induction of the CPCs and examine their continued differentiation. One question that remains is what keeps the cells in the niche? Endogenous CPCs exist in very small populations in the adult heart. What factors keep them in a progenitor cell state? And what factors drive them to continue differentiation? I have only done preliminary characterization of integrin expression for undifferentiated and partially differentiated mES cells. The mechanism(s) underlying the different effects of specific microenvironments on differentiations is still poorly understood. Furthermore, the progenitor cell state could be related to expression of certain integrins. Integrins could potentially explain part of the mechanism keeping CPCs in a progenitor cell state or what drives them towards continued differentiation. While my work has begun initial investigation and provided the necessary foundation and characterization of the CPC niche, there are many questions still remaining to be answered.

Vascular differentiation is another area of further research. The close relationship between vascular endothelial and smooth muscle cells is well-documented, but their differentiation from a CPC state to mature vasculature is still unclear. These studies have highlighted the different contributions from various components of the microenvironment and provided a novel look at vascular differentiation. My work has shown that different components of the microenvironment contribute to their separate differentiation, but there is still work to be done. Researchers have focused on developing an artificial blood vessel or tissue engineered vascular graft for many years, but none have led to viable commercial products. The small-diameter bioengineered vascular graft I have developed is one of the first to be derived from an

ES cell model. It is also one of the first to create layers through a differentiation protocol. Previous work has been done with adult stem cells or creating layers from mature cells. I have demonstrated the capability of using ES cell-derived CPCs and a differentiation protocol to create a layered vascular graft supported by an electrospun scaffold. This proof-of-concept study has great potential for further study and possible commercial product implications.

I have also translated my work on continued cardiovascular differentiation into a human stem cell model. While my work has shown the different effects of ECM proteins both with and without a 3D scaffold, there are still more questions to be answered. My cardiac differentiation protocol was optimized but did not include a step to enrich CPCs. One potential area of research is to evaluate the microenvironment contribution to CPC induction to determine if there are similarities or differences to the mouse ES cell model I used previously. I also found that there appears to be a time delay in the differentiation of the separate components of the troponin complex. Little research has been done on the origins and development of the troponin complex. Further characterization of the specific differentiation of the troponin complex could yield very interesting results with direct clinical applications. My dissertation work could be applied to a cardiovascular tissue engineering project and potentially use the 3D scaffolds I have created to create functional, contractile human cardiac tissue *in vitro*.

Overall, my dissertation work has laid the foundation for understanding the role of the microenvironment in cardiovascular differentiation and has the potential for many exciting future research possibilities.